© by Ritika Mohan. All Rights Reserved.

A MULTIPLEXED MICROFLUIDIC PLATFORM FOR ANTIBIOTIC SUSCEPTIBILITY TESTING

BY

RITIKA MOHAN

DISSERTATION

Submitted in partial fulfillment of the requirements
for the degree of Doctor of Philosophy in Chemical Engineering
in the Graduate College of the
University of Illinois at Urbana-Champaign, 2014

Urbana, Illinois

Doctoral Committee:

Professor Paul J.A. Kenis, Chair
Assistant Professor Charles Schroeder
Assistant Professor Brendan A. Harley
Professor Isaac Cann

Abstract

Antibiotic susceptibility testing represents a key first step for determining therapeutic regimens to treat bacterial infections. Current technologies are slow and cumbersome, require large sample volumes for analysis, have poor detection sensitivity and limited combinatorial capabilities. These factors often preclude the timely administration of correct antibiotics, which complicates the clinical management of infections and exacerbates the escalating problem of antibiotic resistance development in pathogens. My work has focused on developing microfluidic platforms for rapid antimicrobial susceptibility testing with a future potential in point-of-care diagnostics. I have employed the platform to quantify the effects of commonly used antibiotics on *E. coli* cells at various concentrations (0.5-500 μg/mL) of each antibiotic as well as combinations thereof, on cellular proliferation and morphology as a proof-of-concept. I demonstrated that combinations of three or more antibiotics are not necessarily better suited to eradicating pathogens in comparison to antibiotic pairs, which is a significant result for prescribing therapeutic regimens based on antibiotic cocktails. Then, I addressed the effects of initial cell density (ranging from 10^8 -10^{10} cells/mL) on the efficiency of antibiotic action. Finally, I extended the platform to test more clinically relevant pathogens such as *P. aeruginosa* and *K. pneumoniae* in monomicrobial and polymicrobial cultures. I demonstrated that bacteria behave significantly differently when co-cultured and individual susceptibility to antibiotics such as amikacin and tobramycin increases in co-cultures. I illustrate the advantages of using microfluidics over conventional methods for AST for precise determination of antibiotic dosing regimen, which encompass a significant potential to address the issue of antibiotic resistance.

Acknowledgements

Rarely people are successful without other people's help and collaboration and I am no exception to this rule. I have been extremely fortunate to be surrounded with very talented people around me who have helped me in every small and big successes as a graduate student.

First, I would like to thank my advisor a.k.a "Boss" for believing in my capabilities, motivating me to excel, constantly encouraging and providing opportunities for me to network and present our research nationally and internationally, and for being a great friend! **Second**, I would like thank my three undergraduate students who I supervised for approximately 2.5 years and have played an instrumental role in the success of my projects: Jaebum Lee, Emre Sevgen, and Chotitath Sanpitakseree. Specifically, Jaebum Lee helped in the initial stages of the antibiotic project (chapter 3) in the fabrication of microfluidic chips for experiments and also replication of biological experiments. Emre Sevgen was particularly helpful in the manual data analysis in the initial stages of the project (chapter 3 and 4) and also worked on the dye optimization project (chapter 6). Chotitath Sanpitakseree's phenomenal computational skills provided me with invaluable help in reducing the data analysis time from several hours to a few minutes, and replication of polymicrobial experiments. Thanks to Dr. Benjamin Schudel for his help in my first project (chapter 2) as a graduate student. **Third**, I would like to thank our collaborators Prof. Schroeder and Arnab Mukherjee for the intellectually stimulating discussions on the biology aspects of my projects and Prof. Rao's lab for letting us use their laboratory equipment for BL-2 materials.

I would also like to extend a special thanks to Dr. Amit Desai for being a great pseudo-mentor, one of the most amazing people I have met, and for being there throughout my journey as a graduate student ☺

Thanks to my amazing husband, the best of best friends, Dr. Joshua Tice for encouraging, supporting, and waiting for me to finish my PhD before starting his job in a different place! Thanks to my maid of honor and my best friend, Kori Dunn for supporting and teaching me some basic microbiological skills for my research, and for being such an open spirit. Thank you to amazing friends including Kristine Pangan-Okimoto, Samantha Weiss, Chandra Khatri, and Alicia Sorenson for being so enthusiastic and motivating in this journey. Finally, a big hug and love to my parents, brother, grandparents, family and friends for always being there for me.

To my husband

Table of Contents

Chapter 1

Introduction

1.1 Antibiotic resistance

Incorrect use of antibiotics over several decades has led to widespread emergence of antibiotic resistance in clinical pathogens, which poses a rising critical global health issue [1]. Recent years have shown increasing resistance to even one of the most powerful carbapenem antibiotics [1]. For instance, in 2003, *Klebsiella* infections were infrequent and often went unnoticed; however, by 2007 approximately 21% *Klebsiella* infections appeared with carbapenem-resistance in the state of New York and 5% all over the USA [2]. Similarly, methicillin-resistant *Staphylococcus aureus* **(**MRSA) accounts for 60% of the *S. aureus* population, and possesses resistance to multiple antibiotics including quinolones, macrolides, and sulfonamides [3]. Also, since majority of the antibiotics (~ 80%) in the USA are given to chicken, pigs, turkey, and cattle primarily as a preventive measure against illness, trace amounts of antibiotics often end up in milk and food products used for human consumption [4]. Typically, a sub-lethal antibiotic dose gives rise to antibiotic resistance. When a bacterium is exposed to an incorrect antibiotic dose, it gradually develops resistance against that drug even when administered at higher concentrations in the future. Hence, trace amounts of antibiotics found in food products has further exacerbated the issue of antibiotic resistance and has prompted several critical reviews of current agricultural practices [4-6].

One of the key reasons for rising antibiotic resistance is the prescription of incorrect antibiotics and the failure to detect resistance early when treating infections [7]. Current practice for treating infections entails antibiotic susceptibility testing (AST), or determination of

antibiotic susceptibility profiles against various pathogens in infections [8]. Although conventional methods for AST are widely and successfully used for treatment of bacterial infections, several issues exist with these methods. Hence, in the absence of a precise antibiotic susceptibility profile of bacteria resulting from the long assay time and low sensitivity of the conventional methods, physicians often utilize empirical approaches with broad spectrum antibiotics that gives rise to the indiscreet use of antibiotics and is known to intensify the issue of antibiotic resistance [9,10]. ***Development of alternative techniques for generating precise antibiotic susceptibility profiles is indispensable for mitigating antibiotic resistance and for providing better clinical care.*** In this thesis, I discuss approaches to address this issue by utilizing microfluidic platforms. Specifically, I will discuss microfluidic platforms currently being developed for addressing the issue of conventional methods for AST and then I will discuss the application of microfluidics platforms for performing pharmacodynamics/ pharmacokinetics modeling later on in the thesis, which provides superior metrics for determining antibiotic dosing regimen.

1.2. Antibiotic susceptibility testing

1.2.1 Conventional methods

Broth dilution and disk diffusion are two widely used methods for AST. The latter method is the "gold standard" at the clinics and provides qualitative information by categorizing each strain into resistant or sensitive categories without providing any quantitative information about actual concentration of antibiotics that would be effective against infections [11]. In the broth dilution method, which utilizes 96-well plates, minimum inhibitory concentration (MIC) is the most commonly used parameter to describe the efficacy of the antibiotics against the pathogens. In both the methods, the bacteria is first isolated from the patient samples (24 – 48 h)

followed by pre-culturing of isolated bacteria to enrich cell density to detectable levels (24 – 48 h). Then, the cells are incubated with antibiotics in 96-well plates or petri dishes (24 - 48 h) and finally the bacterial growth is determined using absorption spectroscopy or by visual assessment.

Several limitations exist with the current techniques for AST. First, these techniques involve multiple time-consuming steps (3-7 days) [12] leading to long assay times (as long as a few days). Second, these techniques typically require significant quantities (10 - 30 mL) of patient samples such as blood, sputum, or urine for analysis [13], which preclude high-throughput or multiplexed screening for different antibiotic concentrations/ combinations. Third, the limited sensitivity of current techniques for AST makes them unsuitable for detecting the presence of "persister" microbes. Although persister cells represent only a small fraction ($\approx 10^{-5}$) of microbial cells, they tend to evade antibiotic-mediated killing by switching to a metabolically dormant or "persistent" state [14,15]. Persister cells constitute a significant threat due to their ability to re-initiate infection upon discontinuation of antibiotic therapy [16]. Fourth, inconsistencies in results obtained from different AST techniques further complicate diagnosis and treatment [17-22]. Fifth, all the conventional techniques for AST have been standardized for monomicrobial cultures only, while several infections are polymicrobial in nature (*e.g.*, urinary tract infections (UTIs), chronic wounds, cystic fibrosis, and nosocomial bacteremia) caused by more than one microbe [23-25]. The interaction between different microbial species is known to influence the efficacy of the antibiotic treatment [26,27], yet antibiotic dosing regimen is often extrapolated from the monomicrobial AST results from conventional techniques further exacerbating the issue of antibiotic resistance.

1.2.2 Microfluidic approaches

Microfluidics is an attractive technology that can address the issues of the conventional methods for AST. Microfluidic chips/reactors/platforms comprise a simple to complex network of channels, chambers, valves, pumps *etc.* and enable precise spatio-temporal control over flow of reagents. As a result, microfluidics has been explored for a wide range of applications, from chemical synthesis to fundamental biological studies [28-46]. With respect to performing AST, microfluidics offers several advantages compared to conventional techniques including assay with low sample volumes (~ 1-10 µL), enhanced detection sensitivity (~ 1 cell), faster analysis (2-4 h), improved portability, and the ability to perform species-specific AST in polymicrobial infections.

Due to the aforementioned advantages, numerous microfluidic platforms have been developed for antimicrobial susceptibility testing [47-52]. Several of these platforms have focused on improving sensing capabilities to detect changes in metabolic activities of bacteria. For example, electrochemical sensors have been utilized to determine susceptibility by measuring small changes in growth of cells in monomicrobial cultures [48]. A surface-plasmon resonance-based biosensor platform [47] was used to categorize strains as susceptible or resistant by detecting variations in optical properties of bacteria when treated with antibiotics [47]. Another interesting approach for AST utilized an asynchronous magnetic bead rotation biosensor to monitor single cells or cell populations after treatment with antibiotics [53]. Filter chip and optical detection biosensing system have also been developed to provide susceptibility results in one hour [52].

These microfluidic-based biosensor technologies enable sensitive and rapid assays; however, most of these platforms lack multiplexing capabilities. Integrated microfluidics on the

other hand is an attractive technology for the multiplexed implementation of biological assays with rapid turnaround times and minimal sample consumption [54]. Integrated microfluidics enables convenient manipulation of small reagent volumes (nL) within small chambers (μm) enabling the testing of multiple conditions with small volumes in rapidly in a convenient format. Several promising integrated microfluidic platforms for AST have been reported [55-61]. For example, droplet-based microfluidics has been utilized to compartmentalize bacterial cells, nutrients, antibiotics, and fluorescent viability indicators in water-in-oil emulsions [55,57]. A microfluidic platform was developed to confine bacterial cells in square micro-wells connected to a central flow channel that continuously delivers nutrients and antibiotics to cells [59] and a microfluidic agarose channel system was reported for rapid AST by tracking single cell growth [62]. Weibel and colleagues have developed a portable microfluidic chip for AST with the objective of making the device point-of-care [58]. Here, the key advantage of the portable chip is the automatic loading of bacterial cells into microfluidic chambers preloaded with antibiotics using a 'degas driven flow'.

These existing approaches for microfluidic-based antibiotic susceptibility testing offer promising routes towards the development of a rapid and portable screening tool. However, many of these methods suffer from one or more of the following limitations: (1) complicated platform fabrication and/or operation procedures [61], (2) poor portability due to the requirement for syringe pumps, pneumatic actuators, and other ancillary equipment [57,61,62], and (3) unstable droplet formation [63]. In addition, almost all the microfluidic approaches have been developed for monomicrobial cultures, although several infections are polymicrobial in nature.

To address these limitations of existing microfluidic approaches, our group has developed a microfluidic platform featuring a spatially addressable 4x6-array of wells to simultaneously

monitor the effects of multiple antibiotics at different concentrations, as well as their combinations, on bacterial cells for AST. This technology integrates ease-of-fabrication and use with enhanced combinatorial capabilities, and further provides improved portability and usability by circumventing the requirement for expensive syringe pumps and pneumatic actuators by implementing normally closed valves. In addition, the platform is amenable to automated analysis by using time-lapse fluorescence microscopy (TLFM). I employed the microfluidic platform to interrogate the antibiotic sensitivity profile of *Escherichia coli* to four commonly used bactericidal and bacteriostatic antibiotics. Furthermore, I explored synergistic and antagonistic effects of different antibiotic cocktails, as well as the effects of *E. coli* cell densities on the efficiency of antibiotic action. Overall, this platform capitalizes on several key advantages of integrated microfluidics technology including miniaturization of assays, expedited analysis, multiplexing, and improved detection sensitivity along with ease-of-use and portability. I further extended the proof-of-concept AST technology from monomicrobial cultures to polymicrobial cultures comprising *K. pneumoniae* and *P. aeruginosa*, and *E. coli* to determine species-specific bacterial susceptibility. I then used the experimental data from these studies to examine the potential of the microfluidic platform for performing pharmacodynamics/pharmacokinetic modeling, which is expected to provide a more accurate prediction of *in vivo* antibiotic action for a more precise determination of antibiotic dosing regimen.

1.3 Thesis objectives

The overall objective of my research was to develop high throughput microfluidic platforms for antibiotic susceptibility testing (AST) for precise prediction of antibiotic dosing regimen to treat bacterial infections. Empirical approaches to prescribe antibiotics accounts for

as much as 50% incorrect prescription, and these practices have led to an increase in global health issue of antibiotic resistance. Conventional techniques for AST are time consuming, require large sample volumes, low throughput, and have low sensitivities. Hence, Integrated microfluidic platforms are an attractive way to address the limitations of conventional techniques.

My research can be divided into three broad phases. In phase 1, I optimized components used in microfluidic devices for biological screening applications. In phase 2, I validated the optimized microfluidic platform for biological studies and performed antibiotic susceptibility testing on monomicrobial and polymicrobial cultures. Phase 2 encompasses bulk of my research and in phase 3, I utilized the experimental results to perform proof-of-principle pharmacodynamics/pharmacokinetic studies to predict *in vivo* results for accurate prescription of antibiotic dosing regimen.

Specifically, **chapter 2** discusses optimization of normally closed valves with respect to their designs, parameters, and operational considerations for their incorporation into high-throughput biological screening applications with the purpose of reliable sample routing. **Chapter 3** discusses a proof-of-concept microfluidic platform for performing antibiotic susceptibility testing on monomicrobial cultures of *E. coli* cells. First, I first validated the platform by deriving growth profiles of *E. coli*. Second, I performed antibiotic susceptibility testing against *E. coli* cells using single antibiotics followed by antibiotic pairs and combinations of three and four to study the effects of combination therapy utilized in the clinics for treating infections. Third, I discussed the implications of cell density on the efficacy of antibiotics using microfluidic platforms. Finally, I extended the AST platform to be utilized for more clinically relevant pathogens such as *P. aeruginosa*. **In chapter 4**, I utilized the clinically relevant

pathogens such as *K. pneumoniae* and *P. aeruginosa* to perform polymicrobial AST with the aim of determining susceptibility of bacteria in polymicrobial infections. **Chapter 5** introduces the concept of pharmacodynamic/pharmacokinetic modeling that utilizes time-kill curves generated in chapters 3 and 4, to predict the *in vivo* antibiotic action over 24 hours. The screening experiments for AST were performed using genetically modified bacteria (not applicable at the clinical level). Hence, with the objective to further extend the platform for testing "real bacteria", I discussed a range of options with optical dyes (**chapter 6**). Finally, **chapter 7** briefly describes the summary of my research and its future outlook.

1.4 References

1. Toprak E, Veres A, Michel J-B, Chait R, et al. 2012. Evolutionary paths to antibiotic resistance under dynamically sustained drug selection. Nat Genet 44: 101-5.
2. Podschun R, Ullmann U. 1998. Klebsiella spp. as Nosocomial Pathogens: Epidemiology, Taxonomy, Typing Methods, and Pathogenicity Factors. Clinical Microbiology Reviews 11: 589-603.
3. Barrett JF. 2004. MRSA: status and prospects for therapy? An evaluation of key papers on the topic of MRSA and antibiotic resistance. Expert Opinion on Therapeutic Targets 8: 515-9.
4. Heilig S, Lee P, Breslow L. 2002. Curtailing antibiotic use in agriculture. Western Journal of Medicine 176: 9-11.
5. Smith DL, Dushoff J, Morris JG, Jr. 2005. Agricultural Antibiotics and Human Health. PLoS Med 2: e232.
6. Martínez JL. 2008. Antibiotics and Antibiotic Resistance Genes in Natural Environments. Science 321: 365-7.
7. Levy SB, Marshall B. 2004. Antibacterial resistance worldwide: Causes, challenges and responses. Nature Medicine 10: S122-S9.
8. Mohan R, Mukherjee A, Sevgen SE, Sanpitakseree C, et al. 2013. A multiplexed microfluidic platform for rapid antibiotic susceptibility testing. Biosensors and Bioelectronics 49: 118-25.
9. Alanis AJ. 2005. Resistance to antibiotics: are we in the post-antibiotic era? Archives of medical research 36: 697-705.
10 Ang BSP. 2001. Bugs for the next century: The issue of antibiotic resistance. Annals of the Academy of Medicine Singapore 30: 199-202.
11. Reller LB, Weinstein M, Jorgensen JH, Ferraro MJ. 2009. Antimicrobial Susceptibility Testing: A Review of General Principles and Contemporary Practices. Clinical Infectious Diseases 49: 1749-55.
12. Lazcka O, Campo FJD, Munoz FX. 2007. Pathogen detection: A perspective of traditional methods and biosensors. Biosensors and Bioelectronics 22: 1205-17.
13. Mancini N, Carletti S, Ghidoli N, Cichero P, et al. 2010. The Era of Molecular and Other Non-Culture-Based Methods in Diagnosis of Sepsis. Clin Microbiol Rev 23: 235-51.
14. Balaban NQ, Merrin J, Chait R, Kowalik L, et al. 2004. Bacterial Persistence as a Phenotypic Switch. Science 305: 1622-5.
15. Lewis K. 2010. Persister cells. Annual Review of Microbiology. p 357-72.
16. Dawson CC, Intapa C, Jabra-Rizk MA. 2011. "Persisters": Survival at the cellular level. PLoS Pathogens 7: e1002121.
17. Gales AC, Reis AO, Jones RN. 2001. Contemporary assessment of antimicrobial susceptibility testing methods for polymyxin B and colistin: Review of available interpretative criteria and quality control guidelines. Journal of Clinical Microbiology 39: 183-90.
18. Goldstein FW, Ly A, Kitzis MD. 2007. Comparison of Etest with agar dilution for testing the susceptibility of Pseudomonas aeruginosa and other multidrug-resistant bacteria to colistin [2]. Journal of Antimicrobial Chemotherapy 59: 1039-40.

19. Nicodemo AC, Araujo MRE, Ruiz AS, Gales AC. 2004. In vitro susceptibility of Stenotrophomonas maltophilia isolates: Comparison of disc diffusion, Etest and agar dilution methods. Journal of Antimicrobial Chemotherapy 53: 604-8.
20. Tan TY, Ng SY. 2007. Comparison of Etest, Vitek and agar dilution for susceptibility testing of colistin. Clinical Microbiology and Infection 13: 541-4.
21. Traub WH. 1970. Susceptibility of Pseudomonas aeruginosa to gentamicin sulfate in vitro: lack of correlation between disc diffusion and broth dilution sensitivity data. Applied microbiology 20: 98-102.
22. Lo-Ten-Foe JR, De Smet AMGA, Diederen BMW, Kluytmans JAJW, et al. 2007. Comparative evaluation of the VITEK 2, disk diffusion, etest, broth microdilution, and agar dilution susceptibility testing methods for colistin in clinical isolates, including heteroresistant Enterobacter cloacae and Acinetobacter baumannii strains. Antimicrobial Agents and Chemotherapy 51: 3726-30.
23. Hibbing ME, Fuqua C, Parsek MR, Peterson SB. 2010. Bacterial competition: Surviving and thriving in the microbial jungle. Nature Reviews Microbiology 8: 15-25.
24. Korgaonkar A, Trivedi U, Rumbaugh KP, Whiteley M. 2013. Community surveillance enhances Pseudomonas aeruginosa virulence during polymicrobial infection. Proceedings of the National Academy of Sciences 110: 1059-64.
25. Straight PD, Kolter R. 2009. Interspecies chemical communication in bacterial development. Annual Review of Microbiology 63: 99-118.
26. Heizmann WR, Heilmann F, Egeler B, Werner H. 1990. Efficacy of sulbactam in an in vitro model of mixed aerobic/anaerobic infections. Infection 18: 117-21.
27. Werner H, Heizmann WR, Freuer G, Mitinis N, et al. 1989. Efficacy of clavulanate-potentiated antibiotics against Bacteroides species and artificially associated cultures of aerobes and anaerobes. Journal of Antimicrobial Chemotherapy 24: 55-61.
28. Abou-Hassan A, Sandre O, Cabuil V. 2010. Microfluidics in inorganic chemistry. Angewandte Chemie International Edition 49: 6268-86.
29. Andersson H, Berg AVd. 2003. Microfluidic devices for cellomics: a review. Sensors and Actuators B: Chemical 92: 315-25.
30. deMello AJ. 2006. Control and detection of chemical reactions in microfluidic systems. Nature 442: 394-402.
31. Dittrich PS, Manz A. 2006. Lab-on-a-chip: microfluidics in drug discovery. Nature Reviews Drug Discovery 5: 210-8.
32. El-Ali J, Sorger PK, Jensen KF. 2006. Cells on chips. Nature 442: 403-11.
33. Khandurina J, Guttman A. 2002. Bioanalysis in microfluidic devices. Journal of Chromatography A 943: 159-83.
34. Kobel S, Lutolf MP. 2011. Biomaterials meet microfluidics: building the next generation of artificial niches. Current Opinion in Biotechnology 22: 690-7.
35. Kraly JR, Holcomb RE, Guan Q, Henry CS. 2009. Review: Microfluidic applications in metabolomics and metabolic profiling. Analytica chimica acta 653: 23-35.
36. Lecault V, White AK, Singhal A, Hansen CL. 2012. Microfluidic single cell analysis: from promise to practice. Current Opinion in Chemical Biology 16: 381-90.
37. Li L, Ismagilov RF. 2010. Protein crystallization using microfluidic technologies based on valves, droplets, and slipchip. Annual review of biophysics 39: 139-58.
38. Mason BP, Price KE, Steinbacher JL, Bogdan AR, et al. 2007. Greener approaches to organic synthesis using microreactor technology. Chemical Reviews 107: 2300-18.

39. Park JI, Saffari A, Kumar S, Günther A, et al. 2010. Microfluidic synthesis of polymer and inorganic particulate materials. Annual Review of Materials Research 40: 415-43.
40. Streets AM, Huang Y. 2013. Chip in a lab: Microfluidics for next generation life science research. Biomicrofluidics 7: 011302.
41. Tu Q, Pang L, Zhang Y, Yuan M, et al. 2013. Microfluidic Device: A Miniaturized Platform for Chemical Reactions. Chinese Journal of Chemistry 31: 304-16.
42. Velve-Casquillas G, Le Berre M, Piel M, Tran PT. 2010. Microfluidic tools for cell biological research. Nano Today 5: 28-47.
43. Wang J, Ren L, Li L, Liu W, et al. 2009. Microfluidics: a new cosset for neurobiology. Lab on a Chip 9: 644-52.
44. Zhang C, Xing D. 2010. Single-molecule DNA amplification and analysis using microfluidics. Chemical Reviews 110: 4910-47.
45. Zheng XT, Yu L, Li P, Dong H, et al. 2013. On-chip Investigation of Cell-drug Interactions. Advanced drug delivery reviews 65: 1556–74.
46. Ziółkowska K, Kwapiszewski R, Brzózka Z. 2011. Microfluidic devices as tools for mimicking the in vivo environment. New Journal of Chemistry 35: 979-90.
47. Chiang Y-L, Lin C-H, Yen M-Y, Su Y-D, et al. 2009. Innovative antimicrobial susceptibility testing method using surface plasmon resonance. Biosensors and Bioelectronics 24: 1905-10.
48. Karasinski J, White L, Zhang Y, Wang E, et al. 2007. Detection and identification of bacteria using antibiotic susceptibility and a multi-array electrochemical sensor with pattern recognition. Biosensors and Bioelectronics 22: 2643-9.
49. Kinnunen P, McNaughton BH, Albertson T, Sinn I, et al. 2012. Self-Assembled Magnetic Bead Biosensor for Measuring Bacterial Growth and Antimicrobial Susceptibility Testing. Small 8: 2477-82.
50. Koydemir HC, Kulah H, Ozgen C, Alp A, et al. 2011. MEMS biosensors for detection of methicillin resistant Staphylococcus aureus. Biosensors and Bioelectronics 29: 1-12.
51. Nakamura N, Shigematsu A, Matsunaga T. 1991. Electrochemical detection of viable bacteria in urine and antibiotic selection. Biosensors and Bioelectronics 6: 575-80.
52. Tsou P-H, Sreenivasappa H, Hong S, Yasuike M, et al. 2010. Rapid antibiotic efficacy screening with aluminum oxide nanoporous membrane filter-chip and optical detection system. Biosensors and Bioelectronics 26: 289-94.
53. Kinnunen P, Sinn I, McNaughton BH, Newton DW, et al. 2011. Monitoring the growth and drug susceptibility of individual bacteria using asynchronous magnetic bead rotation sensors. Biosensors and Bioelectronics 26: 2751-5.
54. Sia SK, Whitesides GM. 2003. Microfluidic devices fabricated in poly(dimethylsiloxane) for biological studies. Electrophoresis 24: 3563-76.
55. Boedicker JQ, Li L, Kline TR, Ismagilov RF. 2008. Detecting bacteria and determining their susceptibility to antibiotics by stochastic confinement in nanoliter droplets using plug-based microfluidics. Lab on a Chip 8: 1265-72.
56. Chen CH, Lu Y, Sin MLY, Mach KE, et al. 2010. Antimicrobial susceptibility testing using high surface-to-volume ratio microchannels. Analytical Chemistry 82: 1012-9.
57. Churski K, Kaminski TS, Jakiela S, Kamysz W, et al. 2012. Rapid screening of antibiotic toxicity in an automated microdroplet system. Lab on a Chip 12: 1629-37.
58. Cira NJ, Ho JY, Dueck ME, Weibel DB. 2012. A self-loading microfluidic device for determining the minimum inhibitory concentration of antibiotics. Lab on a Chip 12: 1052-9.

59. Sun P, Liu Y, Sha J, Zhang Z, et al. 2011. High-throughput microfluidic system for long-term bacterial colony monitoring and antibiotic testing in zero-flow environments. Biosensors and Bioelectronics 26: 1993-9.
60. Ho JY, Cira NJ, Crooks JA, Baeza J, et al. 2012. Rapid identification of eskape bacterial strains using an autonomous microfluidic device. PLoS ONE 7: e41245.
61. Kalashnikov M, Lee JC, Campbell J, Sharon A, et al. 2012. A microfluidic platform for rapid, stress-induced antibiotic susceptibility testing of Staphylococcus aureus. Lab on a Chip 12: 4523-32.
62. Choi J, Jung Y-G, Kim J, Kim S, et al. 2013. Rapid antibiotic susceptibility testing by tracking single cell growth in a microfluidic agarose channel system. Lab on a Chip 13: 280-7.
63. Theberge AB, Courtois F, Schaerli Y, Fischlechner M, et al. 2010. Microdroplets in microfluidics: An evolving platform for discoveries in chemistry and biology. Angewandte Chemie - International Edition 49: 5846-68.

Chapter 2

Normally closed valves [1]

2.1 Introduction

Miniaturization of various microfluidic components and their integration into dense networks is crucial to enable massively parallel operations on a single device. Fine control is required for a variety of applications where small volumes of fluids (picoliters to nanoliters) are manipulated and mixed [1-4]. Microvalves that route flow are probably one of the most important components in these microfluidic devices. Although significant progress has been made in improving the performance of valves with respect to their response time, leakage, dead volume, power consumption, sensitivity to particulate contamination, and chemical compatibility, further improvements are needed [5, 6].

A new type of valve that incorporates most or all the above ideal characteristics is highly desired. For instance, elastomeric pneumatic microvalves [7] have been successfully used in many applications that require multi-step and high throughput operations on a single device [1, 4]. A significant advantage of these pneumatic microvalves is that the fabrication of the valves is compatible with standard soft lithographic techniques, allowing easy integration of these valves into complex microfluidic devices.

Pneumatic microvalves can be broadly classified into two types: normally open (NO) and normally closed (NC) [2], similar to fail-close and fail-open valve architecture at larger scale

[1] Part of the work has been published: Ritika Mohan, Benjamin R. Schudel, Amit V. Desai, Joshua D. Yearsley, Christopher A. Apblett, and Paul J.A. Kenis, "Design Considerations for Elastomeric Normally Closed Valves", *Sensors and Actuators* B, 160, 2011, 1216-1223.

systems [8]. Although NO valves are widely used in many microfluidic applications [9, 10], devices employing these NO valves have limited portability in applications that require continuous closed state for operation, as these valves need bulky ancillaries (pumps, nitrogen gas cylinders, pneumatic peripherals) for actuation. For example, in my investigations of on-chip protein-antibody interactions [11] or virus detection [12], the valves need to be open only for a short period of time when the solutions are being mixed. Use of NO valves in these applications would have hampered portability between the mixing station and detection ancillaries such as a microscope [11, 12]. NC valves not only address the above limitation of restricted portability, but also retain the ease of fabrication and integration into microfluidic devices. Moreover, NO microvalves typically require actuation pressures of 6 to 30 psi [13, 14], whereas NC valves can be actuated with lower pressures, in the range of 1 to 12 psi, as demonstrated here and by Grover *et al.* [15].

NC valves made out of silicon and glass have been used in several applications, such as portable fuel cell systems using piezoelectric valves [16] and bidirectional gas regulators for micro-gas chromatography systems [17]. The focus of this chapter will be on NC valves made out of elastomeric materials, such as polydimethylsiloxane (PDMS), a commonly used material in microfluidics. Valves made out of elastomeric materials are typically easier to fabricate and actuate at lower pressures. Elastomeric NC valves have been used previously in different microfluidic applications, including cell sorting [18], on-chip electrophoresis [1], combinatorial protein-antibody interaction screening [8], virus detection [12] and on-chip chemical synthesis [19, 20]. Some of these NC valves have been characterized for pumping of fluids for a range of flow rates (0-400 nL/s) and operating pressures (0-30 kPa) [21]. None of these studies, however,

have specifically focused on design rules to optimize the performance of NC valves, in particular with respect to minimizing their actuation pressures and optimizing their reliability.

Formulation of a set of design rules for these microvalves is important because the actuation of these microvalves involves complex interplay between (i) mechanical deformation of the membrane and (ii) adhesion forces between hard and soft materials, which cannot be quantified easily due to the hysteresis that appears when polymeric substrates contact a stiffer surface. In addition, design rules are needed for devices with dense networks of channels because pressure losses across the device may cause failure of the valves that are furthest away from the actuation pressure source. Hence, design rules are needed that will aid in minimizing actuation pressures for these cases. Furthermore, the design rules will enable fabrication of valves with dimensions that can be easily achieved with standard soft lithography.

2.2 Experimental

2.2.1 Soft lithography

I fabricated microfluidic devices with NC valves using standard procedures for PDMS-based multi-layer soft lithography [7]. The fabricated two-layer devices consisted of (a) a control layer composed of microchannels that act as pneumatic lines for applying negative pressure and (b) a fluid layer composed of microchannels. RTV 615 poly(dimethylsiloxane) (PDMS) was obtained from General Electric Company (Waterford, NY). Negative photoresists, SU-8 250 and SU-8 25, were obtained from MicroChem Corporation (Newton, MA). (Tridecafluoro-1,1,2,2-tetrahydrooctyl) trichlorosilane was obtained from Gelest, Inc. (Morrisville, PA). The thickness of the photoresist and PDMS layers were measured using Dektak 3030. Negative patterns of the features of the fluid layer and the control layer were patterned on silicon using 20-25 μm thick negative photoresist. Then, a silane monolayer was evaporated onto the silicon masters to

prevent the covalent adhesion of PDMS to the silicon substrates. Next, a thin layer of 15:1 PDMS (weight ratio of polymer to cross-linker) was spun on the fluid layer master, 5:1 PDMS was poured on to the control layer master to a thickness of 2 mm, and the two layers were partially cured at 65 °C for approximately 30 minutes. The thickness of the valve membrane in the fluid layer was controlled by the spin speed ranging from 1000 to 2000 rpm, yielding 20-60 μm layer thicknesses. After partial curing, the control layer mold was removed from the master, holes were punched for the inlets and outlets of the control layer using a 20 gauge needle (B-D Precision Slide), and the control layer mold was aligned manually with the fluid layer under an optical microscope (Leica MZ6). The aligned layers were further cured at 65 °C for approximately 12 hours to yield the final assembled device. The device was then peeled off the fluid layer master, and holes were punched into the fluid layer using a 20 gauge needle. For experiments studying the reversibly sealed nature of the PDMS devices, the device was placed onto a clean glass substrate by simply bringing the PDMS assembled mold and the glass into contact. I chose a glass substrate, as glass is the most commonly used substrate in microfluidic devices when the channels are fabricated out of PDMS [22, 23]. Since the objective of the research presented here was to study the influence of valve geometry on actuation pressures, I did not modify the material properties of PDMS.

2.2.2 Selective irreversible bonding of PDMS device to glass

In some of the experiments, the PDMS device was irreversibly bonded to glass. In this case, the surface of the assembled device that had the microfluidic features and the glass substrate were treated with atmospheric plasma consisting of oxygen and helium (1:75 volumetric ratio) using a plasma pen (Surfx technologies, Atomflo^{TM} plasma) at 80 W for 2 to 4 seconds. After the plasma treatment, all NC valves were actuated so that the valve stops do not touch the glass

substrate during bonding, and the PDMS device and the glass were brought into contact. The valves were left actuated for approximately 6-8 hours, after which the PDMS device was irreversibly bonded to glass only in the channel areas.

2.2.3 Actuation of NC valves in microfluidic devices

Negative pressure was applied to the NC valves using a pump (Gast DOA-P704-AA Vacuum Pump 1/8 HP 115 VAC), and the actuation pressures of the microvalves were measured using a pressure controller (Cole Parmer, model 68027-78); the schematic illustration of the set-up is shown in **Fig. 2.1**. The valve actuation was performed under an optical microscope (Leica M205) to confirm opening of the valve. Note that the valve is open and will allow fluid flow, when the valve stop is lifted off from the substrate. However, this partial opening of the valve cannot be ascertained by visualizing the device from the top (**Fig. 2.2c**). Hence, I define the open state of the valve based on formation of contact lines. Two sets of contact lines appear upon actuation, one due to gradual delamination of the valve stop and side walls of the fluid channel, and one due to adhesion of the valve membrane to the roof of the control channel. Specifically, the valve is defined as 'completely' open when at least one of the two contact lines (typically circular or oval in shape) links the two opposite edges of the valve stop (**Fig. 2.2c**). I thus define 'actuation pressure' as the pressure required to completely open the valve, based on the definition of 'completely' open valve. After testing 8 different devices, I observed that the actuation pressures for all the valves were in the range of 1 – 6 psi. The standard deviation for actuation pressures for valves with identical geometries (same dimensions) on different devices was ±0.15 psi, which I represent as 0.3 psi error bars. This implies that the device-to-device variability resulted in a 0.3 psi variation in actuation pressures. Each valve on the same device was tested in triplicate, and I observed that the actuation pressures for that same valve were

within 0.01 psi. Note that all the valves were tested without any flow in the fluid channels, and the actuation pressures refer to static values.

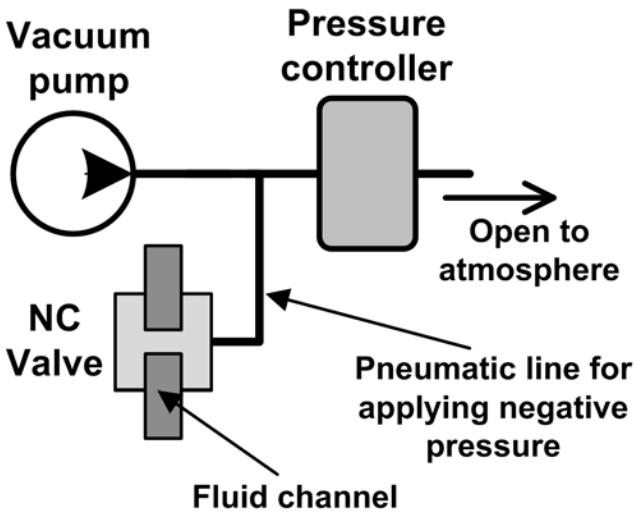

Figure 2.1. Schematic illustration of the setup for actuating NC valves. For clarity, only one valve is shown.

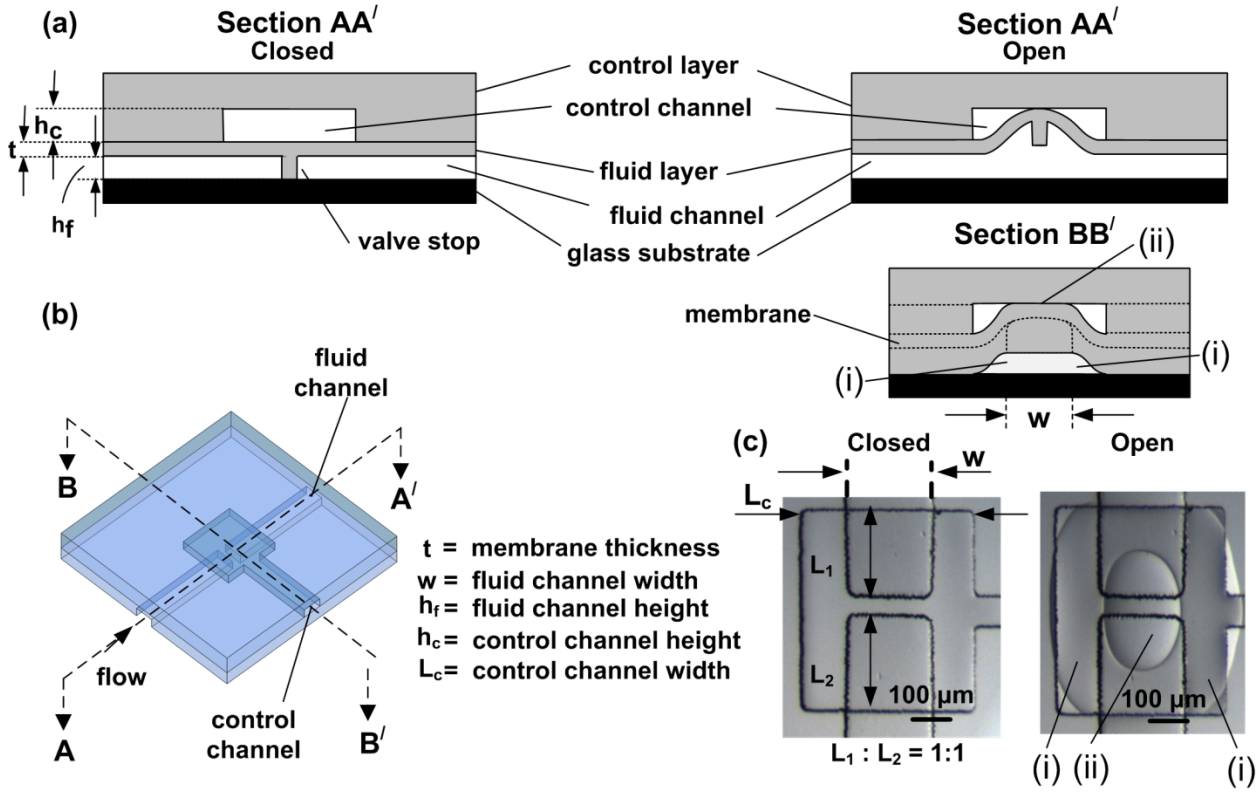

Figure 2.2. (a) Cross-sectional and (b) perspective schematic views of a normally closed straight microvalve in closed and open state. (c) Optical micrographs (top view) of a valve in the

closed and open state. (i) indicates the region of the fluid channel that is lifted off the glass substrate, while (ii) indicates the region of the valve that touches the roof of the control channel.

2.3 Results and Discussion

2.3.1 Design of the valve

To actuate (*i.e.*, open) a NC valve, the membrane that is connected with the valve stop needs to get deflected upwards under the influence of an applied pressure that is lower than ambient (**Fig. 2.2**). The key factors that determine the actuation pressure are (a) the mechanical properties of the membrane, and (b) the adhesion forces between the valve stop and the surface it rests against. In turn, these factors depend on a variety of parameters, including the thickness of the membrane, the bulk and surface properties of materials used, and the dimensions of the control and fluid channels.

Fig. 2.2(a) shows cross-sectional views of a NC valve in the closed and open state. The microvalve consists of a control layer with a channel height (h_c) of 25 – 50 μm and a fluid layer with a channel height (h_f) of 25 – 50 μm. The main operational part of the valve consists of a membrane with a thickness (t) of 15 – 60 μm, and a valve stop with a width of 50 μm to block the flow. **Fig. 2.2(b)** shows a perspective view of the NC valve.

Fig. 2.2(c) shows optical micrographs of a NC valve in the closed and open state. In this figure, the circular or oval-shaped contact area (i) indicates the region of the fluid channel that is lifted off the glass substrate, while (ii) indicates the region of the valve membrane that touches the roof of the control channel. To study the effect of asymmetry on valve performance, I varied two parameters: (1) the shape of the valve stop: straight, diagonal, or v-shaped, and (2) the position of the valve stop within the control chamber, as quantified by the ratio L_1:L_2 ranging from 1:1 to 1:5 (**Fig. 2.2(c)**). The rationale behind introducing asymmetry is the creation of a weak point along the contact line of the adhering substrates, so these surfaces can detach from

each other more easily upon application of a smaller pressure difference. The width of the fluid channel (*w*) was also varied from 50 to 350 μm, which is expected to influence the adhesive contact area between the valve stop and the glass substrate, and consequently the actuation pressures. In addition to these operational, often advantageous characteristics, this valve design can be easily fabricated using standard multi-layer soft lithography [24].

2.3.2 Optimization of valve parameters

Membrane thickness

Membrane thickness influences membrane stiffness, which in turn influences membrane deformation and consequently the actuation pressures. I studied thickness dependence for straight valves only, and the fluid channel width was maintained constant at 175 μm. I observed that the actuation pressures change only marginally (2.4 – 2.6 psi) for valves with different membrane thicknesses, ranging from 16 to 60 μm. Apparently, other parameters also determine the actuation pressure, in particular adhesion forces (see below). I also observed that the actuation pressures decrease with decrease of the membrane thickness without any glass substrate (**Fig. 2.3**). This trend is expected because it is known that the pressure required to deflect membranes increases with increased thickness [25]. Based on the above observations, I conclude that the actuation pressure is primarily governed by the adhesion between the contacting surfaces and not by the membrane stiffness. Since the actuation pressures are not significantly influenced by membrane thicknesses (for the range of values tested here), thicker membranes are preferable, since thinner membranes are susceptible to collapse during fabrication [26] and are usually unreliable during operation (inconsistent actuation pressures). Hence, for all the experiments, I used a membrane thickness of an intermediate value,

approximately 36 μm, which yielded reliable valve operation, *i.e.*, variations in actuation pressures for the same valve were within 0.01 psi for different trials.

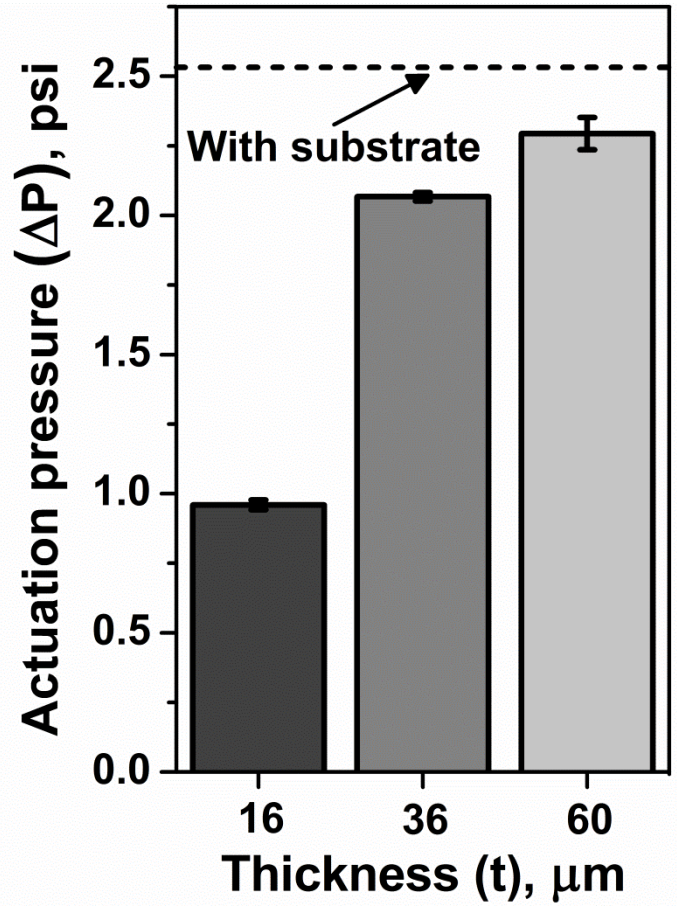

Figure 2.3. Effect of thickness of the membrane (t) on actuation pressures, when tested without any substrate. For comparison, I also include pressure values with a glass substrate. Thicknesses of 16, 36, and 60 μm were tested. Each data point represents the average from experiments on 8 identical valves. Each valve was tested three times.

Fluid channel width

Since adhesion forces were postulated to affect the actuation pressures, fluid channels widths were varied. For all three valve shapes, I observed that the actuation pressures decreased with increasing fluid channel width (**Fig. 2.4**). However, the actuation pressures measured for devices without any substrate do not show dependence on width. Hence, the width-dependence of the actuation pressures is primarily due to the adhesion between the valve and the glass substrate.

To explain this width-dependence, scaling laws were derived for the actuation pressure based on the peeling of soft rectangular strips from hard substrates (supplementary section[24]). For straight valves, the actuation pressure (ΔP) scales as

$$\Delta P \propto \frac{1}{L_0} + \frac{1}{w}, \qquad (1)$$

where w is width of the fluid channel, $2L_0 = L_1 + L_2$ (refer to **Fig. 2.2(c)** for definition of L_1 and L_2). Note that L_0 was maintained constant for all the experiments. The width-dependence of actuation pressures can also be explained by considering the area of valve contact with glass, which increases with decreasing width. In this case, it can be shown that the actuation pressure scales as (supplementary section [24])

$$\Delta P \propto 1 - \frac{w}{L_c}, \qquad (2)$$

where L_c is the width of the square chamber in the control layer (**Fig. 2.2(c)**). I speculate that Eq. (1) (based on peeling) captures the actuation phenomena more accurately compared to Eq. (2) (based on area of contact). In other words, peeling is the more dominant mode of actuation, and hence, I observe a non-linear decrease in actuation pressures with decreasing channel width. In case of v-shaped and diagonal valves, the corner feature determines the actuation pressure, and hence, Eq. (1) may not be applicable, since the equation is derived on the basis of peeling of a rectangular strip. However, the width-dependence of actuation pressures for these valves can still be explained using Eq. (2).

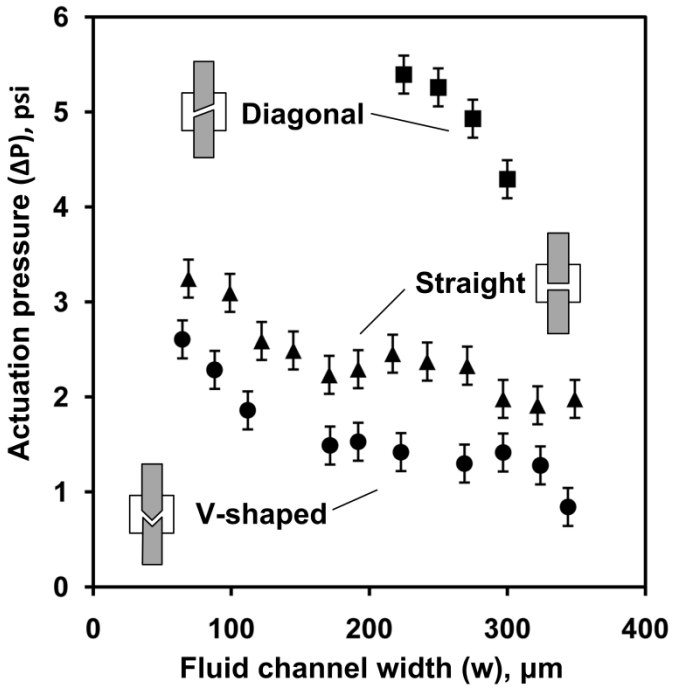

Figure 2.4. Actuation pressure for different microvalve shapes (straight, v-shaped, and diagonal) as a function of the width of the fluid channel. Each data point represents the average value from three experiments using the same valve. The errors represented in the plot originate from device-to-device variability, which were a maximum of 0.3 psi for identical valves on 8 different devices.

Shape of the valve stop

As discussed above, asymmetry may reduce actuation pressures because it introduces a weak point in the adhesion between the valve stop and the substrate. One of the ways I introduced asymmetry was by modifying the shape of the valve stop. **Fig. 2.4** shows the experimentally determined actuation pressures as a function of fluid channel width for three different shapes of the valve stop: straight, diagonal and v-shaped. I observed that the actuation pressures were lower for v-shaped valves compared to those for straight valves (**Fig. 2.4**). To explain this shape dependence, I describe the actuation of the valve as peeling of a soft adhesive strip (PDMS valve) off a hard substrate (glass). The peeling of the strip (*e.g.*, a scotch tape on a hard substrate) is typically easier from a corner as opposed to peeling from the edge, and hence, the actuation pressures are expected to be lower for v-shaped valves with a corner feature than for

straight valves. The lower actuation pressures required for v-shaped valves can be explained semi-quantitatively by considering the relation between the force required to peel (peeling force) and the width of the feature being peeled. Within a first order of approximation, the peeling force is proportional to the width [27, 28]. In case of a v-shaped valve, the corner feature results in a very small local width, on the order of the radius of curvature of the corner (~10 μm), while for a straight valve, the peeling width is the whole channel width (~100 μm). Due to the differences in peeling widths, the actuation pressures for v-shape valves are lower than those for straight ones.

Interestingly, I also observed that the actuation pressures for diagonal valves are higher than those for straight ones, in spite of the presence of a corner feature. This observation mainly results from the fact that for the diagonal valves the corner feature is located away from the central axis. The opening of the valve is initiated along the central axis (**Fig. 2.2(c)**), since the valve is least constrained to deflect upwards at the center of the fluid channel. This deflection profile for the valve can be understood in terms of deflection of a fixed-fixed beam [29] (cross-section BB′ in **Fig. 2.2(a)**). Since valve opening occurs along the central axis of the channel, actuation pressures will be lower only if the peeling forces are small at the center of the valve. In case of diagonal valves, the peeling forces are minimized at the valve edges, and not at the center, thus leading to higher actuation pressures. In contrast, the v-shaped valves have the corner feature along the central axis, and hence actuate at lower pressures. Based on the above discussion, I conclude that the peeling forces should be minimized in the region where the valve opening is initiated to result in lower actuation pressures. A more rigorous explanation for the shape-dependence of actuation pressure based on stress concentration and crack initiation can be found in the supplementary information published [24].

Placement of the valve stop

Another way I lowered symmetry in the valve geometry was by varying the position of the valve stop (**Fig. 2.2**) within the control line chamber, which I quantified using the ratio L_1:L_2 (**Fig. 2.2(c)**). In the case of straight valves, I observed that the actuation pressures were similar for L_1:L_2 ratios of 1:1 and 2:1, and decreased for 5:1 ratio (**Fig. 2.5**). I attribute this decrease in actuation pressure to the fact that in the latter case one of the membrane lengths is significantly larger than the other. A larger membrane length (L_1 here) will lead to lower stiffness of the corresponding membrane (upper membrane in **Fig. 2.2(c)**). As a result, the membrane deflects at a much lower applied pressure and the membrane touches the ceiling of the control channel. Then, upon the application of additional pressure the outer contact line rapidly propagates, since additional deformation of the membrane, and hence extension of the inner contact line is hindered by contact of the membrane with the ceiling. I speculate that this rapid propagation of the outer contact line linking the two opposite edges of the valve stop leads to lower actuation pressures for straight valves with L_1:L_2 ratios of 5:1.

Interestingly, in case of v-shaped valves, I observed a reverse trend, where the actuation pressures increased when the L_1: L_2 ratio was varied as 1:1, 2:1 and 5:1 (**Fig. 2.5**). I speculate that as the L_1: L_2 ratio increases in v-shaped valves the axial distance of the shorter side (L_2) is much shorter than in the case of straight valves, due to the presence of the corner feature in v-shaped valves. As a result, the pressure required to deflect the membrane along the central axis increases significantly due to the shorter length. Hence, the increase in length of the larger side (L_1) is more than offset by the reduction in length of the shorter side. This effect is more pronounced in v-shaped valves compared to straight valves, since the opening of v-shaped valves is predominantly along the central axis due to the sharp corner feature. Consequently, I observed

an increase in actuation pressures with increasing asymmetry in v-shaped valves, due to drastic reduction in the membrane dimension along the central axis and the explanation is published in the supplementary section of the manuscript [24].

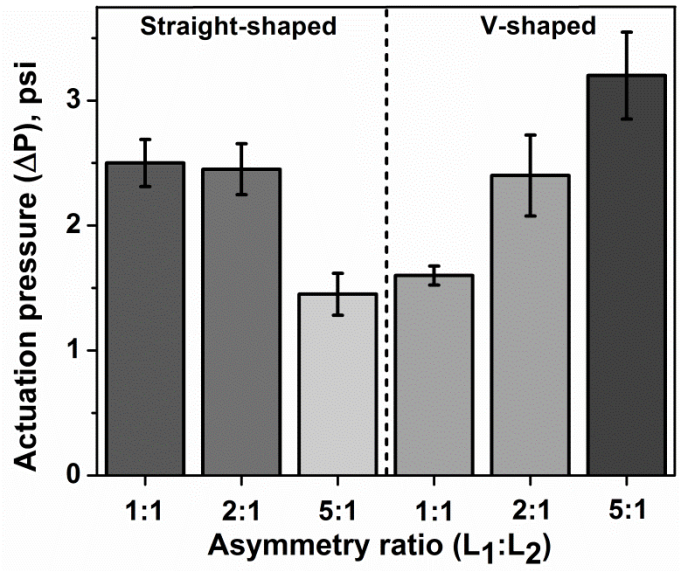

Figure 2.5. Effect of asymmetry on actuation pressures for straight and v-shaped valves. Asymmetry ratios tested were 1:1, 2:1, and 5:1.

Effect of channel height on hysteresis in valve actuation

Hysteresis becomes important during dynamic, repeated actuation of the valve, since the different pressures required to open and close the valve may lead to temporal delays in operation. Hence, minimizing hysteresis is important for precise control of microfluidic metering and flow control [7]. In NC valves, hysteresis primarily results from the valve membrane adhering to the roof of the control channel in the open state, which is illustrated by formation of a circular or oval shaped contact line in **Fig. 2.6**. The hysteresis of adhesion and detachment of the membrane from the roof, typical during adhesive contact between two elastic surfaces, causes hysteresis in the actuation pressures of these valves.

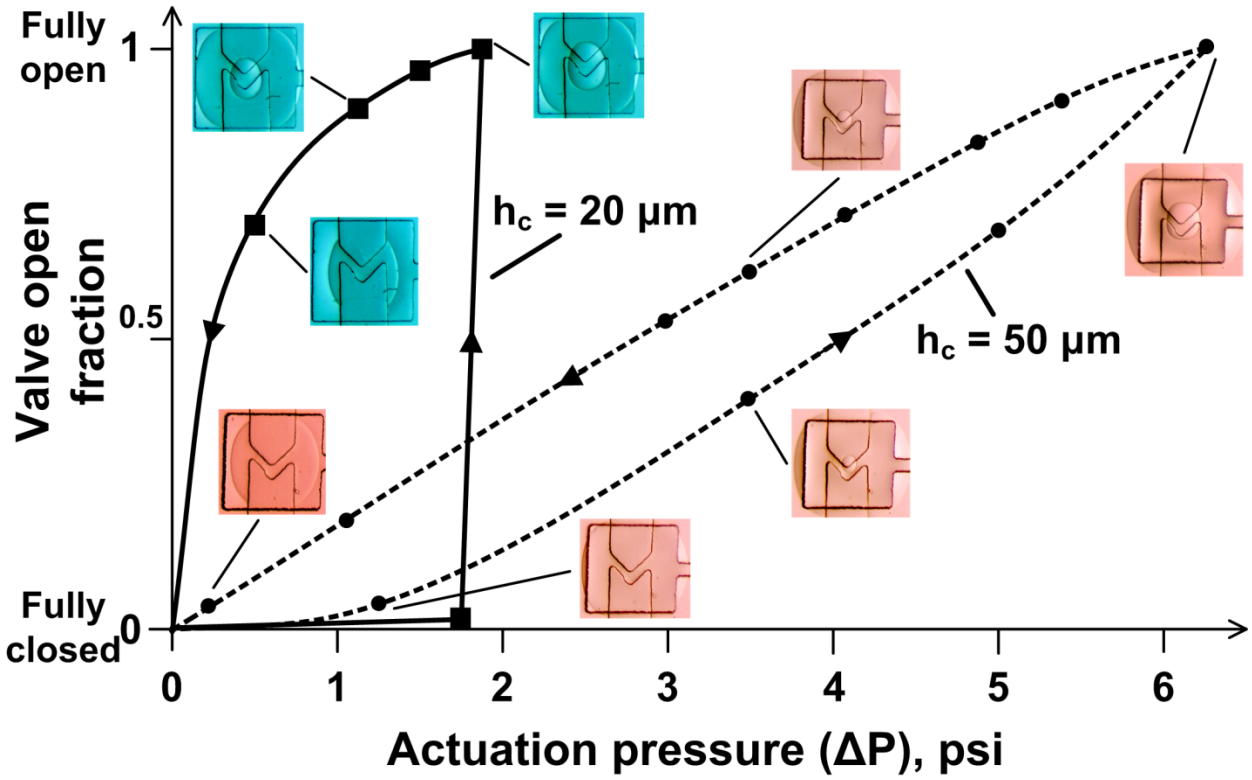

Figure 2.6. Semi-quantitative hysteresis plot of actuation pressures for NC valves. Two different heights for the control channel were tested, 20 and 50 μm. The fluid channel width in all the optical micrographs was 175 μm. The valve is considered open when the oval contact line touches the roof of the control channel and the shorter axis of the oval is approximately the size of the fluid channel width (see Fig. 1(c) for open valve). The colors of the optical micrographs have been artificially modified to differentiate the two types of valves. Lines connecting the data points are added to guide the eye.

In **Fig. 2.6**, I plot the degree by which the valve opens as a function of actuation pressures, where I define the valve as open when the oval contact line touches the roof of the control channel and the shorter axis of the oval is approximately the size of the fluid channel width; **Fig. 2.2(c)** shows an open valve. To estimate the fraction of valve opening, the length of the shorter axis of the oval contact line is compared to that of an open valve. The actuation pressures were higher for the taller control channels, since the valve had to deflect a larger distance upward to touch the roof of the control channel. However, I observed lower hysteresis for the taller control channel, *i.e.* the ratio of the area enclosed within the curve to the actuation pressure is lower for the taller control channel. I attribute the lower hysteresis to the fact that a taller control channel

allows for more relief of the membrane deformation when the pressure is decreased, since the membrane is stretched more in a taller control channel. This additional relief results in easier detachment of the valve membrane from the roof, which leads to lower influence of the adhesion forces between the membrane and the roof when pressure is decreased. Note that the higher actuation pressure for the device with a taller control channel is mainly due to my definition of an open valve. In reality, devices with taller control channels are preferable since the valve can deflect over larger distances, and hence allow more fluid to pass through the channel in the open state.

2.3.3 Operational considerations

Valve performance in a dense network

In microfluidic devices with dense networks, the actuation pressures increase across a network of serially connected valves, due to leakage or pressure losses associated with increasing channel length. As a model for dense microfluidic network, I tested the performance of NC valves by actuating 44 identical valves in series and compared the valve performance to those in a device with only 3 valves in series. Additionally, to demonstrate the advantage of valves operating at lower actuation pressures in dense networks, I compared valve performance in devices with v-shaped (lower actuation pressures) and straight valves. The fluid channel width was 175 μm and the L_1:L_2 ratio was 1:1. In devices with straight valves, 9 out of the 44 valves did not actuate (maximum pressure applied was 12 psi), however, in devices with v-shaped valves, all of the 44 valves actuated in the range of 2 to 5 psi. As expected, all the 3 valves in the simpler microfluidic device actuated for both valve shapes. The above experiments demonstrate that optimization of valve geometry to reduce actuation pressures and to ensure reliable actuation is crucial for the design of integrated microfluidic networks that contain NC valves.

Valve actuation over elongated periods for reversibly and irreversibly bonded devices

Leakage due to weak device-to-substrate bonding presents additional challenges in microfluidics, especially during fluid manipulation. In case of NC valves, the leakage issue becomes even more important due to the requirement of selective bonding, where strong bonding is needed for the channels, while the valves remain non-bonded. Although, Yang *et al.* [20] and Irimia *et al.* [18] were able to achieve selective irreversible bonding, their technique required additional fabrication steps, such as patterning of a metallic or polymeric layer at the valve stop. Here, I developed a simpler alternative to selectively bond microfluidic devices with NC valves. Oxygen plasma treatment of glass and PDMS as an irreversible bonding technique has been characterized in previous work before bonding is known to lead to strong irreversible bonding [30]. I utilized this technique to irreversibly bond the PDMS device to glass substrate. To prevent the valves from permanently sealing to glass, I exposed the PDMS and glass surfaces to oxygen plasma and then actuated the valves before bringing the PDMS and glass substrate into contact, so that the valves do not contact the glass. I left the valves actuated for 6 – 8 hours, which was sufficiently long for the PDMS surface to lose its hydrophobicity and consequently, the tendency to irreversibly bond to glass [31]. As a result, the device is irreversibly bonded to the glass substrate, except in the areas where the valve stop contacts the glass.

Since the adhesion forces between glass and PDMS are known to increase with time [32] and hence expected to influence the valve operation, I measured the actuation pressures of reversibly and irreversibly bonded devices with glass substrate over a period of 4 weeks. For these experiments, I used v-shaped valves, L_1:L_2 ratio of 1:1, and a channel width of 175 μm. In case of reversibly bonded devices, I observed that the actuation pressures increased with time (4 weeks), if the PDMS device and the glass substrate are maintained in contact, while in case of

irreversibly bonded devices, the actuation pressures remained nearly constant over time; a qualitative plot indicating the effect of device-substrate contact time on actuation pressure is shown in **Fig. 2.7**. The increase in actuation pressures for reversibly bonded devices can be attributed to time-dependent plastic deformation (creep) of PDMS over micro and nanoscopic features on the glass substrate. This creep-assisted deformation was observed in one study, where PDMS was shown to plastically deform and encapsulates nanoparticles gradually over time [33]. This encapsulation over time will lead to an increase in contact area of the PDMS valve with the glass substrate and hence stronger adhesion, thus resulting in increasing actuation pressures with time. In case of irreversibly bonded devices, however, the actuation pressures remained almost constant over time (**Fig. 2.7**). This behavior is due to the fact that the plasma treatment used for irreversible bonding hardens the PDMS surface by formation of a thin oxide layer (~100 nm, small compared to the thickness of the valve membrane) [31], which retards the ability of PDMS to plastically deform.

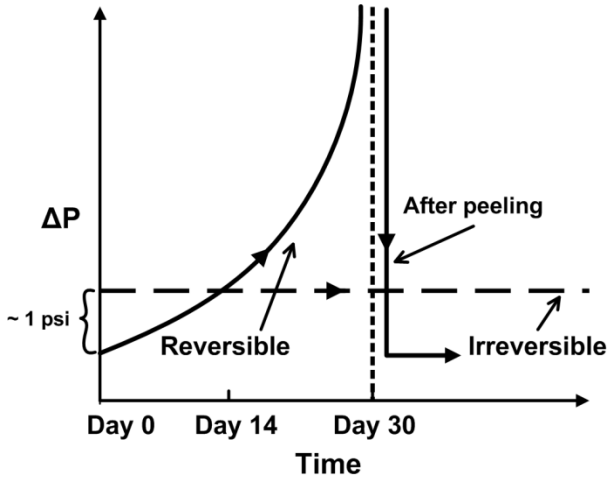

Figure 2.7. Qualitative plot showing the effect of device-substrate contact time on actuation pressures for reversibly and irreversibly bonded devices. The dashed vertical line indicates that reversibly bonded device could not be actuated.

I also observed that the actuation pressures at the beginning for irreversibly bonded devices are approximately 1 psi higher compared to those for reversibly bonded device (**Fig. 2.7**). The

plasma exposure during irreversible bonding decreases the surface roughness of both the PDMS and the glass, which in turn increases the contact area. The increased contact area leads to stronger adhesion, and consequently, higher actuation pressures. However, in the case of reversibly bonded devices, after the PDMS device was peeled off and brought into contact again with the glass substrate, the actuation pressures returned to its original values. I speculate that the peeling of the PDMS breaks the adhesive bonds with the glass surface and new bonds are formed when the PDMS is brought into contact again.

2.4 Conclusions

Design rules for integrating normally closed microvalves in microfluidic devices

Based on the above experimental results and discussion, I formulate the following set of design rules to integrate NC valves into microfluidic devices:

1. *Valve shape*: V-shaped valves are better than straight valves or diagonal valves in terms of actuation pressures and reliability, because they not only actuate at lower pressures than straight for the same fluid channel width, but v-shaped valves also actuate more consistently and their actuation pressure vary less from device to device.
2. *Fluid channel width*: Actuation pressures do not significantly change (only 2 – 3 psi) for a wide range of fluid channel widths (**Fig. 2.4**), 50 - 400 μm. Hence, the NC valves reported in this chapter can be used in microfluidic devices with different channel widths.
3. *Membrane thickness*: For membrane thicknesses in the range of 15 – 60 μm, the actuation pressures did not vary significantly (only 1 – 3 psi). However, thicker membranes are preferable, since valves with thicker membranes actuate more reliably, and valves with thinner membranes are more challenging to fabricate.

4. *Position of valve stop*: For straight valves, inducing asymmetry by changing the position of the valve stop reduces actuation pressures, but fabrication limitations might constrain the extent of asymmetry. For instance, in the devices, I could not lower the symmetry in the position of the valve stop beyond a L_1:L_2 ratio of 5:1. For v-shaped valves, moving the valve stop does not have a beneficial effect.
5. *Hysteresis in valve actuation*: For taller control channels (50 μm), the hysteresis of valve actuation was lower compared to that for shallower channels (25 μm), and hence, taller control channels are preferable, especially for dynamic actuation. Moreover, taller channels allow for more fluid displacement.
6. *Bonding*: Selective irreversible bonding will minimize liquid leakage in devices. However, in applications where the PDMS device needs to be peeled off (*e.g.*, when cleaning of the channels is not possible in an assembled device) or the glass substrate cannot be exposed to plasma treatment (*e.g.*, glass surface has been functionalized with oxygen-sensitive chemical groups), then reversible bonding is preferable.

All the experiments were performed with a glass substrate. Since PDMS also adheres well to other materials typically used for microfluidic devices (*e.g.*, PMMA, COC, PC, and PDMS itself), the design rules derived here will also apply to those cases.

The above analyses and the derived design rules were based on the assumption that adhesion forces between the device and substrate are much larger than the forces required to deflect the membrane. The above assumption is valid for most microfluidic applications because (1) the adhesion forces between device and substrate are high enough to prevent leakage, and (2) the valves are made of soft materials (lower Young's modulus), such as PDMS, to ensure low actuation pressures, and hence the membrane deflection forces will be low. One could encounter

a situation in which the forces needed to deflect the membrane become important, for example when adhesion forces have been reduced due to fouling. As a result, the design rules involving factors that contribute significantly to valve stiffness will change. Specifically, the actuation pressures will increase with decreasing fluid channel width and increasing membrane thickness. However, the actuation pressures will not be significantly influenced by the shape of the valve stop and the asymmetry in the position of the valve stop. To investigate how the design rules change when membrane deflection forces dominate, I studied valve actuation in the absence of the bottom glass substrate (thus eliminating the influence of adhesion) using finite element analysis. The results of these studies and an explanation of how the lack of adhesion forces affects the design rules is provided in Section 7 of the supplementary information of the published manuscript [24].

2.5 References

1. Blazej, R.G., P. Kumaresan, and R.A. Mathies, Microfabricated bioprocessor for integrated nanoliter-scale Sanger DNA sequencing. Proceedings of the National Academy of Sciences of the United States of America, 2006. 103(19): p. 7240-7245.
2. Lee, C.-C., et al., Multistep Synthesis of a Radiolabeled Imaging Probe Using Integrated Microfluidics. Science, 2005. 310(5755): p. 1793-1796.
3. Pal, R., et al., An integrated microfluidic device for influenza and other genetic analyses. Lab on a Chip, 2005. 5(10): p. 1024-1032.
4. Rohde, C.B., et al., Microfluidic system for on-chip high-throughput whole-animal sorting and screening at subcellular resolution. Proceedings of the National Academy of Sciences of the United States of America, 2007. 104(35): p. 13891-13895.
5. Kovacs, G.T.A., Micromachined Transducers Sourcebook. 1998, New York: McGraw-Hill.
6. Oh, K., W. and C.H. Ahn, A review of microvalves. Journal of Micromechanics and Microengineering, 2006. 16(5): p. R13.
7. Unger, M.A., et al., Monolithic Microfabricated Valves and Pumps by Multilayer Soft Lithography. Science, 2000. 288(5463): p. 113-116.
8. Skousen, P.L., Valve Handbook. 1997, New York: McGraw-Hill Professional Publishing.
9. Go, J.S. and S. Shoji, A disposable, dead volume-free and leak-free in-plane PDMS microvalve. Sensors and Actuators A: Physical, 2004. 114(2-3): p. 438-444.
10. Lee, S., W. Jeong, and D.J. Beebe, Microfluidic valve with cored glass microneedle for microinjection. Lab on a Chip, 2003. 3(3): p. 164-167.
11. Schudel, B.R., et al., Microfluidic chip for combinatorial mixing and screening of assays. Lab on a Chip, 2009. 9(12): p. 1676-1680.
12. Schudel, B.R., et al., Multiplexed detection of nucleic acids in a combinatorial screening chip. Lab on a Chip, 2011. 11(11): p. 1916-1923.
13. Kartalov, E.P., et al., Experimentally validated quantitative linear model for the device physics of elastomeric microfluidic valves. Journal of Applied Physics, 2007. 101(6).
14. Studer, V., et al., Scaling properties of a low-actuation pressure microfluidic valve. Journal of Applied Physics, 2004. 95(1): p. 393-398.
15. Grover, W.H., et al., Development and multiplexed control of latching pneumatic valves using microfluidic logical structures. Lab on a Chip, 2006. 6(5): p. 623-631.
16. Zhao, H., et al., Structure and characterization of a planar normally closed bulk-micromachined piezoelectric valve for fuel cell applications. Sensors and Actuators A: Physical, 2005. 120(1): p. 134-141.
17. Bae, B., et al., A Bidirectional Electrostatic Microvalve With Microsecond Switching Performance. Microelectromechanical Systems, Journal of, 2007. 16(6): p. 1461-1471.
18. Irimia, D. and M. Toner, Cell handling using microstructured membranes. Lab on a Chip, 2006. 6(3): p. 345-352.
19. Hosokawa, K. and R. Maeda, A pneumatically-actuated three-way microvalve fabricated with polydimethylsiloxane using the membrane transfer technique. Journal of Micromechanics and Microengineering, 2000. 10(3): p. 415-420.
20. Yang, Y.-N., S.-K. Hsiung, and G.-B. Lee, A pneumatic micropump incorporated with a normally closed valve capable of generating a high pumping rate and a high back pressure. Microfluidics and Nanofluidics, 2009. 6(6): p. 823-833.

21. Grover, W.H., et al., Monolithic membrane valves and diaphragm pumps for practical large-scale integration into glass microfluidic devices. Sensors and Actuators B: Chemical, 2003. 89(3): p. 315-323.
22. Fiorini, G.S. and D.T. Chiu, Disposable microfluidic devices: fabrication, function, and application. BioTechniques, 2005. 38(3): p. 429–446.
23. Kuo, J.S. and D.T. Chiu, Disposable microfluidic substrates: Transitioning from the research laboratory into the clinic. Lab on a Chip, 2011. 11(16): p. 2656-2665.
24. Mohan, R., et al., Design considerations for elastomeric normally closed microfluidic valves. Sensors and Actuators, B: Chemical, 2011. 160(1): p. 1216-1223.
25. Timoshenko, S. and S. Woinowsky-Krieger, Theory of Plates and Shells. 2nd ed. Engineering Societies Monographs. 1959, New York: McGraw-Hill Book Company.
26. Mastrangelo, C.H. and C.H. Hsu, Mechanical stability and adhesion of microstructures under capillary forces - Part II: Experiments. Journal of Microelectromechanical Systems, 1993. 2(1): p. 44-55.
27. Gent, A.N. and G.R. Hamed, Peel Mechanics. The Journal of Adhesion, 1975. 7(2): p. 91 - 95.
28. Kendall, K., Thin-film peeling-the elastic term. Journal of Physics D: Applied Physics, 1975. 8(13): p. 1449.
29. Timoshenko, S., Strength of Materials. 3rd ed. ed. 1983: Krieger Publishing Company.
30. Xia, Y. and G.M. Whitesides, Soft Lithography. Angewandte Chemie International Edition, 1998. 37(5): p. 550-575.
31. Hillborg, H., et al., Crosslinked polydimethylsiloxane exposed to oxygen plasma studied by neutron reflectometry and other surface specific techniques. Polymer, 2000. 41(18): p. 6851-6863.
32. Willis, P.A., et al., Monolithic photolithographically patterned FluorocurTM PFPE membrane valves and pumps for in situ planetary exploration. Lab on a Chip, 2008. 8(7): p. 1024-1026.
33. Demejo, L.P., et al., Time Dependent Adhesion Induced Phenomena: The Flow of a Compliant Silicone-Polyester Copolymer Substrate Over Rigid Micrometer Size Gold and Polystyrene Particles. The Journal of Adhesion, 1995. 48(1): p. 47 - 56.

Chapter 3

Antibiotic susceptibility screening (proof-of-concept) [2]

3.1 Introduction

In recent years, antibiotic resistance traits among microbial pathogens have escalated at alarming rates, which has spurred the development of technologies for rapid and accurate detection of antibiotic susceptibility profiles of pathogens[1]. Established techniques for antibiotic susceptibility testing (AST), such as broth dilution and disc diffusion (**Fig. 3.1**), involve multiple time-consuming steps[2, 3] including: (1) isolation of pathogens from patient samples (24 - 48 hrs.), (2) pre-culturing of isolated bacteria to enrich cell density to detectable levels (24 - 48 hrs.), (3) incubation of cells with antibiotics in 96-well plates or petri dishes (24 - 48 hrs.), and (4) determination of bacterial growth using absorption spectroscopy or by visual assessment. Broth dilution and disc diffusion assays typically require significant quantities (10 - 30 mL) of patient samples such as blood, sputum, or urine for analysis [4]. In addition, the limited sensitivity of macroscale techniques for AST makes them unsuitable for detecting the presence of "persister" microbes. Although persister cells represent only a small fraction ($\approx 10^{-5}$) of microbial cells, they tend to evade antibiotic mediated killing by switching to a metabolically dormant or "persistent" state [5, 6]. Persister cells constitute a significant threat due to their ability to re-initiate infection upon discontinuation of antibiotic therapy [7]. Finally, inconsistencies in results obtained from different AST techniques further complicate diagnosis and treatment [8-13]. Hence, in the absence of precise information about the antibiogram of

[2] Part of the work has been published: Ritika Mohan*, Arnab Mukherjee*, Emre E. Sevgen, Chotitath Sanpitakseree, Jaebum Lee, Charles M. Schroeder, and Paul J.A. Kenis, "A multiplexed microfluidic platform for rapid antibiotic susceptibility testing", Biosensors & Bioelectronics, 49, 2013, 118-125.

particular pathogen, physicians often resort to empirical therapies that utilize broad-spectrum antibiotics. Indiscreet use of antibiotics in this manner is known to intensify the problem of antibiotic resistance [14, 15].

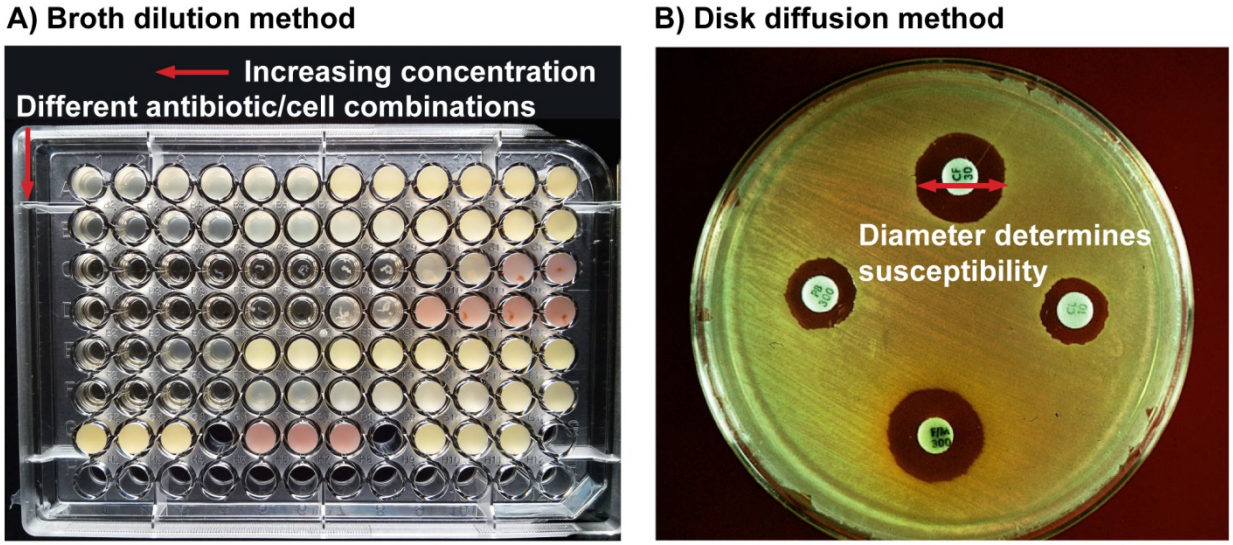

Figure 3.1. Conventional methods for antibiotic susceptibility testing (A) micro-broth dilution method and (B) Disk diffusion method, also known as the "gold standard" method

To address the aforementioned issues, platforms with improved sensitivity and fast analysis time have been developed for antimicrobial susceptibility testing [16-21]. For example, sensors have been utilized to determine susceptibility by measuring small changes in growth of cells [18]. Chiang et al., have developed a surface plasmon resonance-based biosensor platform to categorize strains as susceptible or resistant by detecting variations in optical properties of bacteria when treated with antibiotics [17]. Another interesting approach for antibiotic susceptibility testing utilizes an asynchronous magnetic bead rotation biosensor to monitor single cells or cell populations after treatment with antibiotics [22]. In addition, filter chip and optical detection biosensing system have been developed that can provide susceptibility results in one hour [21]. These microfluidic-based technologies are sensitive and rapid, however, most of these platforms lack multiplexing capabilities [17, 21, 22]. Hence, integrated microfluidics represents

an attractive technology for the multiplexed implementation of biological assays with rapid turnaround times and minimal sample consumption [23]. Several successful microfluidic platforms for AST have been reported [24-30] (**Fig. 3.2**). For example, droplet-based microfluidics has been utilized to compartmentalize bacterial cells, nutrients, antibiotics, and fluorescent viability indicators in water-in-oil emulsions [24, 26]. Sun et al. have reported on the development of a microfluidic platform for the confinement of bacterial cells in square microwells connected to a central flow channel that continuously delivers nutrients and antibiotics to cells [28]. Choi et al. have reported a microfluidic agarose channel system for rapid antibiotic susceptibility testing by tracking single cell growth [31]. Weibel and colleagues have developed a portable microfluidic chip for AST for point-of-care use [27]. The key advantage of the portable chip is the automatic loading of bacterial cells into microfluidic chambers that had been preloaded with dehydrated antibiotics using a 'degas driven flow'.

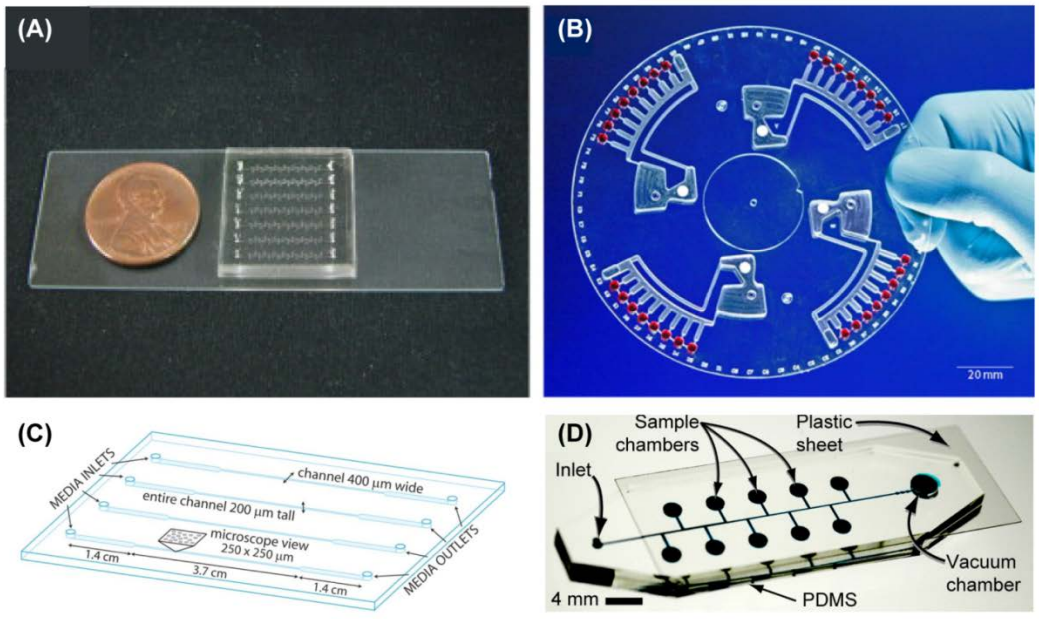

Figure 3.2. Antibiotic susceptibility testing methods. (A) Optical image of the device used for long-term bacterial colony monitoring and antibiotic testing in high throughput manner[28]. (B) Microfluidic biosensor for detection of MRSA[16] (C)Schematic of microfluidic channels geometry used in a device for determining antibiotic susceptibility testing for *S. aureus*[32]. (D) A self-loading device to determine minimum inhibitory concentrations of antibiotics[27].

The existing approaches for microfluidic-based antibiotic susceptibility testing offer promising routes toward the development of a rapid and portable screening tool. However, many of these methods suffer from one or more of the following limitations: (1) complicated platform fabrication and/or operation procedures [30], (2) poor portability due to the requirement for syringe pumps, pneumatic actuators, and other ancillary equipment [26, 30, 31], and (3) unstable droplet formation [33]. In this chapter, I report on the design and fabrication of a microfluidic platform with biosensing capabilities featuring a spatially addressable 4x6-array of wells to simultaneously monitor the effects of multiple antibiotics at different concentrations, as well as their combinations, on bacterial cells for AST. This technology integrates ease-of-fabrication and use with enhanced combinatorial capabilities, and further provides improved portability and usability by circumventing the requirement for expensive syringe pumps and pneumatic actuators by implementing normally closed valves. In addition, the platform is amenable to automated analysis by using time-lapse fluorescence microscopy (TLFM). I employed the microfluidic platform to interrogate the antibiotic sensitivity profile of *Escherichia coli* to four commonly used bactericidal and bacteriostatic antibiotics. Furthermore, I explored synergistic and antagonistic effects of different antibiotic cocktails, as well as the effects of *E. coli* cell densities on dictating the efficiency of antibiotic action. Overall, this platform capitalizes on several key advantages of biosensor based integrated microfluidics technology including miniaturization of assays, expedited analysis, multiplexing, and improved detection sensitivity along with ease-of-use and portability.

3.2 Experimental

3.2.1 Fabrication and experimental setup

The microfluidic chip for AST was fabricated using standard soft lithographic techniques [34] (**Fig. 3.3**). Briefly, molds for casting the fluidic and control layers were made by patterning negative photoresist on silicon wafers using photolithography. A thin layer of 20:1 PDMS (weight ratio of polymer to cross-linker) was spin coated on to the fluidic layer master and 5:1 PDMS was poured on to the control layer master. The two layers were partially cured at 65 °C for 30 minutes. Next, the control layer was carefully peeled off the silanized silicon master, and three holes for actuation of the mixing and sample loading valves were punched using a 20-gauge needle. The control layer was manually aligned with the fluidic layer under an optical microscope (Leica MZ6), and the aligned layers were cured overnight (~ 12 hrs.) at 65 °C to yield a monolithic device. Finally, the assembled device was peeled off the fluid layer master, inlet ports were punched using a 20-gauge needle, and the assembly was placed on a glass coverslip to create a reversible seal.

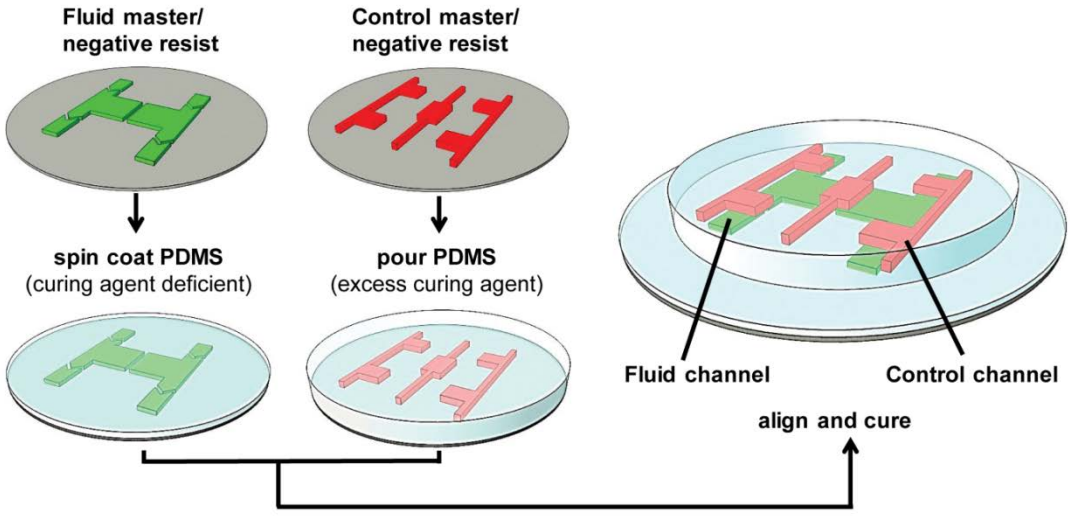

Figure 3.3. Fabrication of the chip using standard two layer soft lithography

3.2.2 Bacterial strains, growth media, and antibiotic solutions

Wild type *E. coli* MG1655 (ATCC 47076) was genetically engineered to constitutively express green fluorescent protein (GFP), thereby enabling detection and enumeration of cells using fluorescence microscopy. Specifically, *E. coli* MG1655 cells were transformed with a low copy plasmid expressing a bright GFP variant from a constitutive promoter derived from bacteriophage lambda [35]. Details of plasmid construction are provided as supporting information (**Table 3.1**). I verified that the recombinant GFP-expressing *E. coli* cells were phenotypically similar to wild type cells with respect to growth rates. *E. coli* cells were routinely cultivated in Lennox broth (10 g/L tryptone, 5 g/L yeast extract, and 5 g/L NaCl) supplemented with kanamycin at a concentration of 30 μg/mL in order to maintain the GFP-expressing plasmid. Kanamycin was omitted for on-chip cultures with no noticeable effect on cellular fluorescence. Antibiotic stock solutions of 10 mg/mL tetracycline hydrochloride and 10 mg/mL chloramphenicol were prepared in 70% ethanol. Stock solutions of 30 mg/mL kanamycin, 100 mg/mL ampicillin, and 1 mg/mL cefalexin hydrate were prepared in sterile deionized water. All stock solutions were filtered using a 0.45 μm syringe filter (Millex- HV filter unit, Millipore) prior to use. Antibiotic dilutions were made directly into Lennox broth.

Construction of GFP-Expressing Plasmid Construct

The GFP-expressing plasmid is based on a previously reported pUA139 promoter probe plasmid [36] that expresses GFP under the control of an upstream promoter. The plasmid was engineered to include a 3-frame stop codon and a strong synthetic ribosome binding site between the GFP gene and the upstream promoter.

Table 3.1. Oligonucleotide sequences employed to construct GFP-expressing plasmid

Seq. No.	Oligonucleotide	Sequence	Reference
1	phage λ-tetO promoter sense strand	TCCCTATCAGTGATAGA GATTGACATCCCTATCA GTGATAGAGATACTGA GCAC	[35]
2	phage λ-tetO promoter antisense strand	GTGCTCAGTATCTCTAT CACTGATAGGGATGTCA ATCTCTATCACTGATAG GGA	[35]
3	Synthetic ribosome binding site	ATTAAAGAGGAGAAA	BioBricks Parts Registry (MIT)
4	rrnB2 transcriptional terminator	AGAAGGCCATCCTGAC GGATGGCCTTTT	BioBricks Parts Registry (MIT)

The promoter was ligated in the plasmid construct using *BamHI* and *XhoI* restriction enzymes and T4 DNA ligase. In addition, a transcriptional terminator was included upstream of the promoter sequence to arrest divergent transcription from the promoter. Sequences for the promoter oligonucleotides, synthetic ribosome binding site, and transcriptional terminator are provided in **Table 3.1**. Cloning was accomplished using standard molecular biology techniques [37].

3.2.3 On-chip antibiotic susceptibility testing

Microfluidic chips were sterilized by autoclaving prior to each experiment. Nonspecific interactions between the chip surface and cells or antibiotics were minimized by passivating the walls of the fluid layer and the glass coverslip with sterile bovine serum albumin (BSA) at a concentration of 10 mg/mL for 15 minutes before each experiment. In a typical experiment (**Fig. 3.4**), the microfluidic chip-cover slip assembly is placed in contact with an aluminum-heating block heated to 35 °C using a temperature controller (Bionomic System BC-110). Antibiotic and

cell solutions (≈1 μL volume for each) are placed on their respective inlet ports and introduced into the wells by actuating the filling valves using a vacuum pump (3 psig; GastDOA-P704-AA VacuumPump 1/8 HP 115 VAC). Enhanced mixing of adjacent sets of antibiotic and cell solutions is initiated by actuating the mixing valves for 15 minutes. To minimize solvent loss due to evaporation during long-term experiments, reservoirs filled with bacterial growth medium (Lennox broth) or sterile water were placed around the device, and the assembly was sealed at the top by affixing a glass slide (**Fig. 3.4**). On-chip measurements were performed by TLFM using an inverted fluorescence microscope (Leica, DMI4000) equipped with a 1600 x 1200 pixel CCD camera (QImaging, Retiga-2000R), a 480/40 nm excitation filter, 527/30 nm emission filter, a motorized stage to raster the imaging field-of-view, and automated focus control implemented with a Z-motor (Ludl Electronic Products). Images were acquired every 10 minutes over a period of 10 hours using a 10x objective (Plan Achromat, NA = 0.25). The shallow fluid channels (15 μm) ensured that all cells were within the depth of focus throughout the experiment. During data acquisition, the exposure time was set to 200 ms and the fluorescent light source was shuttered between successive exposures to minimize photobleaching. Stage rastering, focus control, image acquisition, and capture were implemented using ImagePro Plus software (Media Cybernetics).

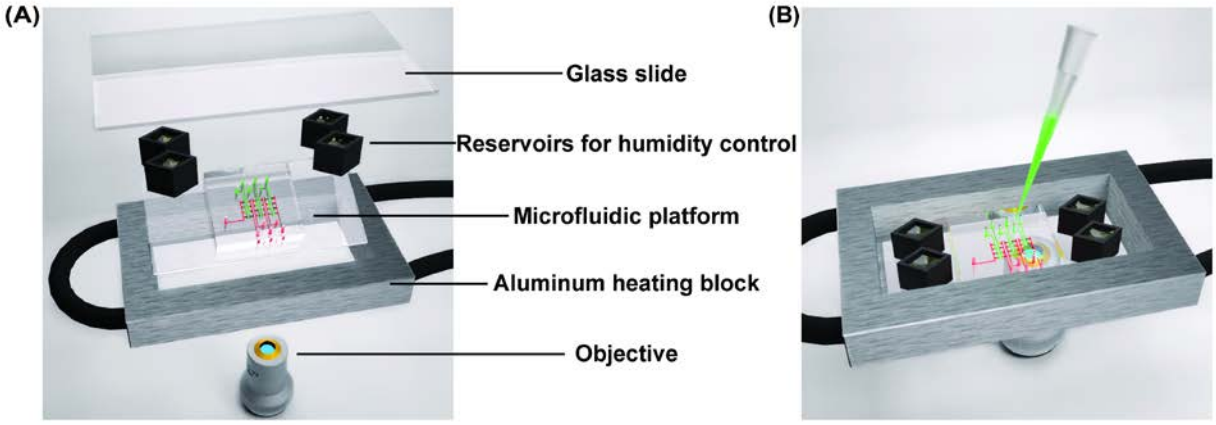

Figure 3.4. Experimental setup for on-chip AST: **(A)** The microfluidic device-coverslip assembly is placed in contact with an aluminum block whose temperature is maintained at 35 °C. Evaporation is minimized by positioning reservoirs filled with sterile growth medium at the four corners of the heating block and sealing the assembly with a glass slide at the top. **(B)** Cells and antibiotics are readily loaded using a micropipette followed by vacuum actuation of the normally closed valves.

3.2.4 Image processing and data analysis

Images were analyzed using ImageJ version 1.46a [38]. Specifically, 8-bit grayscale images were converted to binary images by manual thresholding to capture all cells within a range of fluorescence intensities, which is defined on the low end by a minimum signal-to-noise ratio and determined on the high end by the inability to visualize cells. The number of cells in each chamber was also estimated by counting the local fluorescence intensity maxima, and this algorithm provided consistent results within this range of manual thresholding. In order to highlight long-term trends in cell proliferation (or death), I implemented a moving average filter to smooth the time series data. I quantified antibiotic efficacy in terms of the fraction of the initial cell population that survives antibiotic treatment after 10 hours, which is estimated as:

$$FL_{ab,conc} = \frac{N_{10}}{N_0} \tag{3.1}$$

where $FL_{ab,conc}$ denotes the fraction of live cells at t = 10 hrs., subscripts *ab* and *conc* refer to the antibiotic and its concentration in units of μg/mL, N_o is the total number of cells in a microfluidic chamber at t = 0, and N_{10} is the total number of cells in the same chamber at t = 10 hrs. Synergy and antagonism between pairs of antibiotics are calculated using a criterion variable A:

$$A = \frac{FL_{ab1+ab2}}{min(FL_{ab1}, FL_{ab2,})} \tag{3.2}$$

where $FL_{ab1+ab2}$ denotes the fraction of live cells at t = 10 hours post-treatment with a pair of antibiotics (*ab1+ab2*), and FL_{ab1} and FL_{ab2} denote the fraction of live cells at t = 10 hours post-treatment with each antibiotic individually at the same concentration as in the combination (in a different experiment). Using this convention, an antibiotic combination is defined as being synergistic if $A < 1$ and antagonistic if $A > 1$.

For experiments in which three antibiotics are used, the quantity A is determined by:

$$A = \frac{FL_{ab1+ab2+ab3}}{min(FL_{ab1}, FL_{ab2}, FL_{ab3}, FL_{ab1+ab2}, FL_{ab2+ab3,} FL_{ab3+ab1})} \tag{3.3}$$

For experiments in which four antibiotics are used, the quantity A is determined by:

$$A = \frac{FL_{ab1+ab2+ab3+ab4}}{\min(FL_{singls,} FL_{pairs}, FL_{trpls})} \tag{3.4}$$

where $FL_{ab1+ab2+ab3}$ and $FL_{ab1+ab2+ab3+ab4}$ denotes the fraction of live cells at t = 10 hours after being treated with the antibiotic combination. FL_{sngls} represents these values for each single antibiotic comprising the combination, FL_{pairs} denotes these values for pairs of antibiotics included in the combination and FL_{trpls} stands for combinations of three antibiotics. Using this convention, an antibiotic combination is defined as being synergistic if $A < 1$ and antagonistic if $A > 1$.

3.2.5 Off-chip (macro-scale) antibiotic susceptibility testing

To benchmark our microfluidic platform against macroscale methods for antibiotic screening, we performed antibiotic susceptibility testing on *E. coli* using 96-well plates. *E. coli* cell cultures were prepared as described above and added to the wells of a 127.8 mm x 85.5 mm flat-bottom 96-well plate (Nunclon). Antibiotics were added to each well at the desired concentrations, and the plates were incubated at 35 ^{o}C with linear shaking (linear mode, 3.5 mm amplitude) in a-microplate reader (TECAN Infinite M200 PRO). Cell growth or death was monitored by recording optical density at a wavelength of 600 nm in each well every 15 minutes over a period of 15 hours. In bulk-level experiments, evaporation was minimized by using covered plates.

Estimation of Antibiotic Minimal Inhibitory Concentration

Minimal inhibitory concentration (MIC) is defined as the lowest concentration of an antibiotic that inhibits cell growth as determined by visual inspection. I estimated the MIC of each antibiotic against *E. coli* MG1655 using the broth dilution method as described in the manual of Clinical Laboratory Standards [39]. The results are listed in **Table 3.2**. Specifically, *E. coli* cell cultures were prepared as described above and added to the wells of a 96-well plate (Nunclon) and mixed with an equal volume of antibiotic at the desired concentration. Twelve serial dilutions were prepared for each antibiotic to span a concentration range from 0.1-500 μg/mL. Plates were incubated with shaking (linear mode, 3.5 mm amplitude) at 35 °C in a microplate reader (TECAN Infinite M200 PRO) and the optical density at 600 nm of each well was recorded every 15 minutes over a period of 15 hours. Evaporation was minimized through the use of covered plates. The MIC was defined as the lowest concentration of antibiotic that completely

inhibited cell growth as determined by absorbance readings as well as visual inspection. The antibiotic solutions were diluted using Lennox broth.

Table 3.2. Minimum Inhibitory Concentration (MIC) of antibiotics against *E. coli* MG1655

Seq. No.	Antibiotic	MIC (µg/mL)
1	Ampicillin	8
2	Cefalexin	12
3	Chloramphenicol	8
4	Tetracycline	2

3.3 Results and Discussion

3.3.1 Validation of the platform for biological studies

The microfluidic platform used in this study (**Fig. 3.5**) consists of a two-layer poly (dimethyl-siloxane) chip comprising: (1) a control layer for actuating the mixing and filling valves, and (2) a fluidic layer that houses the flow channels and a 4x6-array of wells. Each well consists of two half wells that house the cells and antibiotic solutions, respectively. Each half well is 400 µm wide, 15 µm tall and 500 µm long. In this way, the 4x6 array design facilitates the treatment of one microbial cell sample with six distinct antibiotic solutions, thereby enabling the execution of up to six unique screens per chip along with four replicates for each screen (**Fig. 3.5**). Antibiotic solutions and cell samples are readily loaded and mixed by actuating the respective filling and mixing valves using a vacuum pump. The incorporation of normally closed valves improves platform portability by obviating the need for continuous actuation using positive pressure [40-43]. To validate the feasibility of the microfluidic platform for biological studies, I determined the doubling times of *E. coli* cultured on-chip and in 96-well plates using two different kinds of media: nutrient-rich Lennox medium and minimal glucose-based M9 medium. I verified that the

on-chip growth profiles of *E. coli* cells were in close agreement with the growth profiles observed in the 96-well plate based experiments (**Fig. 3.6**). Specifically, the on-chip doubling times of *E. coli* were approximately 35 minutes and 70 minutes in Lennox broth and M9 medium, respectively. The corresponding doubling times in the same media when using 96-well plates were 30 minutes and 73 minutes, respectively. The general scheme of the sensing system is shown in **Fig. 3.7**.

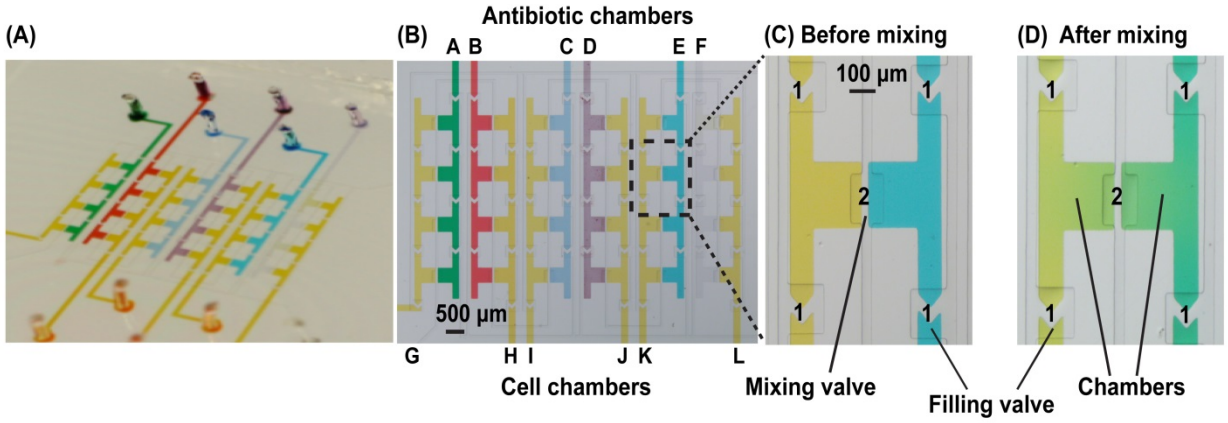

Figure 3.5. Optical micrographs of the microfluidic platform for on-chip AST: **(A)** The device features a 4x6 array of 3 nL volume wells, which are loaded with colored dyes for display purposes. **(B)** Antibiotics at various concentrations and/or different antibiotic combinations are loaded in each well through fluid lines A-F (represented by green, red, blue, magenta, indigo and colorless solutions). *E. coli* cells are loaded in the wells adjacent to the antibiotics through fluid lines G-L (represented by yellow solutions). **(C)** Normally-closed pneumatic valve set 1 is used to control the antibiotic and cell loading in the wells. **(D)** Actuation of mixing valve set 2 is used to mix the antibiotics and cells in adjacent chambers by enhanced diffusion, represented by a change in colors (blue/yellow to green) in the optical micrographs.

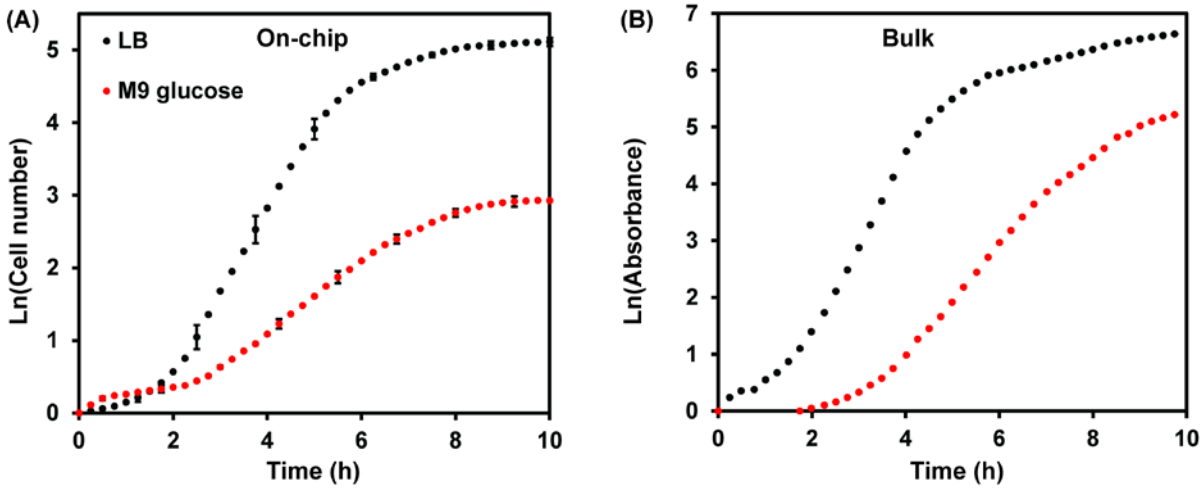

Figure 3.6. Comparison of growth profiles of *E. coli* cultured in Lennox broth and M9 medium using **(A)** the microfluidic chip and **(B)** in conventional 96-well plates. Growth on-chip is quantified by periodically counting cells in each well of the microfluidic device, which is then normalized to the initial cell number loaded in the well. Growth in 96-well plates is quantified by periodically measuring absorbance at 600 nm, which is normalized to the initial absorbance. All measurements are conducted at 35 °C. Each data point represents the mean of at least three experiments. Errors bars represent the standard error of the mean (SEM) and are shown for every fifth data point for visual clarity.

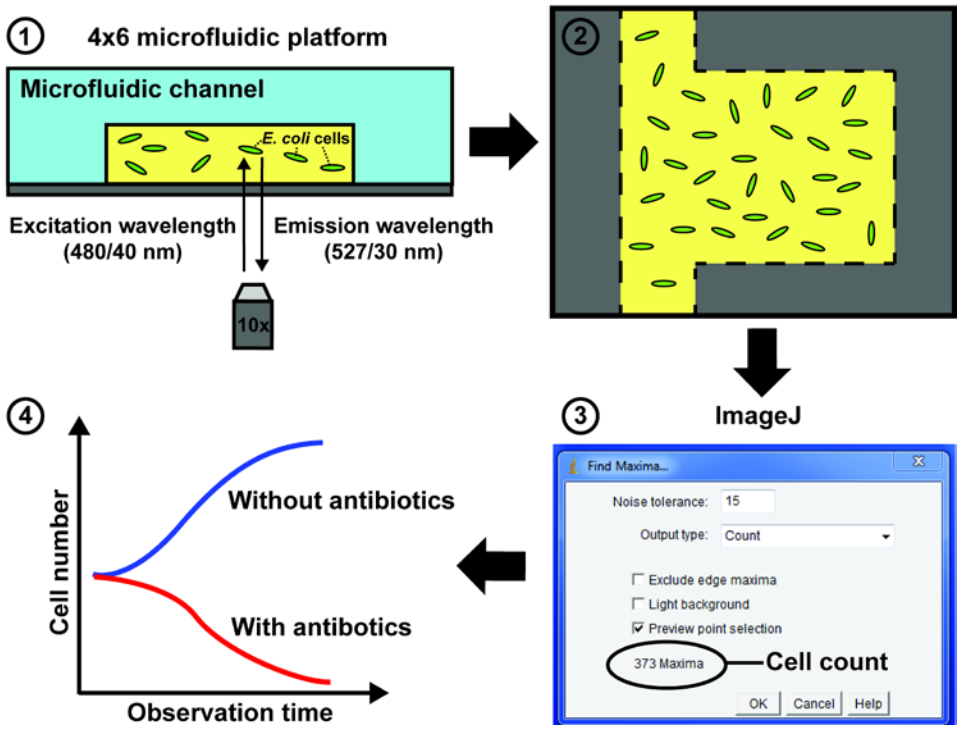

Figure 3.7. General scheme of the sensing system using the 4x6 multiplexed microfluidic platform.

3.3.2 Effects of individual antibiotics on *E. coli* cells

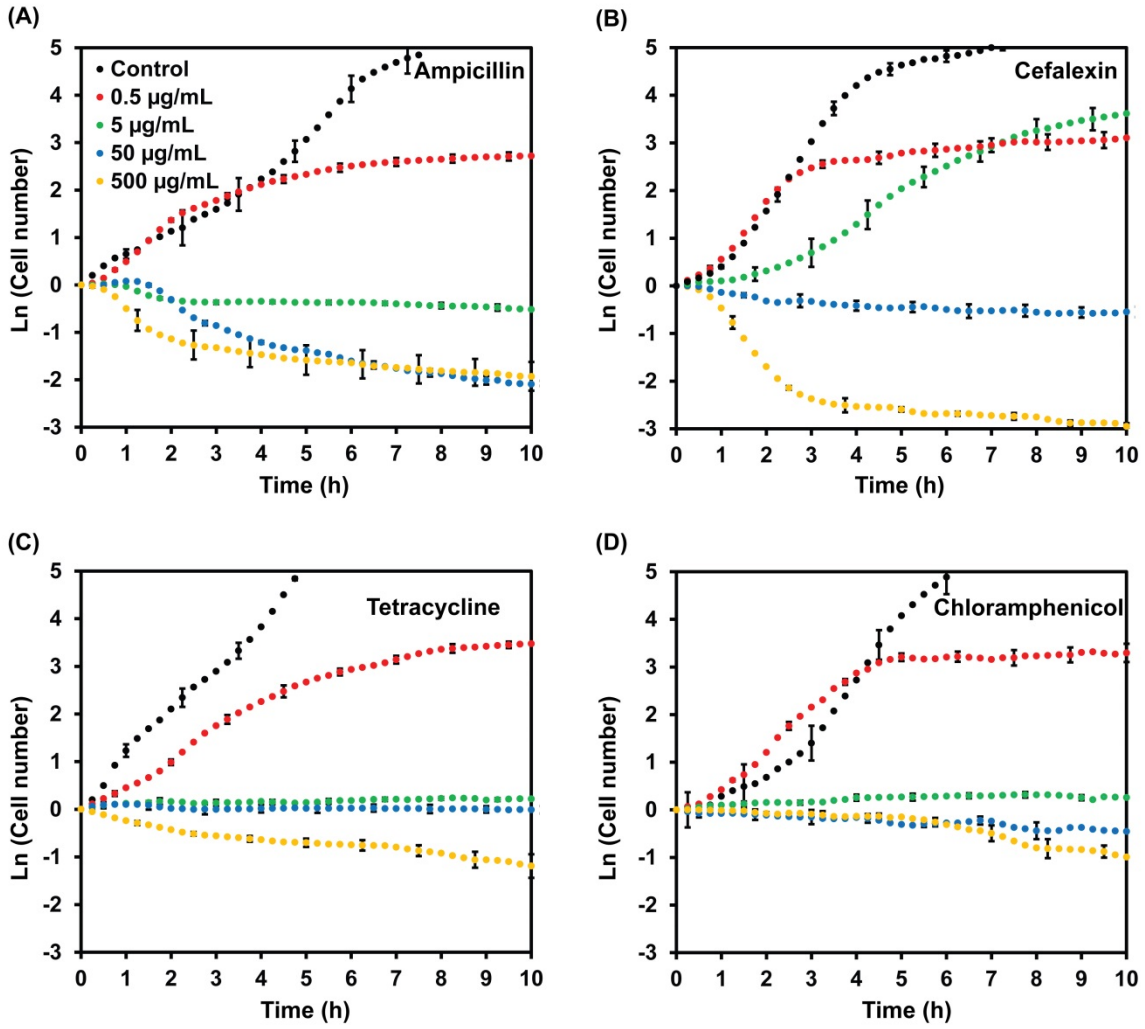

Figure 3.8. Effects of individual antibiotics on *E. coli* growth using an on-chip assay. Time traces represent the effects of bactericidal antibiotics: **(A)** ampicillin and **(B)** cefalexin and bacteriostatic antibiotics: **(C)** tetracycline and **(D)** chloramphenicol on cell growth. Cell growth and death were monitored by counting cells in each well, every 10 minutes, over a period of 10 hours. Cell numbers are normalized to the initial (t = 0) value. Each data point represents the mean of measurements from three experiments. Error bars represent the standard error of the mean (SEM) and are depicted for every fifth data point for visual clarity.

I employed the microfluidic screening chip to investigate the effects of four widely prescribed antibiotics on *E. coli* expressing GFP. The use of GFP as a genetically encodable indicator of cell viability has been previously reported [44]. Transformation of bacteria to

express GFP is a standard procedure routinely used in microbiology or for applications in monitoring cell growth over an extended period of time. Antibiotics were selected to comprise bactericidal (ampicillin, cefalexin) and bacteriostatic (tetracycline, chloramphenicol) classes. I treated early log-phase cultures of *E. coli* with varying concentrations of each antibiotic on-chip and quantified cell numbers using TLFM over a period of 10 hours (**Fig. 3.8**). Representative optical images showing action of an antibiotic on bacteria over a period of 10 hours are shown in **Fig. 3.9**. Although cell numbers are quantified over a period of 10 hours, antibiotic susceptibility information is discernible within 2-4 hours (**Fig. 3.10)**. I estimated antibiotic efficiency in terms of the fraction of the initial cell population in a chamber that survives antibiotic treatment at the end of an experiment ($FL_{ab,\,conc}$) as defined by Eq. (1). $FL_{ab,\,conc}$ values are tabulated in **Table 3.3**. In case of unperturbed cell growth (no antibiotics added), *FL* typically has a value close to 166, which corresponds to 6-8 population doubling events over a period of 10 hours. Bactericidal (cell killing) antibiotic action is expected to result in a value of $FL_{ab,conc} < 1$, whereas bacteriostatic (growth arresting) antibiotic action will lead to $FL_{ab,\,conc} \approx 1$. In this way, $FL_{ab,conc}$ serves as a robust measure of antibiotic potency.

Table 3.3. Efficacy of individual antibiotics quantified in terms of *FL* values

Conc (μg/mL)	FL_{amp}	FL_{cef}	FL_{chl}	FL_{tet}
500	0.16 ± 0.05	0.06 ± 0.00	0.37 ± 0.01	0.33 ± 0.01
50	0.12 ± 0.01	0.58 ± 0.06	0.66 ± 0.02	1.00 ± 0.08
5	0.55 ± 0.04	33.16 ± 3.82	1.24 ± 0.08	1.21 ± 0.04
0.5	15.44 ± 1.41	23.45 ± 3.93	29.19 ± 5.99	32.86 ± 2.57

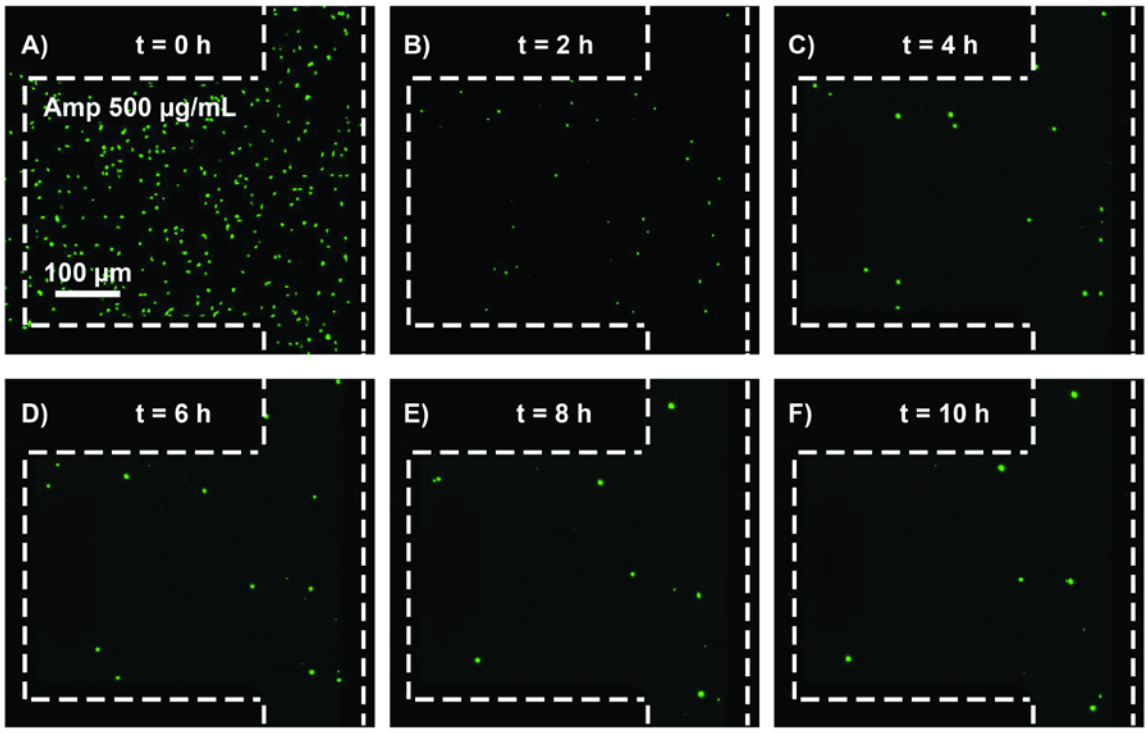

Figure 3.9. Killing of *E. coli* over a period of 10 hours when treated with 500 µg/mL of ampicillin.

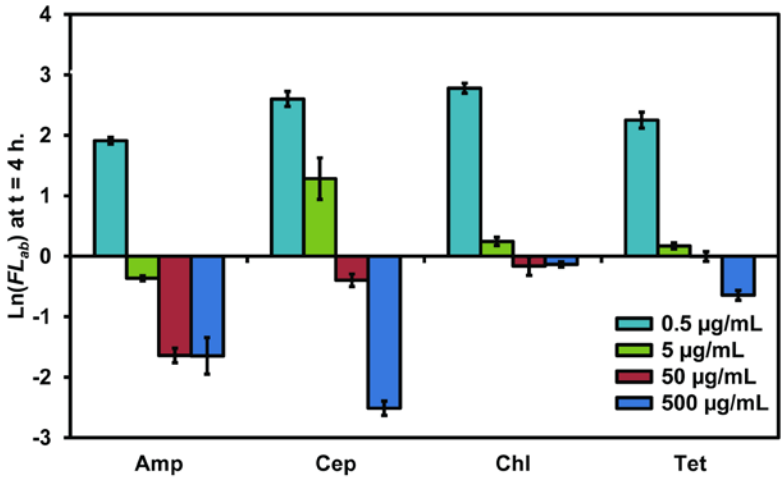

Figure 3.10. *FL* values of single antibiotics on *E. coli* cells, assessed at t = 4 hrs.

I observed that all four antibiotics failed to inhibit cell growth when employed at low concentrations (0.5 μg/mL), although the final cell densities (at t = 10 hrs.) are considerably lower than in the case where cells are not treated with antibiotics ($FL_{amp,0.5} \approx 15.4$, $FL_{cef,0.5} \approx 23.5$, $FL_{chl,0.5} \approx 29.2$, and $FL_{tet,0.5} \approx 32.9$). At a 10-fold higher concentration (5 μg/mL), ampicillin results in a substantial amount of cell death by lysis ($FL_{amp,5} \approx 0.55$), whereas tetracycline and chloramphenicol almost completely abrogate cell division without causing significant lysis ($FL_{tet,5} \approx 1.21$, *and* $FL_{chl,5} \approx 1.24$). These results are consistent with the bactericidal and bacteriostatic mode of action of the respective antibiotics. Interestingly, cell proliferation is observed in the case of cefalexin ($FL_{cef,5} \approx 33.2$). At the highest concentration (500 μg/mL), I observed significant cell death for all antibiotics ($FL_{amp,500} \approx 0.16$ and $FL_{cef,500} \approx 0.06$; $FL_{tet,500} \approx 0.33$ and $FL_{chl,500} \approx 0.37$).

Cell growth data obtained using the on-chip microfluidic assay are generally in good agreement with those obtained in the 96-well plate assays, albeit with a few notable differences (**Figure 3.11**). In particular, 96-well plate based assays revealed robust cell growth upon treatment with cefalexin at 50 μg/mL, whereas complete growth arrest was observed using the on-chip assay for the same antibiotic concentration ($FL_{cef,50} \approx 0.58$). This difference can be explained by the different ways in which cell density is determined using the microfluidic on-chip assay versus the bulk-level 96-well plate assay. At a concentration of 50 μg/mL, cefalexin causes massive cell filamentation because it inhibits cell wall synthesis in *E. coli*. Indeed, in on-chip experiments, I observed a nearly 20-fold increase in cell length within 4 hours of cefalexin treatment (**Figure 3.12**). Cell elongation contributes to increased absorbance at 600 nm; however, in bulk assays that rely on optical absorbance to quantify cell growth, cell filamentation is perceived as an increase in cell density. In an analogous fashion, in the early stages ($t \approx 1.5$

hrs.) of ampicillin treatment (5 μg/mL) and cefalexin treatment (50 and 500 μg/mL), cell filamentation is misconstrued as rapid growth by the bulk absorbance based assay performed in the 96-well plates (See **Fig. 3.12** and **Fig. 3.13**). In this way, the microfluidic-based assay relies on single cell measurements to determine the efficacy of treatment, which intrinsically results in a more accurate measure of antibiotic potency.

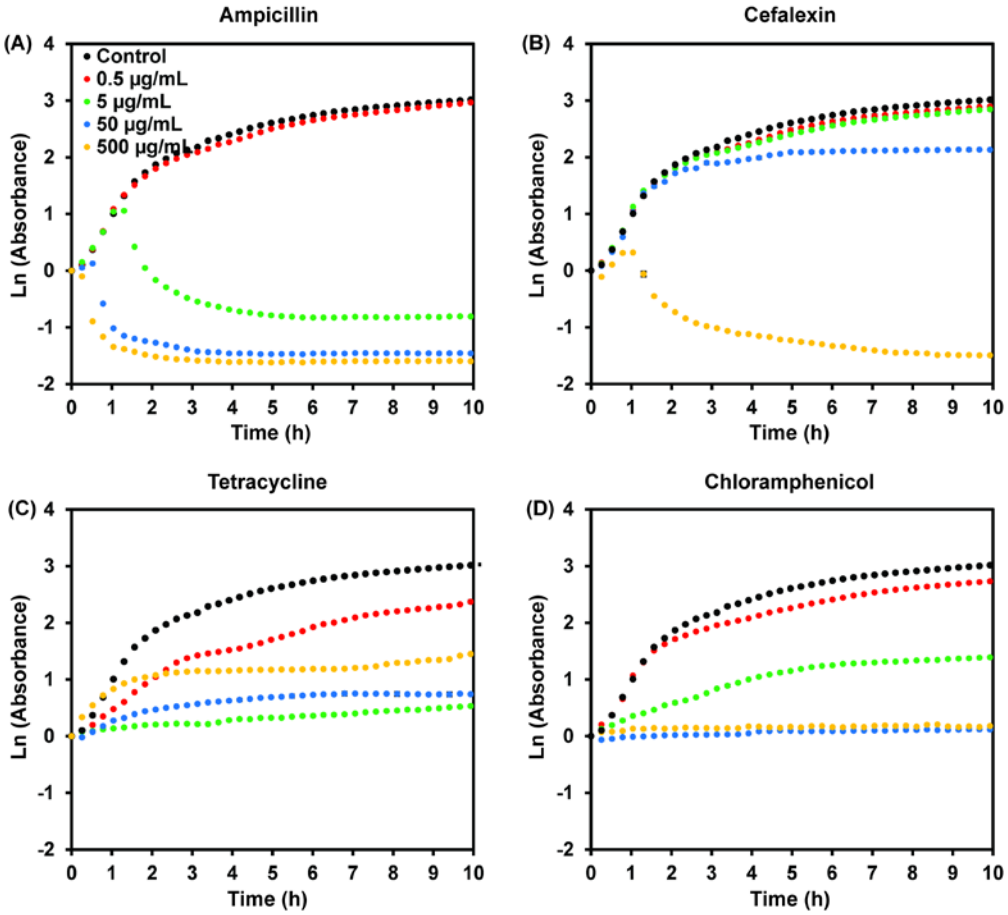

Figure 3.11. Effects of single antibiotics on *E. coli* growth investigated using 96-well plate assays. *E. coli* cells were treated with different concentrations of bactericidal antibiotics: **(A)** ampicillin and **(B)** cefalexin, and bacteriostatic antibiotics: **(C)** tetracycline and **(D)** chloramphenicol. All values are normalized to the absorbance at the initial (t = 0) time point.

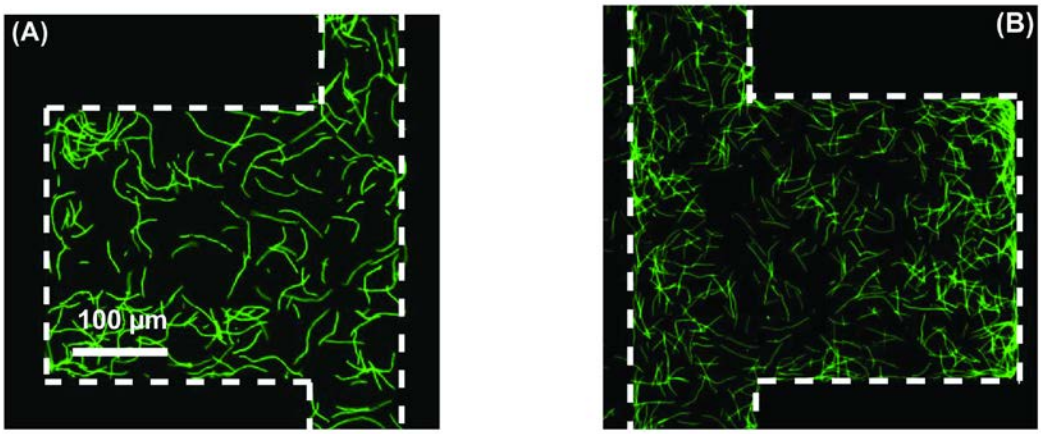

Figure 3.12. Elongation of *E. coli* cells upon treatment with **(A)** cefalexin and **(B)** ampicillin (t = 4 hrs.).

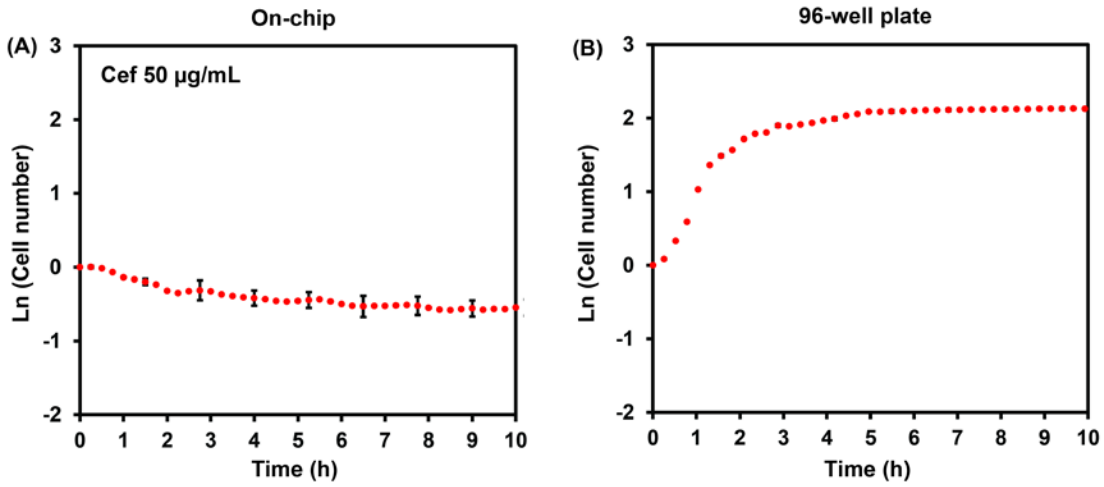

Figure 3.13. Elongation of *E. coli* cells upon treatment with cefalexin during early stage misconstrued as growth in 96-well plate

A second important difference between bulk-level AST and microfluidic-based AST is the possibility of antibiotic precipitation at high concentrations, which can obscure absorbance measurements in bulk-level analysis. We observed this phenomenon in the case of tetracycline. Based on 96-well plate measurements, the highest concentration of tetracycline (500 µg/mL) fails to inhibit cell growth initially (up to $t \approx 1.5$ hrs.), whereas the same concentration results in cell lysis using the on-chip assay ($FL_{tet,500} \approx 0.33$). Moreover, inhibition of cell growth by tetracycline appears to be more effective at lower concentrations of the antibiotic (5 and 50

μg/mL). I attribute this discrepancy to the rapid precipitation of tetracycline in aqueous solution at concentrations exceeding 500 μg/mL [45]. Precipitation of tetracycline from solution in the bulk-level assays results in an erroneous ~3-fold increase in optical absorbance at 600 nm ($Abs_{600,\,0.5\,mg/L\,tet} = 0.25$ *versus* $Abs_{600,\,blank} = 0.08$). In addition, it is well known that hydrophobic small molecules can be absorbed by PDMS. Therefore, I performed a series of control experiments to ensure that the on-chip antibiotic concentrations in the microfluidic platform were not significantly perturbed during the course of the experiments (**Table 3.4**). I quantified antibiotic concentrations before and after on-chip incubation for 10 hours using liquid chromatography-mass spectrometry (LC-MS) discussed in more details in the next section. Based on mass spectrometry, ampicillin, cefalexin, and chloramphenicol showed no significant absorption by PDMS. However, I observed some degree of absorption in case of tetracycline at the endpoint of prolonged 10-hour incubation in PDMS devices. Nevertheless, the on-chip AST results followed the same general trends compared to bulk-level growth experiments, including growth inhibition at low concentrations of tetracycline (5 μg/mL), which is consistent with 96-well plate measurements (**Fig. 3.8 and Fig. 3.11**).

Table 3.4. Fraction of antibiotic lost after 10 hours of incubation in the PDMS chip

Conc (μg/mL)	Amp	Cef	Chl	Tet
1000	0.11	0.03	0.16	0.34
100	0	0.12	0.20	0.57

Study of Antibiotic Absorption by PDMS

PDMS is biocompatible, optically transparent, and inexpensive, which makes it an attractive material for biological assays [23]. However, hydrophobic small molecules such as drugs are often readily lost by absorption by the PDMS bulk material and/or adsorption on the PDMS

surface, which has the potential to interfere with quantitative biological assays [46]. To ensure that the on-chip antibiotic concentrations in the microfluidic platform were not significantly perturbed, I quantified the antibiotic concentrations before and after on-chip incubation for 10 hours using liquid chromatography-mass spectrometry (LC-MS). I used two different concentrations of each antibiotic: 1000 μg/mL and 100 μg/mL. The respective antibiotic solutions were added to the microfluidic chip and incubated at 35 °C for 10 hours. The chip design was modified slightly to include open-ended channels to enable collection of antibiotic samples after incubation. The experiment was set up in exactly the same manner as a typical on-chip experiment with cells, except that the cells were omitted. Based on the results (**Table 3.4**), I conclude that ampicillin, cefalexin, and chloramphenicol concentrations are minimally affected during incubation in a PDMS-based chip, even at high concentrations of the antibiotics. In addition, even though tetracycline is absorbed to some extent, the on-chip results follow the trend as expected including at low concentrations of 5 μg/mL, in which the cell growth is inhibited consistently on-chip and in 96-well plate experiments. I conjecture that tetracycline is absorbed by PDMS owing to its hydrophobic properties [47].

Estimation of Antibiotic Minimal Inhibitory Concentration (MIC)

Minimal inhibitory concentration (MIC) is defined as the lowest concentration of an antibiotic that inhibits cell growth as determined by visual inspection. I estimated the MIC of each antibiotic against *E. coli* MG1655 using the broth dilution method as described in the manual of Clinical Laboratory Standards [39]. The results are listed in **Table 3.2**. Specifically, *E. coli* cell cultures were prepared as described above and added to the wells of a 96-well plate (Nunclon) and mixed with an equal volume of antibiotic at the desired concentration. Twelve serial dilutions were prepared for each antibiotic to span a concentration range from 0.1-500 μg/mL.

Plates were incubated with shaking (linear mode, 3.5 mm amplitude) at 35 °C in a microplate reader (TECAN Infinite M200 PRO) and the optical density at 600 nm of each well was recorded every 15 minutes over a period of 15 hours. Evaporation was minimized through the use of covered plates. The MIC was defined as the lowest concentration of antibiotic that completely inhibited cell growth as determined by absorbance readings as well as visual inspection. Antibiotic stocks were prepared as described in Materials and Methods. The antibiotic solutions were diluted using Lennox broth.

3.3.3 Effect of antibiotics in pairs

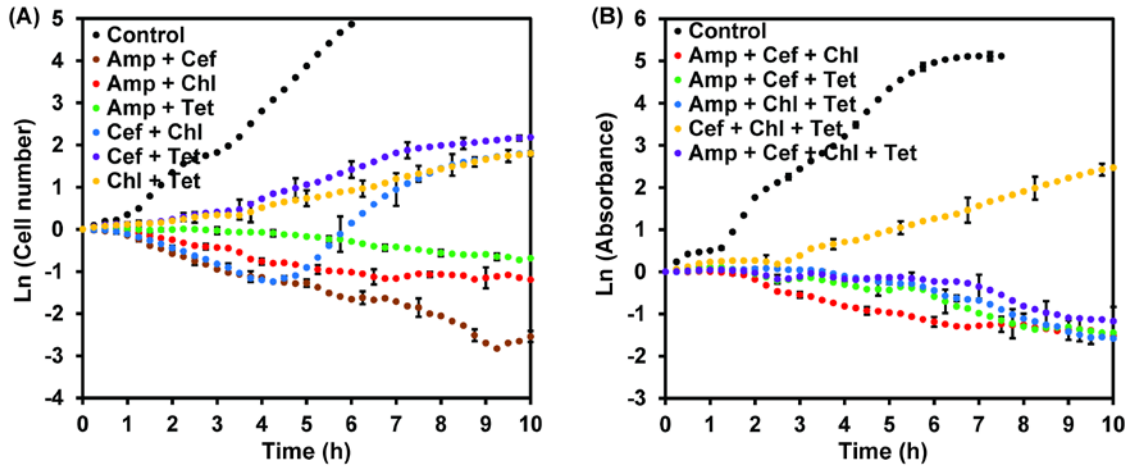

Figure 3.14. Synergistic and antagonistic effects of antibiotic combinations on *E. coli*. Time traces represent the effects of **(A)** pairs of antibiotics and **(B)** combinations of 3 and 4 antibiotics on *E. coli* cell growth. All values are normalized to the initial (t = 0) cell number. Each data point represents the mean of at least three experiments. Errors bars represent the standard error of the mean (SEM) and are depicted for every fifth data point for visual clarity.

The development of novel antimicrobials has lagged in pace relative to the rapid emergence of microbial drug resistance against several existing antibiotics [48]. In the absence of new potent pharmaceuticals, multidrug resistant pathogens are frequently treated with combinations of two or more antibiotics. Combination therapy offers a potential way to mitigate the emergence of drug resistance traits because microbial pathogens are less likely to simultaneously

develop mutations that render them resistant to multiple antibiotics [49, 50]. However, interactions between multiple antibiotics may exhibit either synergistic or antagonistic behavior, wherein the combination shows improved or decreased efficiency compared to each antibiotic applied individually. To evaluate the effects of antibiotic combinations on *E. coli* cell growth, we treated cells with the aforementioned antibiotics administered in pairs at a concentration of 5 μg/mL per antibiotic (**Fig. 3.14**). In this way, I selected an antibiotic concentration that is lower than the antibiotic MIC that we determined using 96-well plates (**Table 3.2**). Discernible changes in cell numbers were obtained within 4 hours of antibiotic treatment (**Fig. 3.15**). I quantify synergistic or antagonistic behavior of a pair of antibiotics based on its ability to eradicate bacterial cells relative to the action of each antibiotic applied individually. For each antibiotic pair, I calculate the value of a criterion variable A as defined above in Eq. (2). Synergistic combinations of antibiotics successfully eradicate *E. coli* cells more effectively than any individual antibiotic ($A < 1$). In contrast, a combination is deemed antagonistic if it eliminates fewer cells relative to the most potent single antibiotic used in the combination ($A >$ 1).

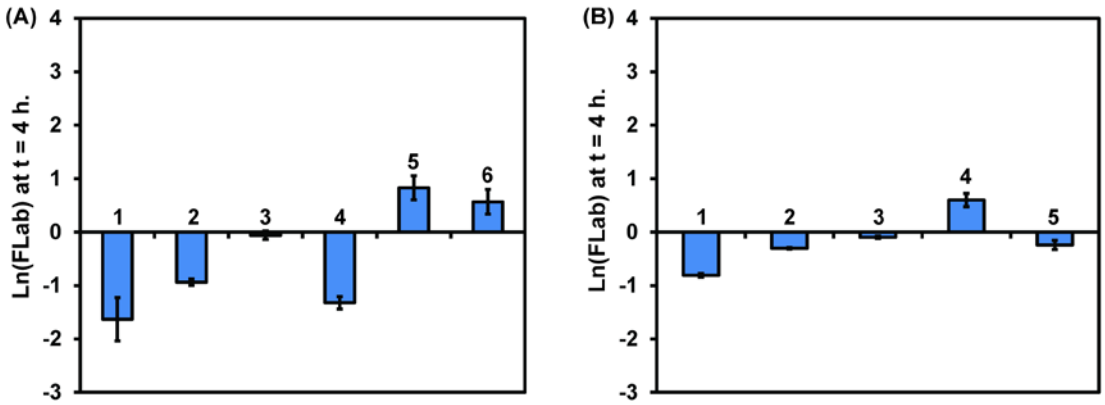

Figure 3.15. *FL* values of antibiotics combinations on *E. coli* cells, assessed using microfluidic chip at t = 4 hrs. **(A)** FL values for antibiotics tested in pairs where 1: Amp + Cef, 2: Amp + Chl, 3: Amp + Tet, 4: Cef + Chl, 5: Cef + Tet, 6: Chl + Tet. **(B)** *FL* values for antibiotics tested in combinations of three and four where 1: Amp + Cef + Chl, 2: Amp + Cef + Tet, 3: Amp + Chl + Tet, 4: Cef + Chl + Tet, 5: Amp + Cef + Chl + Tet

Table 3.5 lists the *FL* and *A* values that I determined for each antibiotic pair after performing the corresponding on-chip experiment. This data indicates that the ampicillin-cefalexin pair exhibited the best antibacterial activity ($FL_{amp+cef} \approx 0.06$). In contrast, neither ampicillin nor cefalexin exhibit appreciable cell killing activity when used individually at 5 μg/mL. The results indicate that a high degree of synergy occurs when the two antibiotics are used in combination (*A = 0.11*). Indeed, synergism between beta-lactam antibiotics, like ampicillin and cefalexin, constitutes the clinical basis for their widespread paired application in treating recalcitrant infections [51, 52].

Table 3.5. Synergistic/antagonistic interactions of antibiotic combinations

Combinations	***FL***	***A***	**Interaction**
Amp + Cef	0.06 ± 0.01	0.11	synergistic
Amp + Chl	0.31 ± 0.04	0.52	synergistic
Amp + Tet	0.46 ± 0.03	0.77	synergistic
Cef + Chl	6.34 ± 0.41	5.12	antagonistic
Cef + Tet	8.85 ± 0.44	7.29	antagonistic
Chl + Tet	7.94 ± 0.45	6.54	antagonistic
Amp + Cef + Chl	0.24 ± 0.04	3.44	antagonistic
Amp + Cef + Tet	0.29 ± 0.12	4.17	antagonistic
Amp + Chl + Tet	0.22 ± 0.01	0.70	synergistic
Cef + Chl + Tet	10.0 ± 2.63	8.23	antagonistic
Amp + Cef + Chl + Tet	0.38 ± 0.16	5.61	antagonistic

In contrast, combinations of the bacteriostatic antibiotics, the chloramphenicol-tetracycline pair resulted in antagonistic behavior. Slow cell growth was observed in this case ($FL_{tet+chl} \approx 7.9$,

$FL_{tet,5} \approx 1.21$ and $FL_{chl,5} \approx 1.24$). Tetracycline and chloramphenicol exert their bacteriostatic effects by inhibiting protein synthesis through their interactions with the bacterial ribosome. As both antibiotics aim for very similar target sites in the ribosome, antagonism may result from mutual exclusion of the antibiotics from their preferred target sites in cells [53].

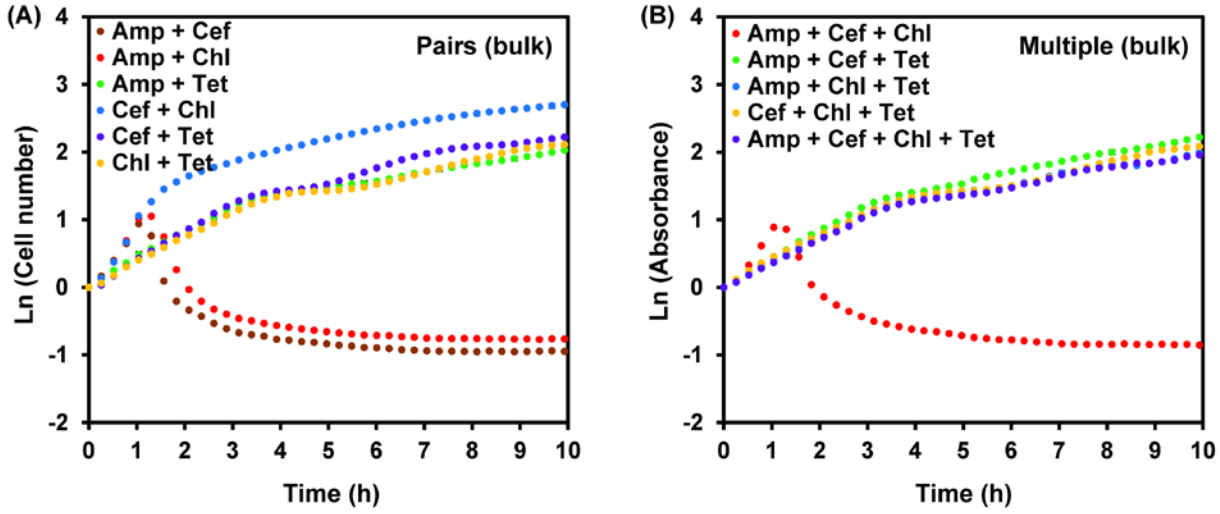

Figure 3.16 Effects of antibiotic combinations on *E. coli* cells, assessed using 96-well plates. Synergistic and antagonistic interactions were explored for **(A)** pairs of antibiotics and **(B)** combinations of three and four antibiotics. Antibiotics were used at a concentration of 5 µg/mL. All values are normalized to the initial absorbance ($t = 0$). Each data point represents the mean of at least three experiments. Errors bars represent the standard error of the mean (SEM) and are depicted for every fifth data point for visual clarity.

Paired combinations of ampicillin with tetracycline or chloramphenicol proved to be moderately synergistic ($FL_{amp+tet} \approx 0.46, FL_{amp+chl} \approx 0.31$) [54]. However, cephalexin resulted in significant antagonism with regards to cell proliferation when combined with tetracycline or chloramphenicol and observed up to 10 hours ($FL_{cef+chl} \approx 6.34, FL_{cef+tet} \approx 8.85$). Antagonism of growth inhibitory effects of the bacteriostatic antibiotics by cefalexin can be attributed to cefalexin's activity on the bacterial cell wall. Consistent with the mode of action of cephalosporin antibiotics, cefalexin interferes with cell wall peptidoglycan synthesis and compromises the integrity of the bacterial cell wall [55]. Enhanced cell wall permeability may

hinder intracellular retention of chloramphenicol and tetracycline to concentrations sufficient for antibacterial activity [53]. Although ampicillin exerts an analogous effect on the bacterial cell wall, antagonism is likely to be less apparent due to the greater potency of ampicillin relative to cefalexin (**Table 3.2**). Specifically, as mentioned above, 5 μg/mL ampicillin is sufficient to prevent cell growth, whereas higher concentrations of cefalexin need to be used to accomplish the same effect. Interestingly, *E. coli* cells respond to the cefalexin-chloramphenicol pair in a biphasic manner; herein, an initial phase of cell elongation and rapid lysis (up to $t = 5$ hrs.) is followed by a period of steady growth. Finally, the microfluidic-based on-chip results agree well with those obtained from 96-well plate assays with similar differences as described in the previous section (**Fig. 3.16**). In particular, cell elongation in the case of antibiotic pairs involving ampicillin or cefalexin is misconstrued as rapid initial growth by the absorbance-based bulk assay.

3.3.4 Effect of antibiotics in combinations of three and four

Moving beyond simple pairs of antibiotics, I also tested combinations of three and four antibiotics together to assess whether higher order antibiotic combinations could significantly enhance the antibacterial activity compared to antibiotic pairs (**Fig. 3.14**). Synergistic or antagonistic interactions between combinations of three or four antibiotics are defined based on the ability of the combination to inhibit cell proliferation relative to the effect of each antibiotic in isolation, as well as to that of sub-groups of antibiotics (pairs and triplets) included in the higher order combination. I calculated the criterion variable A using Eq. (3) in a manner analogous to antibiotic pairs (**Table 3.5**). Interestingly, all tested combinations of three or four antibiotics performed worse than the ampicillin-cefalexin pair ($FL_{amp+cef+chl} \approx 0.24$, $FL_{amp+cef+tet} \approx 0.29$, $FL_{amp+chl+tet} \approx 0.22$, $FL_{cef+chl+tet} \approx 10$, $FL_{amp+cef+chl+tet} \approx 0.38$). This key observation

suggests that a high degree of antagonism results when combinations of beta lactam antibiotics (ampicillin, cefalexin) are supplemented with one or more bacteriostatic antibiotics (chloramphenicol, tetracycline), with the exception of ampicillin-chloramphenicol-tetracycline, which was the only higher order combination that exhibits synergistic effects ($A = 0.70$). Beta lactam antibiotics rely on active cell division with concomitant synthesis of the bacterial cell wall to exert their effects [56]. Bacteriostatic antibiotics have been known to antagonize the effects of beta lactam antibiotics through their inhibition of protein synthesis and consequent stalling of cell wall synthesis [57]. Consistent with my earlier observations, combinations of cefalexin, chloramphenicol, and tetracycline proved to be highly antagonistic ($FL_{cef+chl+tet} \approx 10.0$). Finally, most of the combinations of three and four antibiotics caused substantial cell elongation, which was anomalously interpreted as cell growth by 96-well plate assays (**Fig. 3.16**).

3.3.5 Effect of cell density on killing efficacy of antibiotics

The efficiency of an antibiotic in eradicating pathogen populations is critically dependent on the density of the infecting cells (pathogen load) at the site of infection [58]. Dense bacterial populations often successfully counter antibacterial activities of several potent antibiotics through the initiation of complex genotypic responses based on quorum sensing [59, 60]. Bacterial cells colonizing infection sites can rapidly reach very high densities, because these cells are confined in the constrained space of the host organism. In this work, the microfluidic chambers (dimensions 500 μm x 400 μm x 15 μm and volume = 3 nL) provide a suitable mimic for the microconfinement effects experienced by colonizing pathogens *in vivo* [61]. Therefore, I assessed the effects of initial cell density on the killing efficacy of otherwise lethal doses of antibiotics. For this purpose, I chose the most potent antibiotic combination: the ampicillin-cefalexin pair ($FL_{amp+cef} \approx 0.06$ at an initial pathogen load of 10^8 cells/mL). I varied cell

densities over two orders of magnitude (10^9 - 10^{10} cells/mL). Use of high cell densities precludes direct enumeration of cell numbers due to spatial crowding. In these cases, cell growth was quantified by measuring the integrated fluorescence intensity over time in each microchamber. As depicted in **Fig. 3.17**, the ampicillin-cefalexin combination proved to be ineffective at cell concentrations of 10^9 cells/mL and 10^{10} cells/mL. I obtained similar results using another potent antibiotic cocktail comprising ampicillin, cefalexin, and chloramphenicol ($FL_{amp+cef+chl} \approx 0.23$). The rapid loss of antibiotic efficiency with 10-100 fold variations in population levels emphasizes the acute need to rapidly establish antibiograms of pathogens before infecting populations escalate to untreatable levels. This further highlights the utility of the microfluidic approach used here, which provides practical information within 4 hours. In contract, alternative methods based on current technologies require much longer time (at least 8 hours, more typically 24-72 hours [62] to provide the same observation.

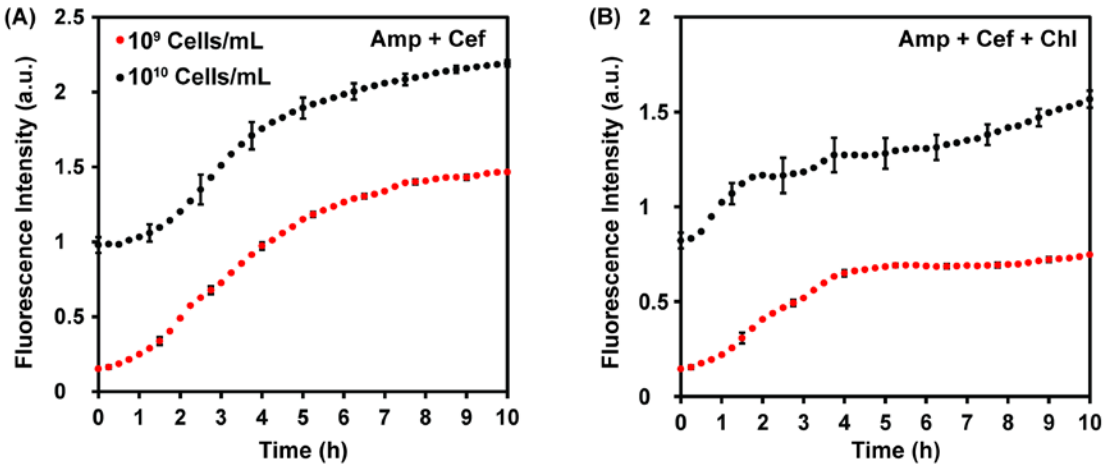

Figure 3.17 Effects of initial *E. coli* cell density on antibiotic efficacy. Population effects of *E. coli* cells were investigated for **(A)** a combination of ampicillin and cefalexin and **(B)** combination of ampicillin, cefalexin, and chloramphenicol. Cell growth was quantified by calculating the integrated fluorescence intensity in a microchamber as the dense crowding hindered counting of single cells. Errors bars represent the standard error of the mean (SEM) and are depicted for every fifth data point for visual clarity.

3.4 Conclusions

In summary, I have developed a multiplexed microfluidic platform comprised of arrays of small volume chambers (3 nL) that enables monitoring the effects of several antibiotics and their combinations on *E. coli* cells. Conventional methods for antibiotic susceptibility testing (*e.g.*, broth dilution and disc diffusion) are time consuming and tedious, generally requiring large sample and reagent volumes. From this perspective, the microfluidic platform provides substantial improvements over existing methods with regard to timescale of analysis and sample volumes. In particular, the platform possesses key several advantages such as low sample and reagent volume requirements (< 6 μL), enhanced detection sensitivity (~ 1 cell), rapid turnaround times (2-4 hours), improved portability, and enhanced combinatorial capabilities compared to several alternative microfluidic techniques. Even though I quantified antibacterial effects on cells over a total time period of 10 hours, changes in cell numbers are already discernible within 2 to 4 hours. In this way, the platform substantially accelerates antibiotic susceptibility testing compared to broth dilution and disk diffusion by circumventing the need for pre-culturing cells to detectable levels, which often takes > 24 hrs. Moreover, the method further enables direct observation and enumeration of cellular phenotypes (growth, morphology). As such, the microfluidic method reported here provides precise quantification of cell numbers, in contrast to bulk methods that rely on population averaged metrics (*e.g.*, optical absorbance) as an indirect proxy for cell number. In addition, the use of normally closed valves in the platform facilitates portability and easy loading of samples and reagents.

On-chip experiments involving combinations of different antibiotics highlight the importance of thorough evaluation of the effectiveness of each combination before use in the clinic. In several instances, antibiotic combinations perform poorly. These results also showcase the

utility of the platform for studies like these, as well as for rapid diagnosis and management of infections. The microfluidic platform described in this chapter relies on genetically modified bacteria for analysis; however, this issue can be circumvented by utilizing fluorescence based or optical dyes. In addition, the methodology reported here relies on the use of fluorescent microscopy, a nearly ubiquitous method that is routinely utilized in medical fields including microbiology, immunology, and pathology testing labs. One can envision using AST chips such as those reported here for further development of point-of-care diagnostic platforms for bacterial infections.

3.5 References:

1. Bisht, R., et al., Antibiotic resistance - A global issue of concern. Asian Journal of Pharmaceutical and Clinical Research, 2009. 2(2): p. 34-39.
2. Lazcka, O., F.J.D. Campo, and F.X. Muñoz, Pathogen detection: A perspective of traditional methods and biosensors. Biosensors and Bioelectronics, 2007. 22(7): p. 1205-1217.
3. White, R.L., et al., Comparison of three different in vitro methods of detecting synergy: Time-kill, checkerboard, and E test. Antimicrobial Agents and Chemotherapy, 1996. 40(8): p. 1914-1918.
4. Mancini, N., et al., The Era of Molecular and Other Non-Culture-Based Methods in Diagnosis of Sepsis. Clin. Microbiol. Rev., 2010. 23(1): p. 235-251.
5. Balaban, N.Q., et al., Bacterial Persistence as a Phenotypic Switch. Science, 2004. 305(5690): p. 1622-1625.
6. Lewis, K., Persister cells, in Annual Review of Microbiology2010. p. 357-372.
7. Dawson, C.C., C. Intapa, and M.A. Jabra-Rizk, "Persisters": Survival at the cellular level. PLoS Pathogens, 2011. 7(7).
8. Gales, A.C., A.O. Reis, and R.N. Jones, Contemporary assessment of antimicrobial susceptibility testing methods for polymyxin B and colistin: Review of available interpretative criteria and quality control guidelines. Journal of Clinical Microbiology, 2001. 39(1): p. 183-190.
9. Goldstein, F.W., A. Ly, and M.D. Kitzis, Comparison of Etest with agar dilution for testing the susceptibility of Pseudomonas aeruginosa and other multidrug-resistant bacteria to colistin [2]. Journal of Antimicrobial Chemotherapy, 2007. 59(5): p. 1039-1040.
10. Lo-Ten-Foe, J.R., et al., Comparative evaluation of the VITEK 2, disk diffusion, etest, broth microdilution, and agar dilution susceptibility testing methods for colistin in clinical isolates, including heteroresistant Enterobacter cloacae and Acinetobacter baumannii strains. Antimicrobial Agents and Chemotherapy, 2007. 51(10): p. 3726-3730.
11. Nicodemo, A.C., et al., In vitro susceptibility of Stenotrophomonas maltophilia isolates: Comparison of disc diffusion, Etest and agar dilution methods. Journal of Antimicrobial Chemotherapy, 2004. 53(4): p. 604-608.
12. Tan, T.Y. and S.Y. Ng, Comparison of Etest, Vitek and agar dilution for susceptibility testing of colistin. Clinical Microbiology and Infection, 2007. 13(5): p. 541-544.
13. Traub, W.H., Susceptibility of Pseudomonas aeruginosa to gentamicin sulfate in vitro: lack of correlation between disc diffusion and broth dilution sensitivity data. Applied microbiology, 1970. 20(1): p. 98-102.
14. Alanis, A.J., Resistance to antibiotics: are we in the post-antibiotic era? Archives of medical research, 2005. 36(6): p. 697-705.
15. Ang, B.S.P., Bugs for the next century: The issue of antibiotic resistance. Annals of the Academy of Medicine Singapore, 2001. 30(2): p. 199-202.
16. Ceylan Koydemir, H., et al., MEMS biosensors for detection of methicillin resistant Staphylococcus aureus. Biosensors and Bioelectronics, 2011. 29(1): p. 1-12.
17. Chiang, Y.-L., et al., Innovative antimicrobial susceptibility testing method using surface plasmon resonance. Biosensors and Bioelectronics, 2009. 24(7): p. 1905-1910.

18. Karasinski, J., et al., Detection and identification of bacteria using antibiotic susceptibility and a multi-array electrochemical sensor with pattern recognition. Biosensors and Bioelectronics, 2007. 22(11): p. 2643-2649.
19. Kinnunen, P., et al., Self-Assembled Magnetic Bead Biosensor for Measuring Bacterial Growth and Antimicrobial Susceptibility Testing. Small, 2012. 8(16): p. 2477-2482.
20. Nakamura, N., A. Shigematsu, and T. Matsunaga, Electrochemical detection of viable bacteria in urine and antibiotic selection. Biosensors and Bioelectronics, 1991. 6(7): p. 575-580.
21. Tsou, P.-H., et al., Rapid antibiotic efficacy screening with aluminum oxide nanoporous membrane filter-chip and optical detection system. Biosensors and Bioelectronics, 2010. 26(1): p. 289-294.
22. Kinnunen, P., et al., Monitoring the growth and drug susceptibility of individual bacteria using asynchronous magnetic bead rotation sensors. Biosensors and Bioelectronics, 2011. 26(5): p. 2751-2755.
23. Sia, S.K. and G.M. Whitesides, Microfluidic devices fabricated in poly(dimethylsiloxane) for biological studies. Electrophoresis, 2003. 24(21): p. 3563-3576.
24. Boedicker, J.Q., et al., Detecting bacteria and determining their susceptibility to antibiotics by stochastic confinement in nanoliter droplets using plug-based microfluidics. Lab on a Chip 2008. 8(8): p. 1265-1272.
25. Chen, C.H., et al., Antimicrobial susceptibility testing using high surface-to-volume ratio microchannels. Analytical Chemistry, 2010. 82(3): p. 1012-1019.
26. Churski, K., et al., Rapid screening of antibiotic toxicity in an automated microdroplet system. Lab on a Chip 2012. 12(9): p. 1629-1637.
27. Cira, N.J., et al., A self-loading microfluidic device for determining the minimum inhibitory concentration of antibiotics. Lab on a Chip, 2012. 12(6): p. 1052-1059.
28. Sun, P., et al., High-throughput microfluidic system for long-term bacterial colony monitoring and antibiotic testing in zero-flow environments. Biosensors and Bioelectronics, 2011. 26(5): p. 1993-1999.
29. Ho, J.Y., et al., Rapid identification of eskape bacterial strains using an autonomous microfluidic device. PLoS ONE, 2012. 7(7).
30. Kalashnikov, M., et al., A microfluidic platform for rapid, stress-induced antibiotic susceptibility testing of Staphylococcus aureus. Lab on a Chip, 2012.
31. Choi, J., et al., Rapid antibiotic susceptibility testing by tracking single cell growth in a microfluidic agarose channel system. Lab on a Chip, 2013. 13(2): p. 280-287.
32. Kalashnikov, M., et al., A microfluidic platform for rapid, stress-induced antibiotic susceptibility testing of Staphylococcus aureus. Lab on a Chip, 2012. 12(21): p. 4523-4532.
33. Theberge, A.B., et al., Microdroplets in microfluidics: An evolving platform for discoveries in chemistry and biology. Angewandte Chemie - International Edition, 2010. 49(34): p. 5846-5868.
34. Xia, Y. and G.M. Whitesides, Soft lithography. Annual Review of Materials Science, 1998. 28(1): p. 153-184.
35. Lutz, R. and H. Bujard, Independent and tight regulation of transcriptional units in escherichia coli via the LacR/O, the TetR/O and AraC/I1-I2 regulatory elements. Nucleic Acids Research, 1997. 25(6): p. 1203-1210.
36. Zaslaver, A., et al., A comprehensive library of fluorescent transcriptional reporters for Escherichia coli. Nature Methods, 2006. 3(8): p. 623-628.

37. Joe Sambrook, D.W.R., Molecular Cloning 3rd ed. 2001: Cold Spring Harbor Laboratory Press.
38. Rasband, W., ImageJ, 2011.
39. Wiegand, I., K. Hilpert, and R.E.W. Hancock, Agar and broth dilution methods to determine the minimal inhibitory concentration (MIC) of antimicrobial substances. Nature Protocols, 2008. 3(2): p. 163-175.
40. Mohan, R., et al., Design considerations for elastomeric normally closed microfluidic valves. Sensors and Actuators, B: Chemical, 2011. 160(1): p. 1216-1223.
41. Schudel, B.R., et al., Microfluidic chip for combinatorial mixing and screening of assays. Lab on a Chip, 2009. 9(12): p. 1676-1680.
42. Schudel, B.R., et al., Multiplexed detection of nucleic acids in a combinatorial screening chip. Lab on a Chip, 2011. 11(11): p. 1916-1923.
43. Thorson, M.R., et al., Microfluidic approach to polymorph screening through antisolvent crystallization. CrystEngComm, 2011. 14(7): p. 2404-2412.
44. Keymer, J.E., et al., Bacterial metapopulations in nanofabricated landscapes. Proceedings of the National Academy of Sciences of the United States of America, 2006. 103(46): p. 17290-17295.
45. Martindale, W., Martindale: The Extra Pharmacopoeia. 29th ed. 1989, London: Pharmaceutical Press. 1984.
46. Toepke, M.W. and D.J. Beebe, PDMS absorption of small molecules and consequences in microfluidic applications. Lab on a Chip, 2006. 6(12): p. 1484-1486.
47. Leive, L., et al., Tetracyclines of various hydrophobicities as a probe for permeability of Escherichia coli outer membranes. Antimicrobial Agents and Chemotherapy, 1984. 25(5): p. 539-544.
48. Keith, C.T., A.A. Borisy, and B.R. Stockwell, Multicomponent therapeutics for networked systems. Nature Reviews Drug Discovery, 2005. 4(1): p. 71-78.
49. Chait, R., A. Craney, and R. Kishony, Antibiotic interactions that select against resistance. Nature, 2007. 446(7136): p. 668-671.
50. Mouton, J.W., Combination therapy as a tool to prevent emergence of bacterial resistance. Infection, 1999. 27(SUPPL. 2): p. S24-S28.
51. Allewelt, M., et al., Ampicillin + sulbactam vs. clindamycin ± cephalosporin for the treatment of aspiration pneumonia and primary lung abscess. Clinical Microbiology and Infection, 2004. 10(2): p. 163-170.
52. Dejace, P. and J. Klastersky, Comparative review of combination therapy: Two beta-lactams versus beta-lactam plus aminoglycoside. American Journal of Medicine, 1986. 80(6 B): p. 29-38.
53. Lorian, V., Antibiotics in Laboratory Medicine. fifth ed, ed. V. Lorian. 1986, Philadelphia: Williams & Wilkins. 1259.
54. Cottarel, G. and J. Wierzbowski, Combination drugs, an emerging option for antibacterial therapy. Trends in Biotechnology, 2007. 25(12): p. 547-555.
55. Rolinson, G.N., Effect of beta-lactam antibiotics on bacterial cell growth rate. Journal of General Microbiology, 1980. 120(2): p. 317-323.
56. Tipper, D.J., Mode of action of beta-lactam antibiotics. Pharmacology and Therapeutics, 1985. 27(1): p. 1-35.

57. Winslow, D.L., J. Damme, and E. Dieckman, Delayed bactericidal activity of beta-lactam antibiotics against Listeria monocytogenes: Antagonism of chloramphenicol and rifampin. Antimicrobial Agents and Chemotherapy, 1983. 23(4): p. 555-558.
58. Udekwu, K.I., et al., Functional relationship between bacterial cell density and the efficacy of antibiotics. Journal of Antimicrobial Chemotherapy, 2009. 63(4): p. 745-757.
59. Butler, M.T., Q. Wang, and R.M. Harshey, Cell density and mobility protect swarming bacteria against antibiotics. Proceedings of the National Academy of Sciences of the United States of America, 2010. 107(8): p. 3776-3781.
60. Dorr, T., K. Lewis, and M. Vulic, SOS response induces persistence to fluoroquinolones in Escherichia coli. PLoS Genetics, 2009. 5(12).
61. Sung, J. and M. Shuler, Microtechnology for Mimicking In Vivo Tissue Environment. Annals of Biomedical Engineering, 2012. 40(6): p. 1289-1300.
62. Jorgensen, J.H. and M.J. Ferraro, Antimicrobial susceptibility testing: A review of general principles and contemporary practices. Clinical Infectious Diseases, 2009. 49(11): p. 1749-1755.

Chapter 4

Antibiotic susceptibility testing of polymicrobial cultures[3]

4.1 Introduction

Microbes seldom exist in isolation[1, 2], hence several infections such as urinary tract infections (UTIs), chronic wounds, cystic fibrosis, and nosocomial bacteremia are polymicrobial in nature, that is they involve more than one microbial agent[3-5]. These infections, in the literature also referred to as mixed, complex, synergistic, or co-infections, are known for their higher mortality rate than their monomicrobial constituents[3]. In spite of the larger debilitating effects, these polymicrobial infections are not well studied [3, 6-8]. Furthermore, since microbes involved in polymicrobial infections are more recalcitrant to several antibiotics compared to the same microbes in monomicrobial cultures, polymicrobial infections frequently require a stronger antibiotic dosing regimen[4]. Billions of dollars are spent each year in USA to treat these infections; however the majority of the treatments are solely based on monomicrobial susceptibility information [9-11], in spite of the fact that monomicrobial antibiotic susceptibility information often does not necessarily apply to polymicrobial cultures[12-15]. This incorrectly assumed correlation can lead to inaccurate antibiotic dosing regimen further exacerbating the global health issue of increasing antibiotic resistance[16]. Due to the severity of these polymicrobial infections and the rising antibiotic resistance, understanding the mechanisms and quantifying the antibiotic susceptibility of the microbes involved in these infections is imperative.

[3] Part of this work has been submitted for publication: Ritika Mohan, Chotitath Sanpitakseree, Amit V. Desai, Emre S. Sevgen, Charles M. Schroeder, and Paul J.A. Kenis, "A microfluidic approach for antibiotic susceptibility testing of polymicrobial infections", submitted.

Conventional antibiotic susceptibility testing (AST) procedures such as disk diffusion and broth dilution are standardized only for monomicrobial cultures[17]. While these methods provide useful insights about the bacterial susceptibility in isolate cultures, they possess several limitations in obtaining analogous information in mixed cultures, including (1) the inability to acquire individual species-specific antibiotic susceptibility information, and (2) the inability to investigate the inter-species interaction, which influences the efficacy of antibiotics. In addition, AST of polymicrobial cultures becomes more tedious than conventional monomicrobial AST, because the number of plates needed increases with the number of bacterial strains in the sample[18]. Also, the conventional methods require (1) large sample volumes (10-30 mL) and long incubation times (>24 h) for pre-culturing the bacteria to detectable levels, leading to cumbersome analysis, and (2) the determination of bacterial growth changes by visual inspection or absorbance-based spectroscopy. Both these factors lead to imprecise results[19, 20].

Only few studies have utilized conventional AST techniques for polymicrobial cultures. For instance, a study involving *P. aeruginosa, B. cenocepacia,* and *E. coli* demonstrated an increase in the antibiotic resistance of the population compared to their monomicrobial cultures and this observation was attributed to the transfer of resistance from a sub-bacterial population[21]. Although this study demonstrated the application of conventional methods of monomicrobial susceptibility to polymicrobial cultures, these methods are still plagued by their limitations, *i.e.*, long time for analysis and low sensitivity, and the inability to determine species-specific susceptibility. Culture-independent techniques, such as the quantitative terminal restriction fragment length polymorphism (qT-RFLP) approach that enumerates genome copies through 16S rRNA gene (proxy for bacterial cell number), have been utilized to obtain species specific information [17, 18, 22]. However, this method is tedious due to the complicated

sample preparation and data analysis procedures, and consists of the inherent problems associated with PCR-based methods such as preparation of precise primers and occasional appearance of false peaks [23].

The few studies that have focused on the effects of bacterial interaction on AST [24-26] have attributed observed changes in antibiotic susceptibility primarily to the production of enzymes such as beta-lactamases, which protect co-existing bacteria[24]. Developing a better understanding of bacterial interactions is crucial for two reasons: (1) investigation of how changes to bacterial susceptibility lead to critical cases of infections, and (2) the possibility of discovering novel molecules that are induced only in the presence of different species [11, 27-30], as these novel molecules may in turn modulate the physiology of other microbes affecting bacterial pathogenesis [30]. Current techniques (*e.g.*, broth dilution) are end-point assays and are unable to quantify bacterial interaction, hence, the development of new techniques for quantifying the effects of antibiotics due to bacterial interaction in polymicrobial infections is indispensable.

The use of integrated microfluidics represents an attractive technology for a range of bio-based applications [31-33] and has the potential to address some of the aforementioned issues associated with the currently used AST methods. Specifically, integrated microfluidics can satisfy key requirements for polymicrobial AST, for example quantification of bacterial interaction and determination of species-specific susceptibility by distinguishing and accurately enumerating different species in a time-resolved fashion. Microfluidic platforms also enable the investigation of bacterial interaction without the need to pre-culture cells to a detectable level, which drastically reduces the assay time. Different microbial species can be easily identified and visualized individually. Other advantages include the low sample and reagent volume

requirements, the high degree of spatial control over reagents, and the option to automate operations for high-throughput studies. Some of these advantages inherent to microfluidics have been exploited previously to study a variety of phenomena in bacterial populations such as the influence of physical (shear stresses) and chemical cues (toxins) on cell viability, motility, functionality, and proliferation[11, 34-37]. In other work, microfluidics has also been utilized to study the co-culture of cells or cell-cell interactions in 2D and 3D environments for a wide range of applications, including tissue engineering and biomimetic niches[38-40], as well as bacterial interaction in biofilms[41]. However, only few studies have focused on the effect of bacterial interactions on AST [42, 43]. Some studies, such as those that utilized microfluidic "lobster traps", microcavities permeable to small molecules, to study antibiotic resistance in low-cell-number/high-density bacterial population[44], have commented on the utility of this approach to study polymicrobial interactions in the future, but such studies have not appeared to my knowledge. Several other microfluidic approaches have been explored for monomicrobial AST [45-51], but none for polymicrobial AST, but these often suffer from issues such as limited portability[47, 50, 52], or complicate platform fabrication and/or operation [50, 53].

In this work, I address the limitations of the conventional AST techniques and current microfluidic approaches by developing a multiplexed microfluidic platform for studying bacterial interaction and species-specific polymicrobial AST. The platform enables measurement of minimum inhibitory concentrations with sample volumes as low as ~ 2.4 nL in less than 4 hours. More importantly, the high sensitivity not only enables accurate quantitation of susceptibility values but also provides species-specific information. I demonstrate the application of this platform to study the interaction between *E. coli*, *P. aeruginosa*, *and K.*

pneumomoniae, in the absence and presence of commonly used antibiotics for MIC determination.

4.2 Experimental

4.2.1 Bacterial strains, media and antibiotics

Bacterial strains of *E. coli, P. aeruginosa* and *K. pneumoniae* were routinely cultivated in Lennox broth (10 g/L tryptone, 5 g/L yeast extract, and 5 g/L NaCl) and supplemented with respective antibiotics as shown in **Table 4.1** to maintain the GFP/ RFP plasmid. Wild type *E. coli* MG1655 cells were transformed with pAM06[54] to constitutively express GFP under control of the P_L promoter from phage lambda. *K. pneumoniae* strain 342 carrying plasmid pRK2073[55] constitutively expressing GFP was generously provided to us by Prof. Eric Triplett at the University of Florida, and *P. aeruginosa* expressing red fluorescent protein (RFP) with the tdtomato gene under the transcriptional control of the nptll promoter on pBBR1-based plasmid pMQ132[56] was generously provided to us by Prof. Robert Shanks at the University of Pittsburgh. Incorporation of GFP and RFP markers enabled easy detection and enumeration of bacterial cells using time lapse fluorescence microscopy. Prior to all monomicrobial and polymicrobial experiments, frozen stocks were revived overnight on LB agar plates supplemented with the appropriate antibiotic. Single colonies from plates were then used to inoculate in 5 mL LB broth and the culture was incubated overnight at 37 °C with aeration (200 rpm).

Table 4.1. Antibiotic supplements in growth media for overnight pathogen culture

Pathogen	Supplemented Antibiotic
pQE80L-P_LGFP/*E. coli*	30 μg mL^{-1} kanamycin
pRK2073-GFP/*K. pneumoniae*	30 μg mL^{-1} kanamycin
pMQ132-P_{nptII}tdtomato/*P. aeruginosa*	40 μg mL^{-1} gentamicin
Wild-type *E. coli*	No antibiotic

For polymicrobial culture preparation (**Fig. 4.1**), 50 μL of the two monomicrobial cultures (cell types 1 and 2 in **Fig. 4.1**) were inoculated into separate tubes containing 5 mL of LB without supplemental antibiotic and were incubated for three hours. The incubated cultures were then concentrated 10X by centrifugation (3200 *g* for 10 min) to remove all traces of antibiotics. A range of cell type 1 and type 2 concentrations were then prepared by diluting in LB as shown in **Fig. 4.1**. The diluted cultures of the two types were then mixed to obtain a range of polymicrobial combinations. In the preparation of polymicrobial cultures, it was ensured that the observations of the competition experiments were solely due to the interaction between bacterial cells and not due to the antibiotics by removing antibiotics by centrifugation and by utilizing LB without antibiotics for the dilution steps. I did not observe a change in cellular fluorescence after cells were sub-cultured in LB without antibiotics in my experiments.

All antibiotic stocks were filtered using a 0.45 μm syringe filter (Millex-HV filter unit, Millipore) prior to use. Antibiotic stock solutions of 10 mg/mL gentamicin sulfate salt, 10 mg/mL tobramycin, 30 mg/mL kanamycin sulfate and 10 mg/mL amikacin were prepared in sterile deionized water. The antibiotics gentamicin sulfate and tobramycin were purchased from Sigma-Aldrich, kanamycin sulfate was purchased from Invitrogen, and amikacin was purchased from Fisher Scientific.

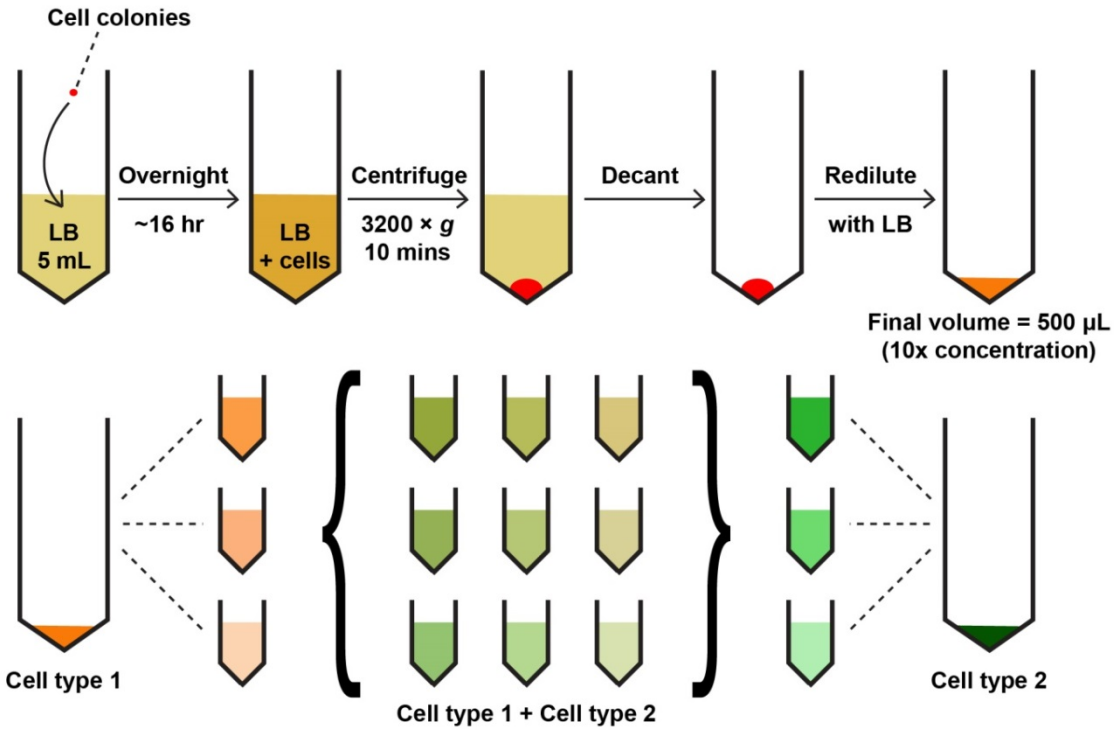

Figure 4.1. Preparation of mixed cultures of *E. coli*, *P. aeruginosa*, and *K. pneumoniae* in pairs

4.2.2 Pyocyanin extraction assay

The extraction procedure for pyocyanin was followed as previously described by Essar (**Fig. 4.2**).[57] Briefly, pyocyanin was extracted from 4 mL of overnight culture using 3 mL of chloroform. The chloroform layer (blue) was separated and extracted with 1 mL of 0.2 M HCl yielding an acidic layer (red). Absorbance of this acidic layer was measured at 520 nm (OD_{520}) and the concentration of pyocyanin was determined by comparison to calibration curves.

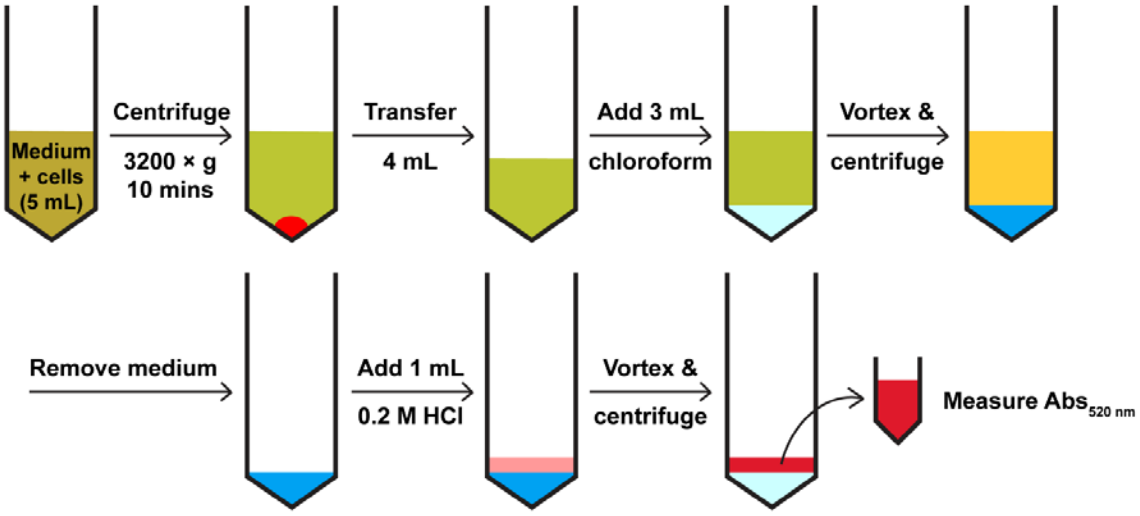

Figure 4.2. Extraction of pyocyanin by procedure outlined by Essar [57]

4.2.3 Antibiotic susceptibility testing off-chip

To compare the MIC obtained on-chip to conventional methods, I performed AST against *E. coli*, *K. pneumoniae*, and *P. aeruginosa* using 96-micro-well plates with each well 360 µL in volume (broth dilution method) or the conventional two-fold dilution protocol. The monomicrobial cell cultures were prepared as described previously [58] and polymicrobial cultures were prepared as shown in **Fig. 4.1**. Bacterial solution (100 µL) and antibiotics (100 µL) were added to the wells of a 127.8 mm x 85.5 mm flat-bottom 96-well plate (Nunclon), and the plates were incubated overnight at 37 °C. The MICs were determined by visual inspection of the bacterial density in each well, where the minimum concentration of antibiotic that prevented cell growth was determined to be the MIC. Since the antibiotic concentrations were prepared by the two-fold dilution protocol, the precision of the method is considered to be plus or minus one two-fold concentration [59]. I report a range of MIC values in several cases since occasionally a particular antibiotic concentration would allow for only slight growth of the cells, while the next higher concentration would cause cell death.

4.2.4 Antibiotic susceptibility testing on-chip

All microfluidic devices were sterilized by autoclaving prior to each experiment and the chips were treated with 10 mg/mL bovine serum albumin (BSA) for 15 minutes to prevent nonspecific interactions between chip surface and cells or antibiotics. The experimental set up and operation of the microfluidic platform is an adaptation of previously described protocols[58].

All fluorescent images were analyzed (**Fig. 4.3**) and post processed using ImageJ version 1.47c. The number of cells in each chamber was determined using local fluorescence intensity maxima as previously described[58]. Briefly, the function 'Enhance Contrast' was used to improve the visual perception of the bacterial cells. Then, an ImageJ function 'Find Maxima' was used to determine the number of cells by counting the local fluorescence intensity maxima. Finally, I plotted time-kill curves of the bacteria for different antibiotics (cell number vs. time). To better highlight long-term trends in cell growth (or death), I implemented a two-point moving average filter which smoothens the time kill curves. The concentration range of an antibiotic that leads to a negligible change in cell numbers over 10 h was considered to be the MIC range of the antibiotic for the pathogen. Similar to bulk scale experiments, if a concentration of an antibiotic caused a slight increase in cell numbers before inhibition of cell growth and the next higher concentration led to obvious cell death, I reported a range of MIC values (**Table 4.2**).

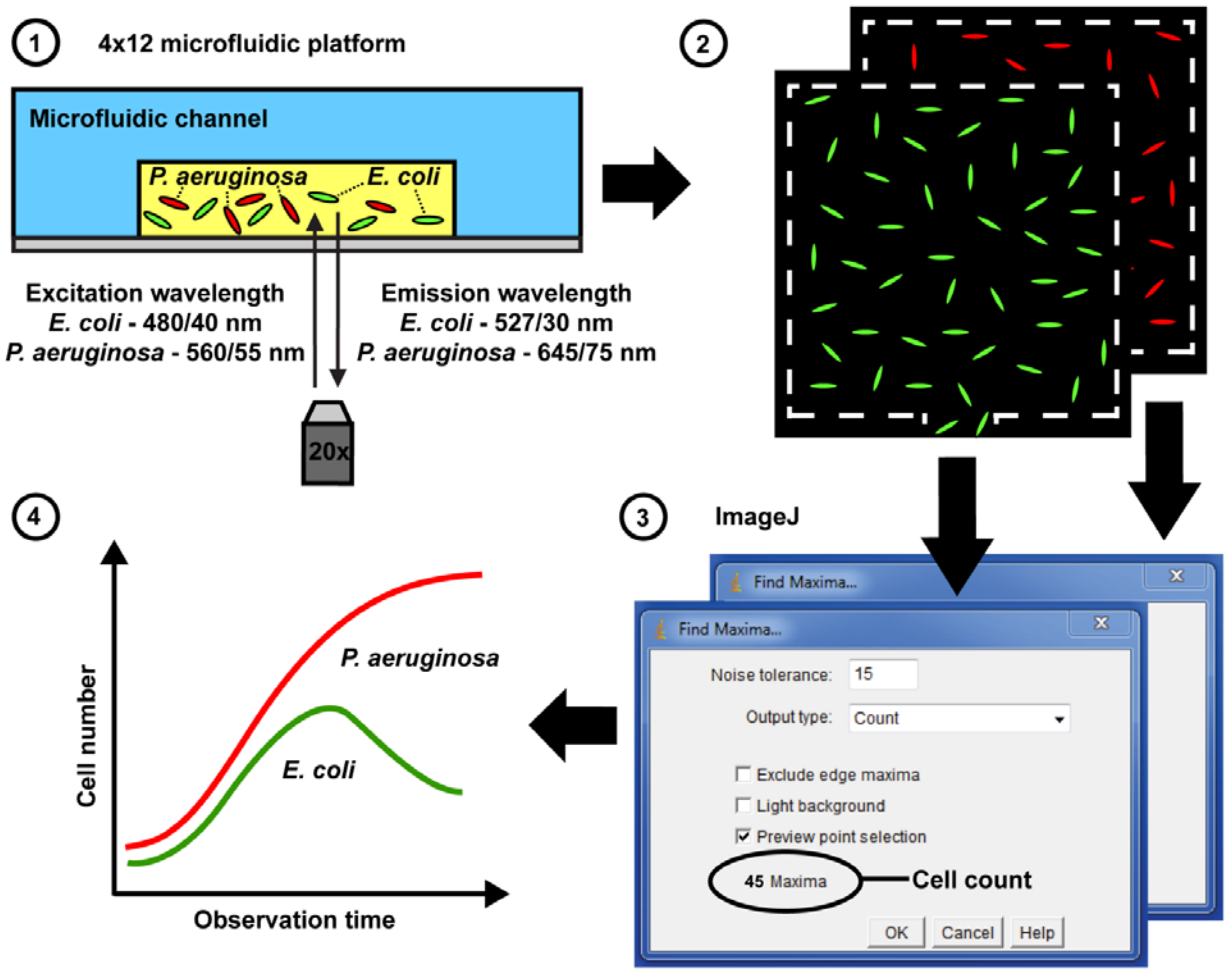

Figure 4.3 A general schematic showing data analysis procedure for AST in polymicrobial cultures using multiplexed microfluidic platform

4.3 Results and Discussion

4.3.1 Design of the microfluidic platform

I developed a two-layer PDMS microfluidic platform for a high-throughput AST (**Fig. 4.4**). The platform comprises (1) a control layer for actuating the mixing and filling valves, and (2) a fluidic layer that houses the flow channels and 48 wells (4.8 nL each). Each well comprises two half-wells that are 400 µm by 400 µm and visualization of the entire well is possible using a

20X objective. Visualization of all bacterial cells in the z direction is ensured with 15 μm tall flow channels, which is approximately equal to the depth of focus of the microscope. For polymicrobial susceptibility testing, each half-well holds bacterial cells of one or more bacterial species and the adjacent half-well holds the antibiotic solutions, so that a set of 12 unique conditions can be tested in quadruplicates (48 experiments) on a single microfluidic platform. In case of bacterial interaction studies, each half-well holds a unique combination of bacterial species in terms of number and/ or type, so that 24 unique conditions can be tested in quadruplicates (96 experiments) on a single platform. Each half-well is isolated from the remaining wells by normally-closed valves, which enhance the portability of the platform by circumventing the need for continuous actuation during the experiment. The current platform design is an improvement over my prior platform[58], with respect to the position of the quadruplicate half-wells such that these wells are equidistant from their respective inlets. This configuration ensures uniform distribution of cell numbers in each of the quadruplicate half-wells due to the equal hydraulic resistance between the inlet and each of the half-well (**Fig. 4.4**).

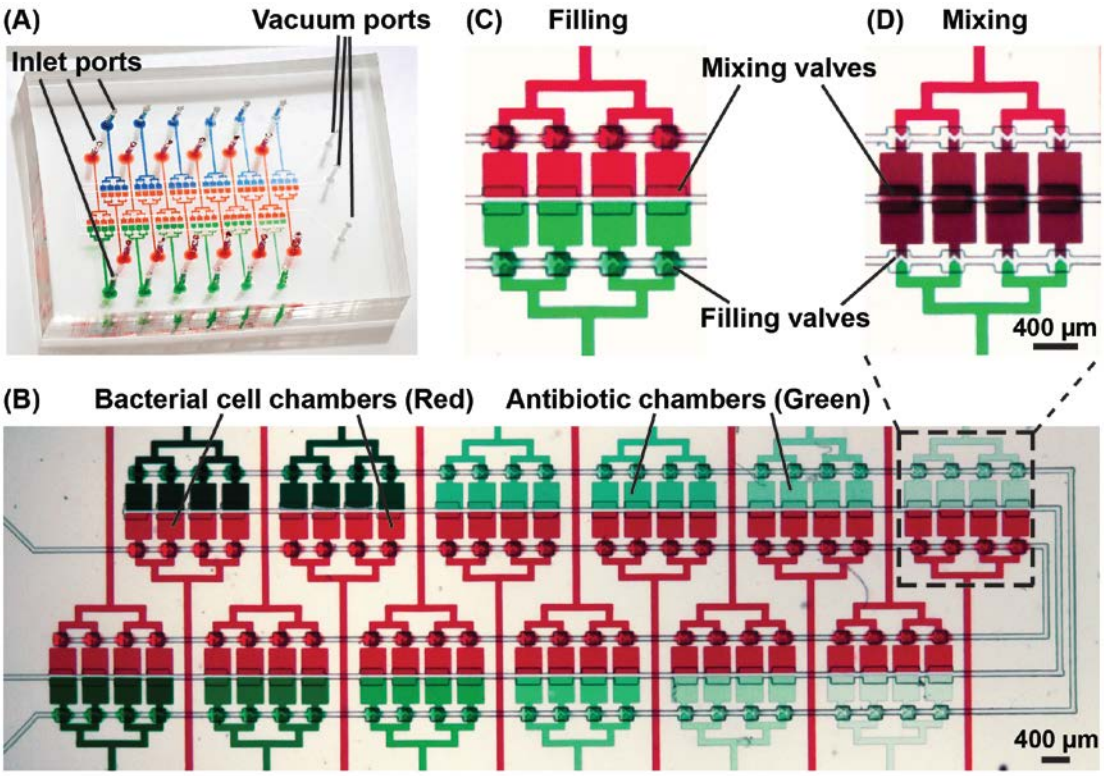

Figure 4.4. Optical micrographs of the high throughput microfluidic platform for quantifying on-chip polymicrobial interactions as well as the susceptibility of bacteria to antibiotics in polymicrobial cultures: **(A)** 48 well-array chip in which each well is comprised of two 2.4 nL half-wells, here filled with dyed aqueous solutions. **(B)** Close up 48-well array able to screen 24 unique conditions in quadruplicates. For example: 12 unique antibiotic concentrations and/or different antibiotic combinations can be loaded in each well through fluid lines (green solutions) and 12 unique polymicrobial bacterial cell solutions can be loaded in the adjacent wells (red solutions). **(C)** Antibiotic and bacterial cell chambers are isolated by mixing valves. **(D)** Same set of wells after opening of the mixing valves, which results in uniform diffusional mixing of the antibiotics and cells in adjacent chambers, here represented by the dark red solution.

I validated the multiplexed microfluidic platform by comparing the MIC of tobramycin and amikacin (**Table 4.2**) obtained on-chip to a conventional AST method (micro-broth dilution), against *E. coli*, a model bacterium, as well as against *P. aeruginosa* and *K. pneumoniae*, which are more clinically-relevant pathogens. The latter two bacteria along with *Enterococcus faecium*, *Staphylococcus aureus*, *Acinetobacter baumanii*, and *Enterobacter* species belong to the ESKAPE category, widely known to "escape" the bactericidal action of antibiotics and are clinically significant since they are known to possess inherit resistance to

several antibiotics[49]. The MIC values obtained using micro-broth dilution (bulk) and on-chip experiments were found to be in close agreement. Occasional discrepancies between bulk and on-chip outcomes can be attributed to the inherent differences in the analysis procedures. For on-chip experiments, the MIC is determined by counting the changes in cell numbers over time, whereas in bulk experiments the MIC is determined by visually detecting changes in bacterial growth (micro-broth dilution method). The key advantages of the microfluidic approach are: the rapid determination of MIC (2 - 4 h) with low sample volumes (< 3 nL), real time monitoring of growth dynamics, high sensitivity (single cell), high-throughput (compared to the current "gold standard" technique for AST, *i.e.*, disk diffusion), amenability to automation, and ease of operation along with enhanced portability. In this work, I utilize this high-throughput microfluidic platform to quantify bacterial interaction over time in the presence and absence of antibiotics.

Table 4.2. Minimum Inhibitory Concentration (MIC) of monomicrobial cultures

	Amikacin [µg mL^{-1}]		**Tobramycin [µg mL^{-1}]**	
	Bulk	**On-chip**	**Bulk**	**On-chip**
E. coli	8	4	8	4
K. pneumoniae	8	8-16	4-8	4-8
P. aeruginosa	2-4	4	2	2

4.3.2 Interaction dynamics of *E. coli* and *P. aeruginosa* (absence of antibiotics)

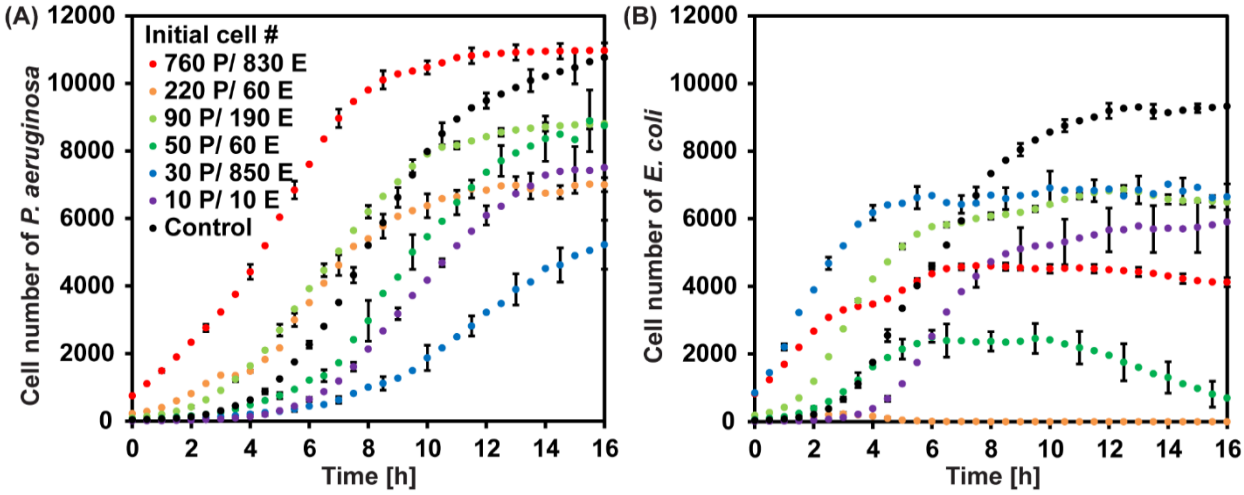

Figure 4.5. On-chip real-time monitoring of cell numbers of *P. aeruginosa* (P) and *E. coli* (E) in the absence of antibiotics for different initial conditions (absolute and relative initial cell numbers of each). Cell growth and death for (A) *P. aeruginosa* and (B) *E. coli* were monitored by counting cells in each well, every 30 minutes, over a period of 16 h. Each data point represents the mean of the measurements from three experiments, and error bars represent the standard error of the mean and are depicted for every third data point for clarity.

Since *P. aeruginosa* and *E. coli* are ubiquitous, they at times occur simultaneously in polymicrobial infections[60]. I employed the microfluidic platform to monitor changes in cell numbers using time-lapse fluorescence microscopy (TLFM) in mixed cultures of *P. aeruginosa* and *E. coli* expressing RFP and GFP, respectively. The use of GFP and RFP as genetically encodable indicators of cell viability has been reported previously[61, 62]. I prepared co-cultures of *P. aeruginosa* and *E. coli* prior to introducing them in the microfluidic platform (**Fig. 4.1**). The co-cultures were prepared such that the initial cell numbers for *P. aeruginosa* and *E. coli* varied across a wide range (10 to 900) for studying diverse cases of bacterial interaction that can occur in mixed infections. The pre-mixed cells were introduced in the microfluidic platform and then TLFM was used to visualize and quantify the cell numbers of the different bacterial species over a period of 16 h (**Fig. 4.5** and **Fig. 4.6**).

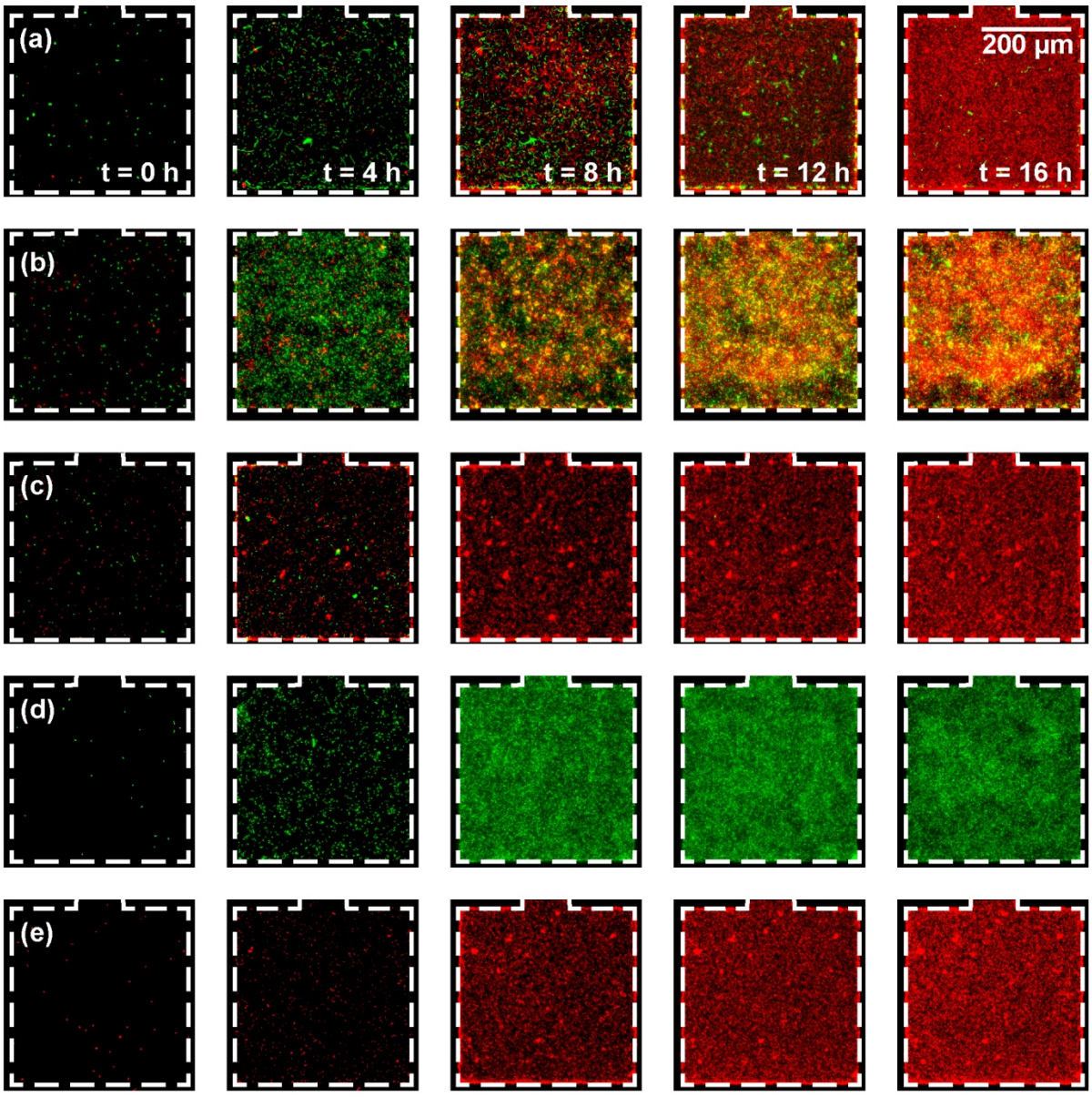

Figure 4.6. Optical micrographs of individual microfluidic wells visualizing changes in cell numbers of *P. aeruginosa* (expressing red fluorescent protein, rfp) and *E. coli* (expressing green fluorescent protein, gfp) in the absence of antibiotics for different initial conditions: initial cell numbers of *P. aeruginosa* and *E. coli* of respectively (a) 50 and 60, (b) 90 and 190, and (c) 220 and 60. (d) and (e): Control experiments, cell growth of monomicrobial solutions of *E. coli* and *P. aeruginosa*, respectively.

I observed that at higher initial cell numbers of *P. aeruginosa* compared to *E. coli* (220 and 60), *E. coli* is completely eradicated within 8 hours (**Fig. 4.5B**). When *P. aeruginosa*'s cell

numbers are higher than *E. coli*, *P. aeruginosa* is hypothesized to produce high concentrations of toxic metabolites such as pyocyanin, which are known to have antimicrobial properties against *E. coli*[63]. I tested this hypothesis by mixing supernatant of an overnight *P. aeruginosa* culture with *E. coli*, and observed drastic reduction in growth of *E. coli* suggesting toxicity of metabolites generated by *P. aeruginosa* against cell cultures of *E. coli* (data not shown). However, in a co-culture of *P. aeruginosa* and *E. coli* when mixed in 1:1 at high (~800) or low (~10) initial cell numbers, I observe an initial growth of *E. coli* followed by growth arrest in 7-8 hours. Similarly, at higher initial cell numbers (~ 190 and 850) of *E. coli* compared to those of *P. aeruginosa* (~90 and 30), the cell growth of *E. coli* levels of at about 6300 after 6 to 8 hours. I attribute these observations to the production of indole by *E. coli*[60]. Indole enables *E. coli* to grow in mixed planktonic populations that includes *P. aeruginosa* by inhibiting pyocyanin production and consequently disrupting quorum sensing in *P. aeruginosa*[60]. In gram negative bacteria, cell-to-cell communication based on density is referred to as quorum sensing, and occurs through the release of fatty-acid-based molecules known as autoinducers (AIs) to coordinate gene expression within a population[64]. At high cell numbers of *E. coli* relative to *P. aeruginosa*, I speculate that sufficiently high accumulation of indole aids in survival and growth of *E. coli* in presence of *P. aeruginosa*.

Interestingly, when starting with ~50 *P. aeruginosa* cells and a similar number of *E. coli* cells (ratio 1:1), *E. coli* first grows for 6 hours (to ~2700 cells), followed by growth arrest for 4 hours and then cell death such that the *E. coli* cell number after 16 hours is ~1000 cells. Here, I speculate that the killing of *E. coli* occurs after 10 hours due to higher cell number of *P. aeruginosa* (~6500) compared to *E. coli* (~2500), which leads to *E. coli* lysis due to accumulation of sufficiently high amounts of toxic metabolites such as pyocyanin. However, the

production of indole by *E. coli* counters the effects of pyocyanin[60], so the *E. coli* population does not get completely eradicated. In the other two cases (90 P, 190 E & 30 P, 850 E) where the initial cell number of *P. aeruginosa* was lower than that of *E. coli*, *E. coli* expectedly does not lyse. The increased viability is probably due to sufficient production of indole by *E. coli* and suppression of pyocyanin production by *P. aeruginosa*, both of which leads to *E. coli's* survival and growth arrest in about 6 h. I also observed that the doubling time of *P. aeruginosa* increases from ~50 minutes in monomicrobial cultures to ~109 minutes in presence of high initial cell numbers of *E. coli* (~850) relative to the number of *P. aeruginosa* cells (~30). This observation is in agreement with recent literature that describes growth inhibition of *P. aeruginosa* in presence of metabolites such as indole produced by *E. coli*[60]. The *results demonstrate that the growth dynamics in co-culture of E. coli and P. aeruginosa depend on their interaction which in turn is dependent on the absolute initial number of cells and the ratio of the initial cell numbers*.

4.3.3 Interaction dynamics of *P. aeruginosa* and *K. pneumoniae* (absence of antibiotics)

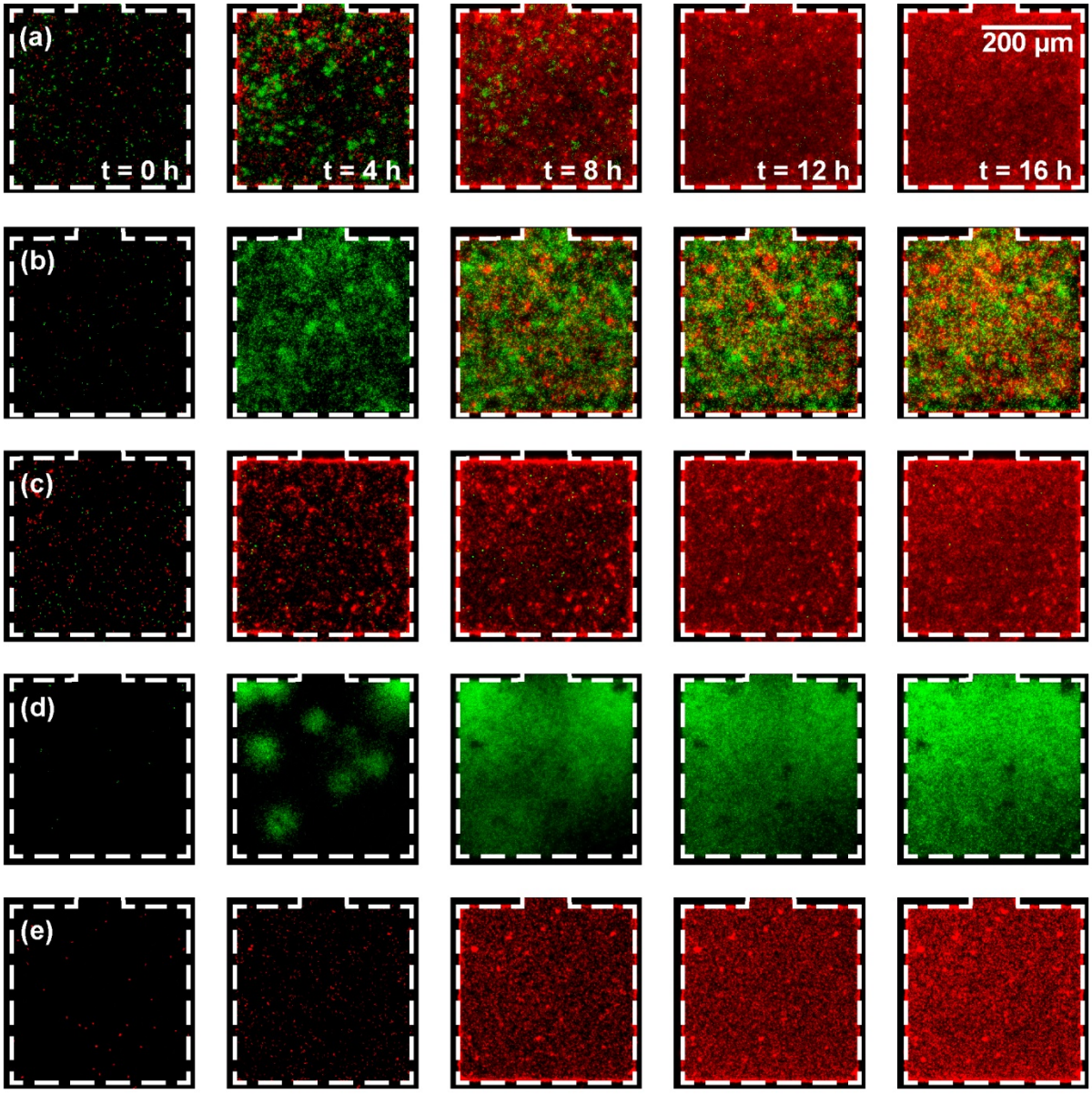

Figure 4.7 Optical micrographs of individual microfluidic wells visualizing changes in cell numbers of *P. aeruginosa* (expressing red fluorescent protein, rfp) and *K. pneumoniae* (expressing green fluorescent protein, gfp) in the absence of antibiotics for different initial conditions: initial cell numbers of *P. aeruginosa* and *K. pneumoniae* of respectively (a) 480 and 370, (b) 170 and 150, and (c) 490 and 130. (d) and (e): Control experiments, cell growth of monomicrobial solutions of *E. coli* and *K. pneumoniae*, respectively.

Study of the dynamics of interaction between *P. aeruginosa* and *K. pneumoniae* is of key interest because several urinary tract infections (UTIs) are known to be polymicrobial communities involving *P. aeruginosa* and *K. pneumoniae* [65] and this co-culture also exists on the perinea of males with spinal cord injuries [66]. Similar to the co-culture studies of *P. aeruginosa* and *E. coli*, I employed the microfluidic platform to monitor changes in cell numbers using time lapse fluorescence microscopy (TLFM) in mixed cultures of *P. aeruginosa* and *K. pneumoniae* expressing RFP and GFP, respectively (**Fig. 4.7** and **Fig. 4.8**). Cultures of mixed bacterial cells were prepared similar to that of *P. aeruginosa* and *E. coli* co-cultures (**Fig. 4.1**). In experiments with low initial cell numbers of *P. aeruginosa* (<200), I observed that the cell number of *K. pneumoniae* increased until a threshold value (~6700), independent of the ratio of the cell numbers, followed by growth arrest between 6-8 hours. However, in experiments with initial cell numbers of *P. aeruginosa* >200, I observe almost complete cell lysis of *K. pneumoniae* after 16 hours irrespective of the initial cell numbers of *K. pneumoniae*. We hypothesize that the different responses of *K. pneumoniae* for different cell numbers are due to the interspecies interaction. When a small number of bacteria release AIs, their concentration is too low to be detected or sensed. However, when a critical cell mass of bacteria are present, the surrounding bacteria are able to sense, and in response, activate transcriptional activator (or R protein), *i.e.*, quorum sensing[67]. I speculate that quorum sensing in this particular co-culture occurs when *P. aeruginosa* is at approximately 200 cells (which correspond to a concentration of ~10^8 cells/mL). This in turn leads to growth arrest after 6-8 h and eventually lysis of *K. pneumoniae*. On the other hand, *K. pneumoniae* is unable to quorum-sense as effectively as *P. aeruginosa* and probably requires a lot more than 3000 cells (1.2 x 10^9 cells/mL) to survive in the presence of *P. aeruginosa* as shown in **Fig. 4.7**. *The results for co-culture of P. aeruginosa and K. demonstrate*

that the growth dynamics is influenced by bacterial interaction which in turn is largely dependent on the initial cell number of P. aeruginosa, but independent of the ratio of their initial cell numbers. This behavior is different from what I observed for the co-cultures of *P. aeruginosa* and *E. coli.*

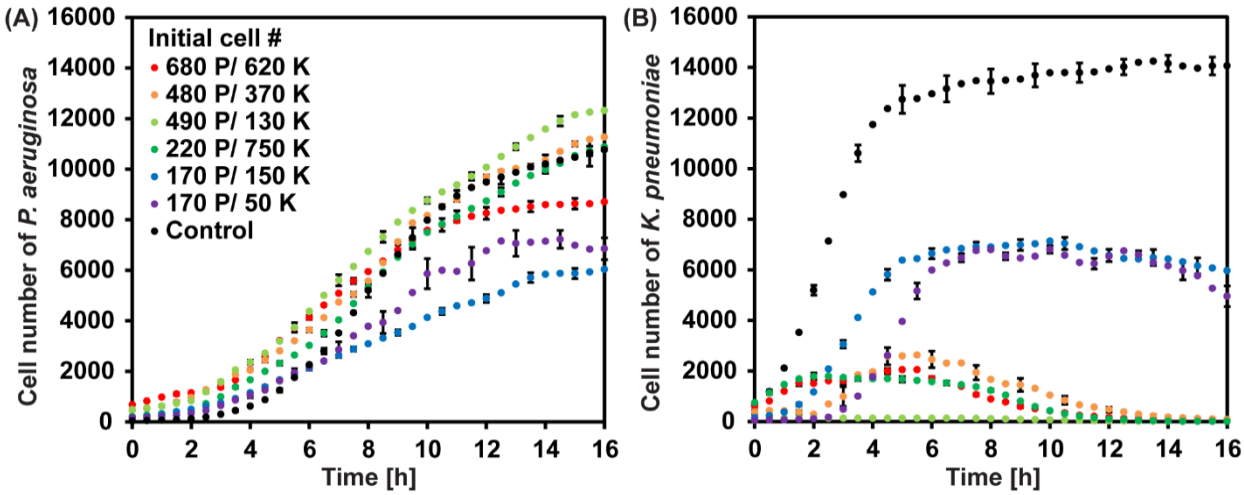

Figure 4.8. On-chip real-time monitoring of cell numbers of *P. aeruginosa* (P) and *K. pneumoniae* (K) in the absence of antibiotics for different initial conditions (absolute and relative initial cell numbers of each). Cell growth and death for (A) *P. aeruginosa* and (B) *K. pneumoniae* were monitored by counting cells in each well, every 30 minutes, over a period of 16 h. Each data point represents the mean of the measurements from three experiments, and error bars represent the standard error of the mean and are depicted for every third data point for clarity.

The co-culture studies indicate significant differences in the growth dynamics of bacteria and these growth dynamics are further dependent upon on bacteria's absolute and relative initial cell numbers in their polymicrobial cultures. Using microfluidics and TLFM, I are able to resolve growth dynamics at different time intervals ranging from growth of cells followed by growth stasis or cell lysis, which could be misinterpreted as solely growth by conventional methods that are typically end point assays.

4.3.4 Antibiotic tolerance in polymicrobial cultures for *P. aeruginosa*

Since *P. aeruginosa* is one of the primary pathogens found in many polymicrobial infections of humans [4], I performed AST against *P. aeruginosa* in co-cultures with *E. coli* and with *K. pneumoniae*, as well as with all three pathogens present (**Table 4.3**). In each experiment, the total initial cell number was set at ~100-300 cells, which corresponds to a cell density of ~10^8 cells/mL, similar to values published in literature for antibiotic susceptibility testing[58]. In these polymicrobial experiments equal cell numbers of each bacterium were mixed to get to an initial number of cells of 100-300. I chose to start all the experiments at roughly similar number of total cells to avoid inoculum effects that can lead to increases in the observed MICs of antibiotics against bacteria, if more are present at the onset[68]. In addition, since inoculum effects do not generally occur with aminoglycosides such as tobramycin and amikacin against *Pseudomonas* species, the increases in the MICs described against *P. aeruginosa* later in this section cannot be attributed to slight changes in total initial cell numbers[69].

I used two commonly used antibiotics (tobramycin and amikacin) against polymicrobial infections involving *P. aeruginosa* and observed that the MIC of *P. aeruginosa* in co-cultures increases 4- to 16-fold compared to isolates (**Table 4.3**). In addition, supra-lethal antibiotic concentrations (as high as 256 μg/mL) failed to cause cell death of all three bacteria in co-culture. Hence, although changes in MIC values for *E. coli* and *K. pneumoniae* in isolate vs. mixed cultures are small (they decrease by a factor of 2 in some cases), the antibiotic tolerance of both the bacteria in co-cultures increased as evident by the inability of high concentrations of the antibiotics (256-512 μg/mL) to kill the bacterial cells. Furthermore, the observed increase in the antibiotic resistance of *P. aeruginosa* in co-cultures corroborates well with literature [30, 44].

Table 4.3. MIC of amikacin and tobramycin obtained on-chip in different mixed cultures

	MIC of Amikacin [μg mL^{-1}]	MIC of Tobramycin [μg mL^{-1}]
Monomicrobial conditions		
E. coli	4	4
K. pneumoniae	8-16	4-8
P. aeruginosa	4	2
Polymicrobial conditions		
E. coli* + *P. aeruginosa		
E. coli	4-8	4
P. aeruginosa	8-16	8-16
K. pneumoniae* + *P. aeruginosa		
K. pneumoniae	4-8	8
P. aeruginosa	8-16	8-16
E. coli* + *K. pneumoniae* + *P. aeruginosa		
P. aeruginosa	16	16-32

Three mechanisms are known to potentially cause the observed increase in antibacterial resistance in co-cultures: (1) the drug is prevented from interacting with the target due to inactivity of antibiotic targets; (2) efflux of the antibiotic from the bacterial cells before they reach their target site of attack; and (3) direct destruction or modification of the antibiotic molecule[70]. The antibiotic resistance mediated by the first mechanism can occur in scenarios such as differences in the metabolic activities of bacteria in co-cultures which in turn can lead to competition for the available nutrients. Bacteria sensing limited nutrients initiates a mechanism known as stringent response, which leads to growth arrest and consequently inactivity of the antibiotic targets (*e.g.*, binding elements such as ribosomal RNA), and thus an increased antibiotic tolerance[71].

With respect to the second mechanism, interspecies communication in bacteria is known to change gene expression patterns, which may cause efflux of antibiotic molecules out of the cell, leading to increased antibiotic resistance. Indeed efflux pump genes in *P. aeruginosa* are known to be up-regulated in co-culture[72].

The third mechanism, the destruction or modification of the antibiotic molecule, may be different in mono- *vs*. co-cultures due to differences in production of molecules that may modify the antibiotic molecule. Induction of novel metabolites being produced as a result of bacterial interactions is in fact an exciting area of study as the specifics of chemistry involved have yet to be fully unraveled[30]. However, already known metabolites that are specific to certain pathogens can be monitored. For example, in the case of *P. aeruginosa*, the increased production of pyocyanin observed in co-cultures with gram positive bacteria (such as *S. aureus*) is often associated with increased virulence[30, 73], whereas a decreased amount of pyocyanin is produced in the presence of bacteria such as *E. coli* ZK126[60]. Furthermore, in co-cultures of *E. coli* and *P. aeruginosa*, increased production of another metabolite, indole, aids in survival of *E. coli*[60].

In the following sections, the objective is to test hypotheses driven by first and third mechanism mentioned above, with the goal to explain apparent increases in antibiotic tolerance that I observe in the polymicrobial experiments. I did not test the second mechanism since it would require extensive gene expression studies, and the screening of specific genes involved in this mechanism is beyond the scope of this study.

4.3.5 Antibiotic tolerance in nutrient deficit medium

Bacteria in co-cultures have to compete for resources and often inherently differ in their metabolic rates. Hence, after a certain period of time, the bacteria may encounter a limit in the amount of remaining available nutrients. In literature, bacteria have been shown to become highly tolerant to antibiotics when nutrients are limited[71], which can be problematic, because antibiotics are effective only on actively growing cells[74]. In other words, nutrient limitation leads to growth arrest or slow growth, rendering the antibiotics ineffective even at supra-lethal

concentrations. I observed an increase in doubling time of *P. aeruginosa* in mixed culture experiments, a clear indication of slower growth. One of the reasons for this slower growth is the competition for limited resources in presence of other bacteria. Hence, the reduced growth of *P. aeruginosa* indeed may result from limited resources, which leads to activation of stringent response [71]. The resulting increased antibiotic tolerance is evident from the observed increase in MIC values against *P. aeruginosa* in polymicrobial cultures evaluated on-chip, as well as from failure to kill the bacterial cells even at high concentrations (> 256 μg/mL). To confirm this hypothesis, I compared the MIC values against *P. aeruginosa* observed in the polymicrobial on-chip experiments to the MIC values against *P. aeruginosa* observed in monomicrobial cultures in nutrient-rich and nutrient-poor media (**Table 4.4**). I observed increases by factors of 16 to 32 in the MIC of the antibiotics amikacin and tobramycin against *P. aeruginosa* in nutrient-poor medium, which validates the hypothesis of the first mechanism. Similar results were observed for *K. pneumoniae* and *E. coli* in nutrient-poor medium. Hence, activation of stringent response due to competition of resources in polymicrobial cultures is a possible reason for the observed increase in antibiotic resistance.

Table 4.4. Minimum Inhibitory Concentration (MIC) of *P. aeruginosa* in poor (M-9) medium

	Bulk MIC [μg mL^{-1}]	**On chip MIC [μg mL^{-1}]**
Amikacin	16	16
Tobramycin	16-32	64

4.3.6 Effect of pyocyanin on susceptibility of *P. aeruginosa*

Next, I tested whether virulence in co-cultures due to pyocyanin production has a correlation with increased antibiotic resistance (mechanism three, see above). Specifically, I hypothesized that an increased antibiotic tolerance of *P. aeruginosa* could be due to increased

production of pyocyanin, which is the major virulent factor produced by *P. aeruginosa* and acts as a signaling factor in quorum sensing of the pathogen to protect itself from other surrounding species[4]. When quantifying the concentrations of pyocyanin in monomicrobial and polymicrobial cultures, I observed a significant decrease in its production in case of co-cultures of *P. aeruginosa* & *E. coli*, *P. aeruginosa* & *K. pneumoniae*, and in a co-culture of all three bacteria compared to pyocyanin production in monomicrobial cultures of *P. aeruginosa* (**Table 4.5**). These results demonstrate that lower virulence (reduction in production of pyocyanin) does not imply a decrease or an increase in the antibiotic tolerance. Since the production of pyocyanin is *suppressed* in co-cultures, it appears that change in production of pyocyanin is not responsible for the resulting increases in antibiotic tolerance, as the decreased production should have led to decreased MIC values, which is contrary to my observations.

Table 4.5. Effect of mixed population on production of pyocyanin by *P. aeruginosa*

Initial conditions [cells mL^{-1}]			Pyocyanin concentration [µg mL^{-1}]
P. aeruginosa	***E. coli***	***K. pneumoniae***	
P. aeruginosa			
$35x10^{6}$	-	-	25.5 ± 6.0
P. aeruginosa + E. coli			
$35x10^{6}$	$125x10^{6}$	-	3.5 ± 4.7
$35x10^{6}$	$60x10^{6}$	-	2.3 ± 1.5
$35x10^{6}$	$30x10^{6}$	-	3.2 ± 1.5
P. aeruginosa + K. pneumoniae			
$35x10^{6}$	-	$310x10^{6}$	11.0 ± 4.8
$35x10^{6}$	-	$160x10^{6}$	15.6 ± 3.6
$35x10^{6}$	-	$80x10^{6}$	18.3 ± 4.4

4.3.7 Effect of indole on the susceptibility of P. aeruginosa

As the production of indole is known to aid in the survival and growth of *E. coli* in co-cultures by inhibiting quorum sensing in *P. aeruginosa* [60], I explored this effect on the

susceptibility of *P. aeruginosa*. To simulate the effect of increased indole production in co-cultures, I determined the MIC of tobramycin and amikacin against monomicrobial cultures of *P. aeruginosa* in the presence of varying concentrations of indole (500 µm to 5 mM) (**Table 4.6**). The experiments showed that the presence of indole at physiologically relevant concentrations (500 µm to 1 mM) had negligible effect on the MIC values against *P. aeruginosa* and concentrations >= 5 mM of indole were toxic to both *P. aeruginosa* and *E. coli*[60]. Furthermore, the production of pyocyanin decreased as expected based on the color of the overnight culture. *These observations suggest that, although indole suppresses the production of pyocyanin in P. aeruginosa, the presence of indole by itself is not necessarily responsible for the higher antibiotic tolerance observed in P. aeruginosa.*

Table 4.6. Minimum Inhibitory Concentration (MIC) of *P. aeruginosa* with indole concentration ranging from 500 µM-1 mM

	Bulk MIC [µg mL^{-1}]	**On chip MIC [µg mL^{-1}]**
Amikacin	2-4	2-4
Tobramycin	2	2

4.4 Conclusions

Here, I reported a multiplexed microfluidic platform for quantification of interactions between *P. aeruginosa, E. coli,* and *K. pneumoniae* in the presence and absence of antibiotics. This approach allows for the study of species-specific antibiotic susceptibility information and real-time monitoring of bacterial interaction, a seemingly neglected aspect in studying polymicrobial infections. Furthermore, these types of experiments are challenging to perform using conventional techniques. The current practice often involves extrapolating monomicrobial AST results to determine treatment of polymicrobial infections. In contrast, the approach reported here offers the potential to prescribe an appropriate antibiotic dosing regimen in a

timely fashion based on polymicrobial AST results. In addition, the technique presents an opportunity to study dynamic bacterial interactions for extended periods of time. Notably, the existing conventional methods are standardized only for monomicrobial susceptibility and possess several limitations including the use of large sample volumes, time consuming steps, low sensitivity, and inability to provide bacterial species specific susceptibility information.

The results demonstrate that the growth dynamics of bacteria in polymicrobial cultures depend on bacterial interactions, the starting cell numbers, and the ratio of starting cell numbers. The antibiotic tolerance of *P. aeruginosa* increases in mixed populations significantly, highlighting the need to standardize polymicrobial AST. Since polymicrobial interactions are widely dependent upon the type and the number of bacteria, technologies to study these interactions need to be developed for better clinical treatment of polymicrobial infections.

In summary, the microfluidic platform presented not only enables fundamental investigations correlations between bacterial interactions and antibiotic tolerance, but also has the potential to serve as a clinical diagnostic platform for determining AST in polymicrobial infections. The microfluidic approach reported here relies on genetically modified bacteria to ensure compatibility with TLFM analysis, which is not appropriate to analyze clinical samples. In chapter 6, I have tried to address this drawback by using optimized optical dyes for long-term monitoring of wild-type bacterial growth dynamics.

Finally, the ability of the platform to perform long-term polymicrobial cell studies in multiplexed fashion may also have significant potential in the field of microbiology, for example to study responses of mixed bacterial populations to external stresses.

4.5 References

1. Straight, P.D. and R. Kolter, Interspecies chemical communication in bacterial development. Annual Review of Microbiology, 2009. 63: p. 99-118.
2. West, S.A., et al., Social evolution theory for microorganisms. Nature Reviews Microbiology, 2006. 4(8): p. 597-607.
3. Brogen, K.A. and J.M. Guthmiller, Polymicrobial diseases. 2002: ASM Press.
4. Korgaonkar, A., et al., Community surveillance enhances Pseudomonas aeruginosa virulence during polymicrobial infection. Proceedings of the National Academy of Sciences, 2013. 110(3): p. 1059-1064.
5. Hibbing, M.E., et al., Bacterial competition: Surviving and thriving in the microbial jungle. Nature Reviews Microbiology, 2010. 8(1): p. 15-25.
6. Weinstein, M.P., L.B. Reller, and J.R. Murphy, Clinical importance of polymicrobial bacteremia. Diagnostic Microbiology and Infectious Disease, 1986. 5(3): p. 185-196.
7. Kiani, D., et al., THe increasing importance of polymicrobial bacteremia. JAMA, 1979. 242(10): p. 1044-1047.
8. McKenzie, F.E., Case mortality in polymicrobial bloodstream infections. Journal of Clinical Epidemiology, 2006. 59(7): p. 760-761.
9. Brown, S.P., M.E. Hochberg, and B.T. Grenfell, Does multiple infection select for raised virulence? Trends in Microbiology, 2002. 10(9): p. 401-405.
10. Cillóniz, C., et al., Community-acquired polymicrobial pneumonia in the intensive care unit: aetiology and prognosis. Critical care (London, England), 2011. 15(5).
11. Wessel, A.K., et al., Going local: Technologies for exploring bacterial microenvironments. Nature Reviews Microbiology, 2013. 11(5): p. 337-348.
12. Ryan, R.P. and J.M. Dow, Diffusible signals and interspecies communication in bacteria. Microbiology, 2008. 154(7): p. 1845-1858.
13. Gupta, P., et al., Clinical significance of polymicrobial bacteremia in newborns. Journal of Paediatrics and Child Health, 2005. 41(7): p. 365-368.
14. Marra, A.R., et al., Comparison of the systemic inflammatory response syndrome between monomicrobial and polymicrobial Pseudomonas aeruginosa nosocomial bloodstream infections. BMC Infectious Diseases, 2005. 5.
15. Park, S.Y., et al., Clinical significance and outcome of polymicrobial Staphylococcus aureus bacteremia. Journal of Infection, 2012. 65(2): p. 119-127.
16. Levy, S.B. and B. Marshall, Antibacterial resistance worldwide: Causes, challenges and responses. Nature Medicine, 2004. 10(12 SUPPL.): p. S122-S129.
17. Riedele, C. and U. Reichl, Interspecies effects in a ceftazidime-treated mixed culture of Pseudomonas aeruginosa, Burkholderia cepacia and Staphylococcus aureus: analysis at the single-species level. Journal of Antimicrobial Chemotherapy, 2011. 66(1): p. 138-145.
18. Riedele, C. and U. Reichl, Time-kill studies with a ceftazidime-treated mixed culture consisting of Pseudomonas aeruginosa, Burkholderia cepacia and Staphylococcus aureus. Engineering in Life Sciences, 2012. 12(2): p. 188-197.
19. Lazcka, O., F.J.D. Campo, and F.X. Muñoz, Pathogen detection: A perspective of traditional methods and biosensors. Biosensors and Bioelectronics, 2007. 22(7): p. 1205-1217.
20. White, R.L., et al., Comparison of three different in vitro methods of detecting synergy: Time-kill, checkerboard, and E test. Antimicrobial Agents and Chemotherapy, 1996. 40(8): p. 1914-1918.

21. El-Halfawy, O.M. and M.A. Valvano, Chemical Communication of Antibiotic Resistance by a Highly Resistant Subpopulation of Bacterial Cells. PLoS ONE, 2013. 8(7).
22. Schmidt, J.K., B. König, and U. Reichl, Characterization of a three bacteria mixed culture in a chemostat: Evaluation and application of a quantitative terminal-restriction fragment length polymorphism (T-RFLP) analysis for absolute and species specific cell enumeration. Biotechnology and Bioengineering, 2007. 96(4): p. 738-756.
23. Avis, P.G., I.A. Dickie, and G.M. Mueller, A 'dirty' business: testing the limitations of terminal restriction fragment length polymorphism (TRFLP) analysis of soil fungi. Molecular Ecology, 2006. 15(3): p. 873-882.
24. Heilmann, F., Ampicillin and ampicillin-sulbactam dilution tests with mixed culture of Bacteroides fragilis, Escherichia coli and Enterococcus. Infection, 1993. 21(3): p. 187-190.
25. Heizmann, W.R., et al., Efficacy of sulbactam in an in vitro model of mixed aerobic/anaerobic infections. Infection, 1990. 18(2): p. 117-121.
26. Werner, H., et al., Efficacy of clavulanate-potentiated antibiotics against Bacteroides species and artificially associated cultures of aerobes and anaerobes. Journal of Antimicrobial Chemotherapy, 1989. 24(SUPPL. B): p. 55-61.
27. Diggle, S.P., Microbial communication and virulence: Lessons from evolutionary theory. Microbiology, 2010. 156(12): p. 3503-3512.
28. Oh, D.-C., et al., Libertellenones A–D: Induction of cytotoxic diterpenoid biosynthesis by marine microbial competition. Bioorganic & Medicinal Chemistry, 2005. 13(17): p. 5267-5273.
29. Oh, D.-C., et al., Induced Production of Emericellamides A and B from the Marine-Derived Fungus Emericella sp. in Competing Co-culture. Journal of Natural Products, 2007. 70(4): p. 515-520.
30. Shank, E.A. and R. Kolter, New developments in microbial interspecies signaling. Current Opinion in Microbiology, 2009. 12(2): p. 205-214.
31. Yeo, L.Y., et al., Microfluidic Devices for Bioapplications. Small, 2011. 7(1): p. 12-48.
32. Mu, X., et al., Microfluidics for Manipulating Cells. Small, 2013. 9(1): p. 9-21.
33. Gan, M., et al., Massively Parallel Bacterial and Yeast Suspension Culture on a Chip. Small, 2012. 8(6): p. 863-867.
34. Zheng, Y., et al., Recent advances in microfluidic techniques for single-cell biophysical characterization. Lab on a Chip, 2013. 13(13): p. 2464-2483.
35. Wu, J., X. Wu, and F. Lin, Recent developments in microfluidics-based chemotaxis studies. Lab on a Chip, 2013. 13(13): p. 2484-2499.
36. Dmytryshyn, B. Microfluidic cell culture systems and cellular analysis. 2011.
37. Lagus, T.P. and J.F. Edd, A review of the theory, methods and recent applications of high-throughput single-cell droplet microfluidics. Journal of Physics D: Applied Physics, 2013. 46(11).
38. Breslin, S. and L. O'Driscoll, Three-dimensional cell culture: The missing link in drug discovery. Drug Discovery Today, 2013. 18(5-6): p. 240-249.
39. Gao, D., et al., Recent developments in microfluidic devices for in vitro cell culture for cell-biology research. TrAC - Trends in Analytical Chemistry, 2012. 35: p. 150-164.
40. Moraes, C., et al., Organs-on-a-Chip: A focus on compartmentalized microdevices. Annals of Biomedical Engineering, 2012. 40(6): p. 1211-1227.
41. Mitchell, R.J., et al., Microbial linguistics: Perspectives and applications of microbial cell-to-cell communication. BMB Reports, 2011. 44(1): p. 1-10.

42. Park, S., et al., A microfluidic concentrator array for quantitative predation assays of predatory microbes. Lab on a Chip, 2011. 11(17): p. 2916-2923.
43. Park, J., et al., Microdroplet-Enabled Highly Parallel Co-Cultivation of Microbial Communities. PLoS ONE, 2011. 6(2): p. e17019.
44. Connell, J.L., et al., Probing prokaryotic social behaviors with bacterial "lobster traps". mBio, 2010. 1(4).
45. Boedicker, J.Q., M.E. Vincent, and R.F. Ismagilov, Microfluidic Confinement of Single Cells of Bacteria in Small Volumes Initiates High-Density Behavior of Quorum Sensing and Growth and Reveals Its Variability. Angewandte Chemie International Edition, 2009. 48(32): p. 5908-5911.
46. Chen, C.H., et al., Antimicrobial Susceptibility Testing Using High Surface-to-Volume Ratio Microchannels. Analytical Chemistry, 2010. 82(3): p. 1012-1019.
47. Churski, K., et al., Rapid screening of antibiotic toxicity in an automated microdroplet system. Lab on a Chip, 2012. 12(9): p. 1629-1637.
48. Cira, N.J., et al., A self-loading microfluidic device for determining the minimum inhibitory concentration of antibiotics. Lab on a Chip, 2012. 12(6): p. 1052-1059.
49. Ho, J.Y., et al., Rapid Identification of ESKAPE Bacterial Strains Using an Autonomous Microfluidic Device. PLoS ONE, 2012. 7(7): p. e41245.
50. Kalashnikov, M., et al., A microfluidic platform for rapid, stress-induced antibiotic susceptibility testing of Staphylococcus aureus. Lab on a Chip, 2012. 12(21): p. 4523-4532.
51. Sun, P., et al., High-throughput microfluidic system for long-term bacterial colony monitoring and antibiotic testing in zero-flow environments. Biosensors and Bioelectronics, 2011. 26(5): p. 1993-1999.
52. Choi, J., et al., Rapid antibiotic susceptibility testing by tracking single cell growth in a microfluidic agarose channel system. Lab on a Chip, 2013. 13(2): p. 280-287.
53. Theberge, A.B., et al., Microdroplets in Microfluidics: An Evolving Platform for Discoveries in Chemistry and Biology. Angewandte Chemie International Edition, 2010. 49(34): p. 5846-5868.
54. Mukherjee, A., et al., Characterization of Flavin-Based Fluorescent Proteins: An Emerging Class of Fluorescent Reporters. PLoS ONE, 2013. 8(5): p. e64753.
55. Chelius, M.K. and E.W. Triplett, Immunolocalization of dinitrogenase reductase produced by Kiebsiella pneumoniae in association with Zea mays L. Applied and Environmental Microbiology, 2000. 66(2): p. 783-787.
56. Shanks, R.M.Q., et al., New yeast recombineering tools for bacteria. Plasmid, 2009. 62(2): p. 88-97.
57. Essar, D.W., et al., Identification and characterization of genes for a second anthranilate synthase in Pseudomonas aeruginosa: interchangeability of the two anthranilate synthases and evolutionary implications. Journal of Bacteriology, 1990. 172(2): p. 884-900.
58. Mohan, R., et al., A multiplexed microfluidic platform for rapid antibiotic susceptibility testing. Biosensors and Bioelectronics, 2013. 49(0): p. 118-125.
59. Jorgensen, J.H. and M.J. Ferraro, Antimicrobial susceptibility testing: A review of general principles and contemporary practices. Clinical Infectious Diseases, 2009. 49(11): p. 1749-1755.
60. Chu, W., et al., Indole production promotes escherichia coli mixed-culture growth with Pseudomonas aeruginosa by inhibiting quorum signaling. Applied and Environmental Microbiology, 2012. 78(2): p. 411-419.

61. Keymer, J.E., et al., Bacterial metapopulations in nanofabricated landscapes. Proceedings of the National Academy of Sciences of the United States of America, 2006. 103(46): p. 17290-17295.
62. Shaner, N.C., P.A. Steinbach, and R.Y. Tsien, A guide to choosing fluorescent proteins. Nature Methods, 2005. 2(12): p. 905-909.
63. Baron, S.S. and J.J. Rowe, Antibiotic action of pyocyanin. Antimicrobial Agents and Chemotherapy, 1981. 20(6): p. 814-820.
64. Hughes, D.T. and V. Sperandio, Inter-kingdom signalling: Communication between bacteria and their hosts. Nature Reviews Microbiology, 2008. 6(2): p. 111-120.
65. Jacobsen, S.M., et al., Complicated catheter-associated urinary tract infections due to Escherichia coli and Proteus mirabilis. Clinical Microbiology Reviews, 2008. 21(1): p. 26-59.
66. Gilmore, D.S., D.G. Schick, and J.Z. Montgomerie, Pseudomonas aeruginosa and Klebsiella pneumoniae on the perinea of males with spinal cord injuries. Journal of Clinical Microbiology, 1982. 16(5): p. 865-867.
67. De Kievit, T.R. and B.H. Iglewski, Bacterial quorum sensing in pathogenic relationships. Infection and Immunity, 2000. 68(9): p. 4839-4849.
68. Bidlas, E., T. Du, and R.J.W. Lambert, An explanation for the effect of inoculum size on MIC and the growth/no growth interface. International Journal of Food Microbiology, 2008. 126(1-2): p. 140-152.
69. Brook, I., Inoculum Effect. Review of Infectious Diseases, 1989. 11(3): p. 361-368.
70. Wright, G.D., Bacterial resistance to antibiotics: Enzymatic degradation and modification. Advanced Drug Delivery Reviews, 2005. 57(10): p. 1451-1470.
71. Nguyen, D., et al., Active Starvation Responses Mediate Antibiotic Tolerance in Biofilms and Nutrient-Limited Bacteria. Science, 2011. 334(6058): p. 982-986.
72. Duan, K., et al., Modulation of Pseudomonas aeruginosa gene expression by host microflora through interspecies communication. Molecular Microbiology, 2003. 50(5): p. 1477-1491.
73. Vega, N.M., et al., Salmonella typhimurium intercepts Escherichia coli signaling to enhance antibiotic tolerance. Proceedings of the National Academy of Sciences of the United States of America, 2013. 110(35): p. 14420-14425.
74. Jass, J. and H.M. Lappin-Scott, The efficacy of antibiotics enhanced by electrical currents against Pseudomonas aeruginosa biofilms. Journal of Antimicrobial Chemotherapy, 1996. 38(6): p. 987-1000.

Chapter 5

Pharmacodynamic/Pharmacokinetics modeling using microfluidics

5.1 Introduction

Three goals must be met for an optimal antibiotic treatment: (1) maximized rate of clearance of an infection, (2) minimized toxicity and side effects, and (3) minimized likelihood of resistance ascending and being transmitted during the course of therapy [1]. To achieve the above three goals, the clinician is required to determine optimal drug or drug combination effective against the pathogen, optimal dose and dosing regimen (frequency of administration), and an optimal term of treatment. As described in previous section, MIC is the most commonly used parameter in AST to describe the efficacy of an antibiotic against a specific bacterial strain and is often reported in a "range" format where the acceptable range can vary by two-folds. However, MIC is not an optimal parameter since it reflects only a range estimate of the effect of antibiotic on the bacteria and does not take the time course of the effect into account [2]. In fact, the use of MIC alone to determine antibiotic treatment regimens has led to prescription of sub-lethal concentrations of antibiotics for several years [3], leading to increased antibiotic resistance. Consequently, determination of optimal antibiotic regimen based on superior metrics is important to address the issue of antibiotic resistance [4]. Hence, studies on pharmacodynamics are increasing in the hopes of establishing new breakpoints to clear bacterial infection effectively, thereby minimize the spread of antibiotic resistance.

Pharmacodynamics (PD) analysis of time kill curves can be used to precisely determine the MIC (instead of a range) in conjunction with other PD parameters, which provides time-dependent information on the effect of antibiotics on bacteria [3, 5-7] and an understanding of

the PD characteristics can provide insights into the optimal regimen for antibiotics [8]. For instance, for concentration-dependent antibiotics, a high once-daily dose is the best way to eradicate pathogens, while for concentration-independent drugs, the goal is to maximize the duration of antibiotic exposure above MIC at the site of infection [3]. Due to differences in the PD properties, antibiotics with same MIC can behave differently. The PD parameters can further be used to perform pharmacokinetic (PK) modeling for predicting *in vivo* antibiotic dosing regimen. Although, the right choice of antibiotic (determined by MIC) is important in treating bacterial infections, the optimum dose and dosing interval (determined by PK/PD analysis) is critical for achieving optimal clinical responses to prevent the emergence of resistant pathogens.

Several models have been explored for PD analysis of antibiotics [2-7, 9-11], where the advantages of PD analysis to better predict clinical outcomes have been demonstrated. In a typical PD analysis, first, *in-vitro* time-kill curves (number of bacteria as a function of time) for varying antibiotic concentrations are acquired. Then, models such as the Zhi modeling methods are used to fit the data and determine PD parameters such as (1) the ratio of C_{max} to MIC (C_{max}:MIC), (2) the ratio of the drug's AUC to MIC (AUC:MIC), and (3) the time the drug concentration exceeds the MIC (T>MIC), where C_{max} is the drug's peak concentration and AUC is area under the plasma concentration-time curve [7]. These parameters could then be used to predict the optimal antibiotic dosing regimen therapy.

Microfluidics provides several advantages for such PD analysis. First, microfluidics enables automated, rapid, generation of precise time-kill curves (cell number *vs.* time) without the need to manually collect samples every 30 minutes to estimate the change in bacterial counts, and the high sensitivity enables knowing precise quantitative information about cell numbers at different time points. Hence, this feature also increases the temporal resolution of the technique

allowing us to more effectively discern the dynamics of antibiotic-bacteria interactions. Second, microfluidics provides capabilities for high-throughput, multiplexed screening allowing us to test a large number of antibiotic concentrations and/or combinations. This capability further enables acquisition of more data compared to conventional methods, which will lead to more accurate data-fitting and consequently more accurate prediction of PD parameters. Third, the ability to perform rapid, high-throughput analysis with low sample volumes will enable determination of patient-specific PD parameters. This specificity is important as significant variation exists between response of different individuals to the same antibiotic regimen, which precludes the universal application of empirical results [6]. Motivated by these advantages, researchers have explored the use of microfluidic platforms to better predict the *in vivo* effect of several drugs including antibiotics [12-15]. Hence, microfluidics has the potential to significantly impact the field of AST by enabling faster and more accurate PD analysis of the effect of antibiotics on bacteria.

The antibiotic concentration in bloodstream decreases exponentially after injection due to the excretion mechanisms in the human body. Hence, in cases of bacterial infection, several antibiotic doses over a time period are needed to keep the drug concentration above MIC to effectively inhibit bacterial growth. While pharmacodynamics modeling provides precise effective antibiotic concentration, it cannot predict the change of antibiotic concentration over time *in vivo* resulting in a transient growth of bacteria. Pharmacokinetics can effectively address the issue by describing the relationship between antibiotic concentration and bacterial growth/death rate as a function of time. The values of MIC, growth rate constant, maximum killing rate, and Hill coefficient derived from pharmacodynamics modeling are generally employed to construct the pharmacokinetics model [8]. We utilized the precise parameters

obtained from the microfluidic platform to construct proof-of-concept pharmacokinetic models in monomicrobial cultures of *P. aeruginosa*. The modeling concept can further be extended to polymicrobial susceptibility results for treating polymicrobial infections. In this chapter, I will discuss the pharmacokinetics modeling procedure for amikacin and tobramycin against *P. aeruginosa* cultures.

5.2 Materials and Methods

Proof-of-concept PD model was developed to determine precise values of MIC. **Fig. 5.1** describes the general flow of how an antibiotic dosing regimen can be predicted from PK/PD modeling.

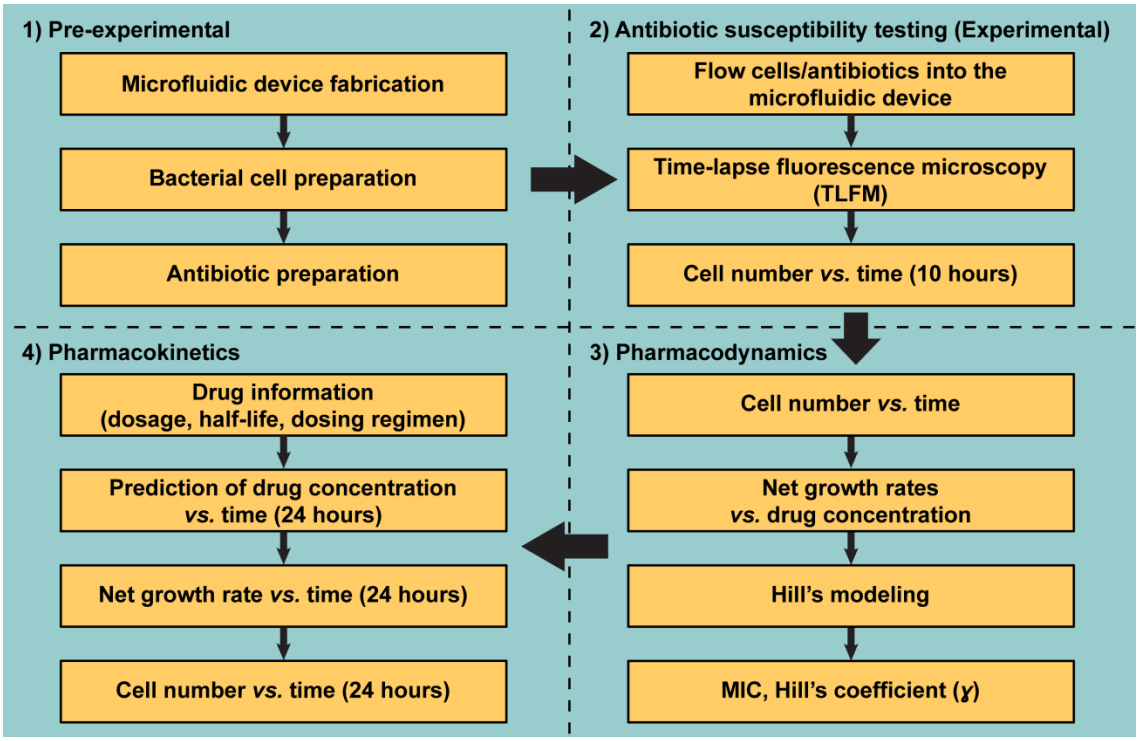

Figure 5.1 Illustration of steps leading to prediction of cell numbers *in vivo* using high-throughput microfluidic platform with a prescribed antibiotic dosing regimen. The main steps include (1) pre-experimental set-up such as fabrication of microfluidic platforms and sample (cell) preparation, (2) antibiotic susceptibility testing, entailing derivation of time-kill curves, (3) pharmacodynamic modeling to determine parameters *in vitro*, and (4) pharmacokinetic modeling to predict *in vivo* action of the antibiotics on bacterial cell numbers over time

5.2.1 Hills modeling

Hill's modeling was used to determine the precise MIC and the Hill coefficient values in monomicrobial and polymicrobial cultures since this type of modeling has been commonly used in pharmacodynamics [16]. In order to simplify the model, the antibiotics concentration is assumed to be constant inside microfluidic chambers over the experiment duration (no absorption into PDMS) [17]. Monomicrobial growth model in presence of an antibiotic can be described by the following equation [8]:

$$\frac{dB}{dt} = (G - K_t) \cdot B, \tag{5.1}$$

where B is the cell number in a microfluidic chamber, G is the growth rate constant in exponential phase in absence of the antibiotic [h^{-1}], and K_t is the bacterial killing rate in presence of the antibiotic at time t [h^{-1}]. The bacterial killing rate constant, K_t, can be expressed by the sigmoid $E_{\max}$ model [18]:

$$K_t = \frac{K_{\max} \cdot C_t^{\gamma}}{C_{50}^{\gamma} + C_t^{\gamma}}, \tag{5.2}$$

where C_t [μg mL^{-1}] is the antibiotic concentration at time t, K_{max} [h^{-1}] is the maximum bacterial killing rate for an antibiotic, C_{50} [μg mL^{-1}] is the concentration corresponding to the time when the maximum bacterial killing rate is half, and γ is the Hill coefficient.

At MIC, the net growth rate of bacteria is zero, hence, the concentration, C_t, is equal to MIC. This implies that bacterial killing rate constant, K_t, is equal to the growth rate constant, G, at MIC which is given by the following expression:

$$G = \frac{K_{\max} \cdot MIC^{\gamma}}{C_{50}^{\gamma} + MIC^{\gamma}}. \tag{5.3}$$

Hence,

$$C_{50} = MIC \cdot \sqrt[\gamma]{\frac{K_{\max} - G}{G}}. \tag{5.4}$$

Substituting the value of C_{50} (**Equation 5.4**) in to **Equation 5.3** and rearranging, we obtain the following equation:

$$\ln\left(\frac{K_t \cdot (K_{\max} - G)}{G\left(K_{\max} - K_t\right)}\right) = \gamma \ln C_t - \ln(MIC^{\gamma}) \tag{5.5}$$

Using the above expression, γ can be calculated from the slope of the equation, and the MIC from the intercept [$-\ln(MIC^{\gamma})$].

The antibiotic concentration in bloodstream decreases exponentially after injection due to the excretion mechanisms in the human body. Hence, in cases of bacterial infection, several antibiotic doses over a time period are needed to keep the drug concentration above MIC to effectively inhibit bacterial growth. While pharmacodynamics modeling provides precise effective antibiotic concentration, it cannot predict the change of antibiotic concentration over time *in vivo* resulting in a transient growth of bacteria. Pharmacokinetics can effectively address the issue by describing the relationship between antibiotic concentration and bacterial growth/death rate as a function of time. The values of MIC, growth rate constant, maximum killing rate, and Hill coefficient derived from pharmacodynamics modeling are generally employed to construct the pharmacokinetics model [8]. We utilized the precise parameters obtained from the microfluidic platform to construct proof-of-concept pharmacokinetic models

in monomicrobial cultures of *P. aeruginosa*. The modeling concept can further be extended to polymicrobial susceptibility results for treating polymicrobial infections. Here, I discuss the pharmacokinetics modeling procedure for amikacin and tobramycin against *P. aeruginosa* cultures.

5.3 Results and Discussion

5.3.1 MIC determination from hills modeling

The following sections will describe an example for computing Hill coefficient and MIC in (1) monomicrobial and (2) polymicrobial cultures.

Monomicrobial cultures: MIC determination of *E. coli* against Amikacin

Growth curves of the bacteria in the absence of antibiotics are used to determine G using **Equation 5.1** as described below:

$$\ln(B) = G \cdot t + \ln(B_0) \qquad (5.6)$$

From **Fig. 5.2**, G is the slope of the straight line section of the plot and is 1.0841 h^{-1}, corresponding to a doubling time of ~ 38 minutes.

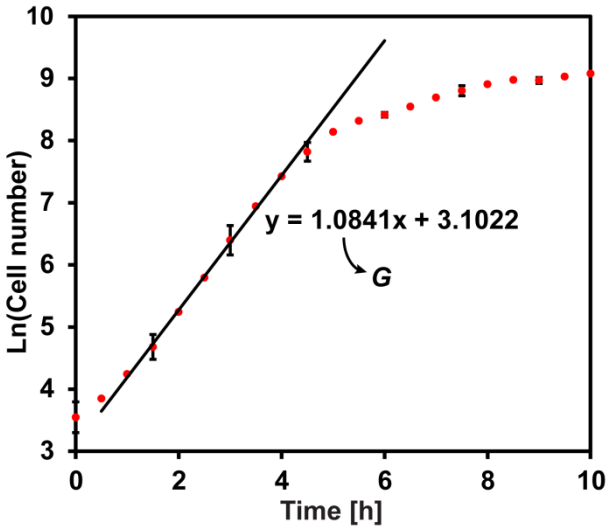

Figure 5.2. Ln(Cell number) or ln(*B*) *vs*. time (*t*) to determine *G* from **Equation 5.6** for the growth curve of *E. coli*.

In the presence of antibiotics, the growth rate is expected to be lower than in the absence of antibiotics. Hence, the net growth rate in presence of antibiotics can be determined by subtracting the growth rate constant, G, from the antibiotic killing rate constant, K_t. Hence, the growth rate in **Equation 5.6** can be modified to give the net growth (G-K_t) as shown in **Equation 5.7**.

$$\ln(B) = (G - K_t) \cdot t + \ln(B_0) . \qquad (5.7)$$

Fig. 5.3 represents the time-kill curves for *E. coli* for different concentration of amikacin, which can be described using **Equation 5.7**. The slope of the straight line portions of these plots will provide the net growth rate, G-K_t, which in turn can be computed to calculate K_t, knowing the value of G from growth curves. These values of G and K_t (and hence K_{max}) can be used to plot **Equation 5.5** (**Fig. 5.4**), which can then be used to compute γ and MIC. The Hill coefficient, γ, is determined to be 2.02 ± 0.16, and MIC is calculated as 4.2 ± 0.6 μg mL-1. The net growth

rate (G-K_t) can also be plotted as a function of antibiotic concentration (**Fig. 5.5**) to obtain the Hill curve, which is a sigmoid as predicted in literature (**Equation 5.2**).

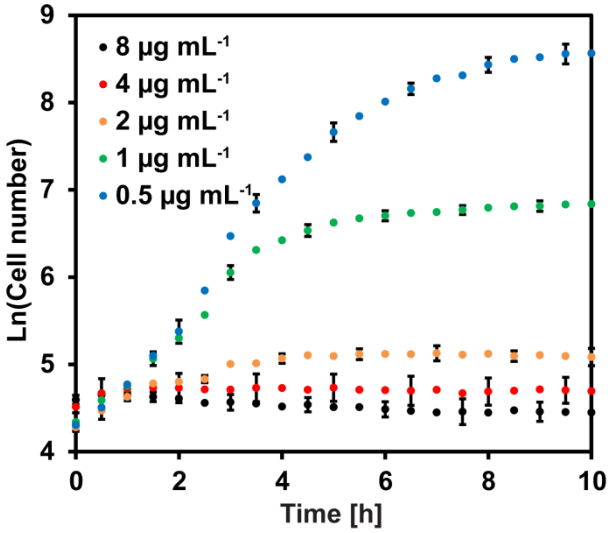

Figure 5.3. ln(cell number) or ln(B) vs. time (t) or time-kill curves (**Equation 5.7**) for *E. coli* at different antibiotic concentrations of amikacin

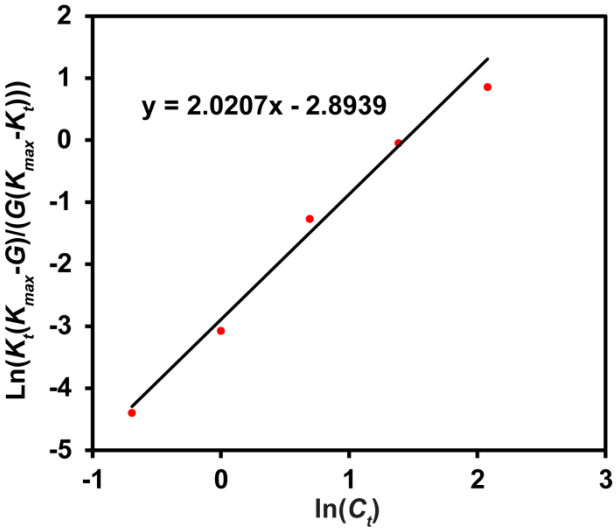

Figure 5.4. Determination of Hill coefficient (γ) and MIC using **Equation 5.5** [8]

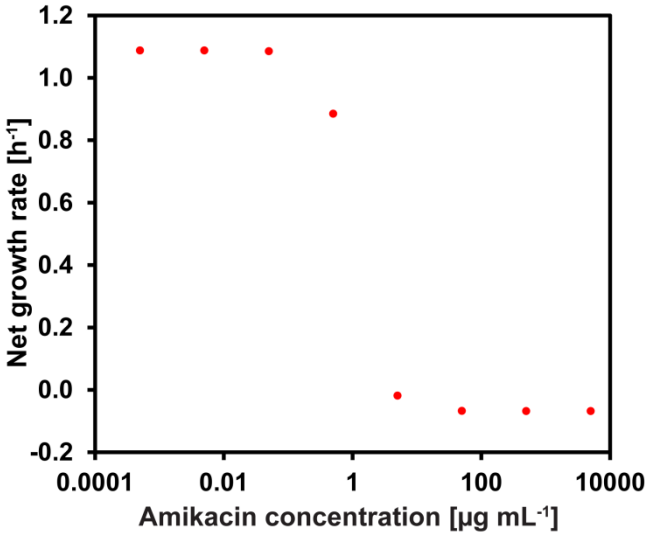

Figure 5.5. Net growth rate of *E. coli* as a function of amikacin concentration, *i.e.*, the Hill model.

Polymicrobial AST: MIC determination of *E. coli* and *P. aeruginosa* against Amikacin

Similar to MIC determination in monomicrobial cultures, I calculate the species-specific growth rate constants for *E. coli* and *P. aeruginosa* in polymicrobial cultures (**Fig. 5.6**) since the effect of bacterial interaction on *G* is already accounted in the observed experimental data. Species-specific net growth rate for the two bacteria in the presence of antibiotics can be determined from slopes similar to monomicrobial cultures (**Fig. 5.7-5.9**). For *E. coli*, the Hill coefficient is determined to be 1.06 ± 0.09, and MIC is determined to be 5.1 ± 1.0 µg mL^{-1}. For *P. aeruginosa*, the Hill coefficient is determined to be 1.32 ± 0.06, and MIC is determined to be 7.8 ± 0.9 µg mL^{-1}.

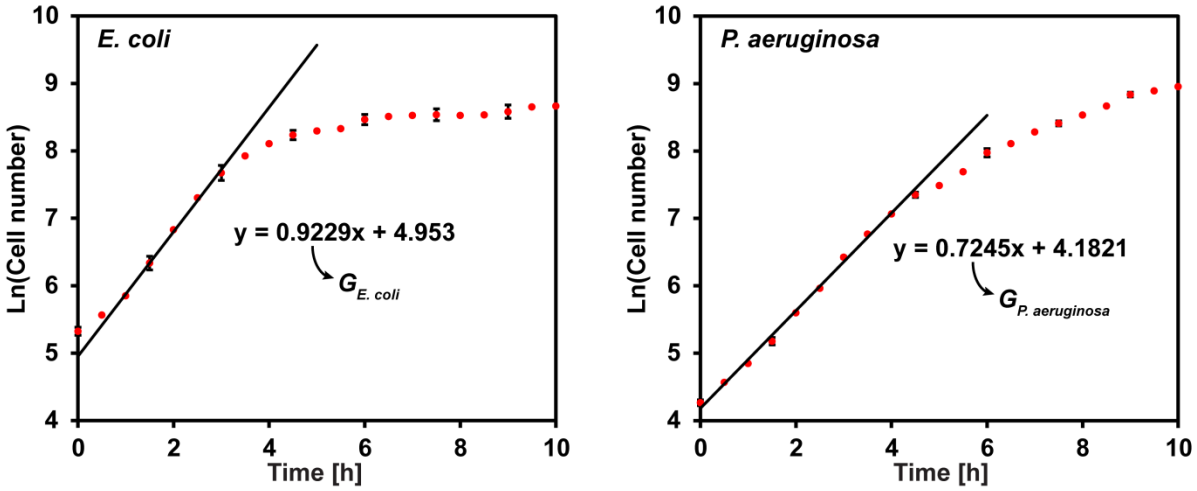

Figure 5.6. Ln(Cell number) or ln(*B*) *vs*. time (*t*) to determine *G* from **Equation 5.6** for the growth curves of *E. coli*. and *P. aeruginosa* in co-cultures

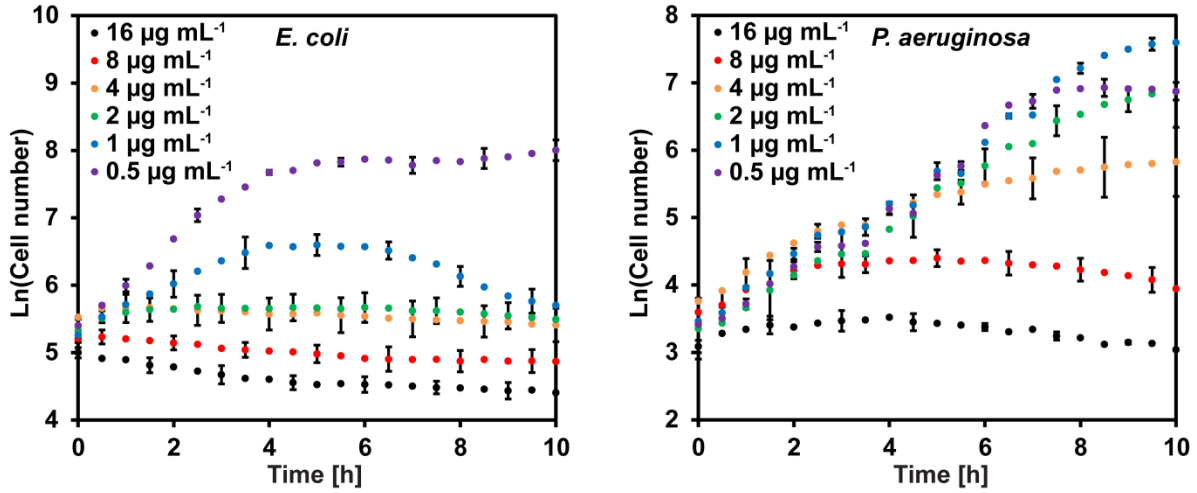

Figure 5.7. ln(cell number) or ln(*B*) vs. time (*t*) or time-kill curves (**Equation 5.7**) for *E. coli* and *P. aeruginosa* in co-cultures at different antibiotic concentrations of amikacin

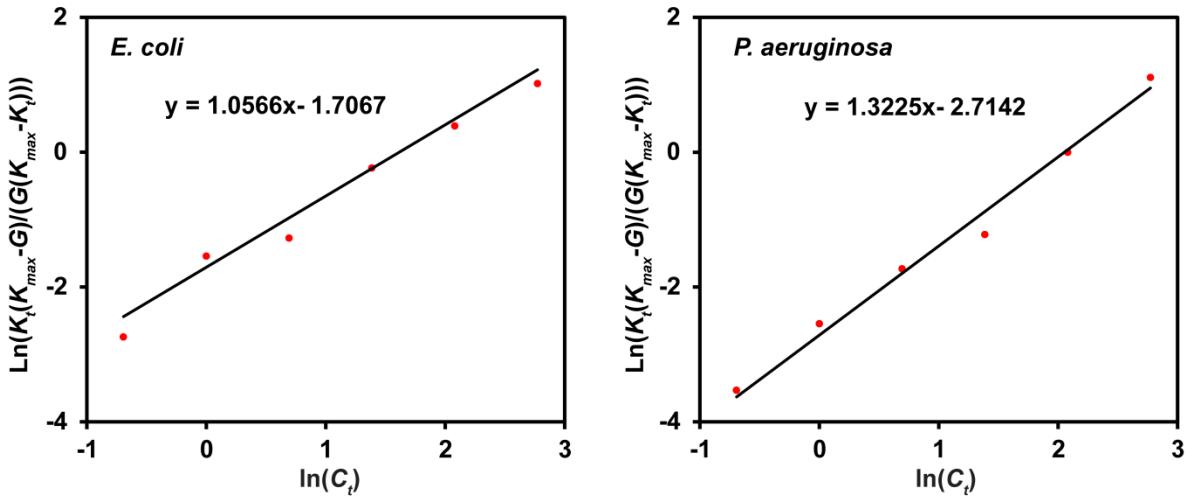

Figure 5.8. Determination of Hill coefficient (γ) and MIC using **Equation 5.5** [8] for amikacin against *E. coli* and *P. aeruginosa* polymicrobial cultures

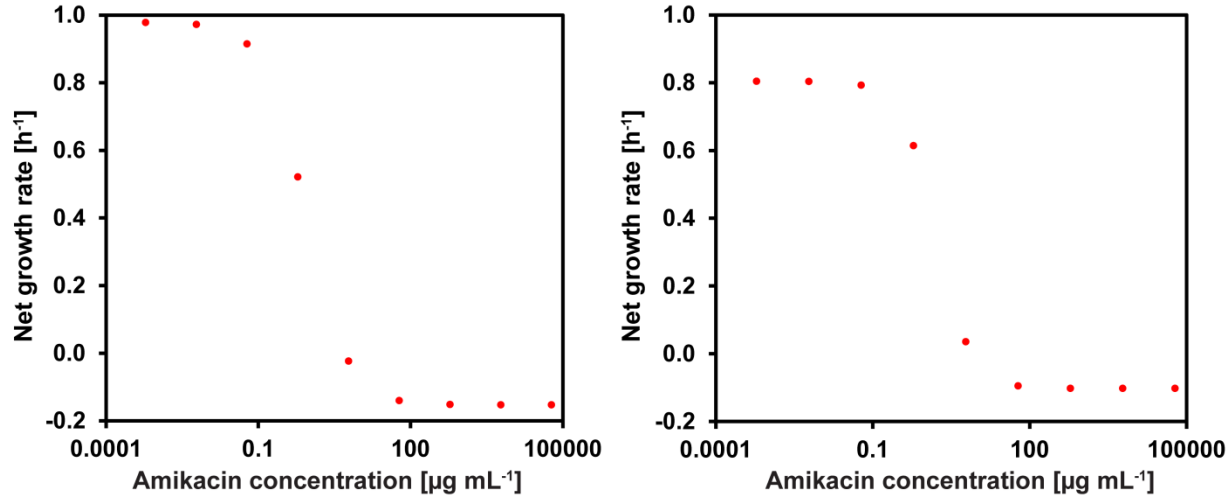

Figure 5.9. Net growth rate of *E. coli* and *P. aeruginosa* as a function of Amikacin concentration, *i.e.*, the Hill curves.

MIC determination *via* conventional method, specifically microbroth dilution method, can provide a reliable range of MIC as discussed previously. However, the method still lacks precision as the MIC is reported in a range of concentration between wells. By utilizing Hill's equation, a precise MIC was calculated (within the range of MIC reported in literature) (**Table 1** and **Table 2**). Hill's equation also provides a Hill coefficient, which describes sensitivity of the changes in killing rates of bacteria to the changes in antibiotic concentration. Comparing the two

antibiotics with the same MIC, the antibiotic with higher Hill coefficient is considered to be more effective, as the killing rate will be higher at the same concentration above MIC [8].

The MICs indicate that *P. aeruginosa* is more resistant to Amikacin than *E. coli* in *P. aeruginosa-E. coli* co-culture. In addition, the higher Hill coefficient in *P. aeruginosa* also signifies that increasing Amikacin concentration will increase the killing rate, K_t, of *P. aeruginosa* more than increasing the killing rate of *E. coli*. Finally, compared to monomicrobial antibiotic screening, *E. coli* is more resistant to amikacin, as evident from the increased MIC and the Hill coefficient of *E. coli* amikacin in co-culture is also lower than microbial culture implying that increasing amikacin concentration in co-culture will increase the killing rate less effectively than in *E. coli* monomicrobial culture (**Table 5.1** and **Table 5.2**)

Table 5.1: Determination of precise MIC and Hill coefficient using pharmacodynamics modeling in monomicrobial cultures

	Amikacin		**Tobramycin**	
	MIC	γ	MIC	γ
E. coli	4.2 ± 0.6	2.0 ± 0.2	4.0 ± 0.7	2.5 ± 0.2
K. pneumoniae	10.4 ± 2.5	1.3 ± 0.1	5.8 ± 1.5	2.0 ± 0.2
P. aeruginosa	6.4 ± 2.0	1.6 ± 0.2	3.1 ± 0.4	0.9 ± 0.1

Table 5.2: Determination of precise MIC and Hill coefficient using pharmacodynamics modeling in polymicrobial cultures

	Amikacin		**Tobramycin**	
	MIC	γ	MIC	γ
E. coli* + *P. aeruginosa				
E. coli	5.1 ± 0.9	1.1 ± 0.1	4.0 ± 0.7	0.3 ± 0.1
P. aeruginosa	7.8 ± 0.9	1.3 ± 0.1	11.5 ± 2.9	1.2 ± 0.1
K. pneumoniae* + *P. aeruginosa				
K. pneumoniae	10.2 ± 2.8	3.4 ± 0.4	10.7 ± 3.4	2.7 ± 0.2
P. aeruginosa	8.1 ± 1.6	1.7 ± 0.1	9.4 ± 2.1	3.2 ± 0.2
E. coli* + *K. pneumoniae* + *P. aeruginosa				
P. aeruginosa	20.5 ± 2.4	2.8 ± 0.1	14.3 ± 3.7	2.2 ± 0.2

5.3.2 Proof-of-concept pharmacokinetics modeling

From pharmacodynamics modeling discussed previously and antibiotic information from literature [19, 20], I obtain the PD parameters for amikacin and tobramycin against *P. aeruginosa* listed in **Table 5.3.**

Table 5.3. Parameters used in pharmacokinetic modeling

	***P. aeruginosa* + Amikacin**	***P. aeruginosa* + Tobramycin**
Growth rate constant, G	0.83 $hour^{-1}$	0.83 $hour^{-1}$
MIC	5.91 μg mL^{-1}	3.06 μg mL^{-1}
Maximum killing rate, K_{max}	1.01 $hour^{-1}$	0.98 $hour^{-1}$
Hill coefficient, γ	1.57	0.95
Initial concentration, C_0	25.0 μg mL^{-1}	10.0 μg mL^{-1}
Dosing regimen	8.0 hour	8.0 hour
Drug half-life, $t_{1/2}$	3.01 hour	3.03 hour

It was assumed that amikacin is usually injected every 8 hours such that the peak concentration in blood serum is approximately 25 μg mL^{-1} (roughly 4 times MIC) as recommended in literature since higher concentrations can be toxic to humans [21, 22], although the injection amount usually depends on the size of the person. Similarly, tobramycin is injected every 8 hours to give a peak concentration of approximately 10 μg mL^{-1} (roughly 3 times MIC). The half-life of amikacin was determined from the predicted blood serum concentration to be 3.01 h [23]. Similarly, the half-life of tobramycin was determined to be 3.03 hours [20]. The initial cell numbers in the microfluidic chambers were 200 to 300, which approximately equals to ~ 10^8 cells/mL. The concentration of antibiotic, C_t, over time is given by [24]:

$$C_t = C_0 \cdot e^{\frac{\ln(0.5)}{t_{1/2}} t}, \tag{5.8}$$

where C_0 is the initial antibiotic concentration [μg mL^{-1}], $t_{1/2}$ is the antibiotic half-life in human body [hour], and t is the time elapsed [hour]. **Equation 5.8** is modified to describe C_t over time, where additional doses are administered after every 8 hours as shown in **Fig. 5.10.**

$$C_t = \sum_{i=0}^{n} C_0 \cdot e^{\frac{\ln(0.5)}{t_{1/2}}(t-8i)} \; ; (t\text{-}8i) \geq 0 \qquad (5.9)$$

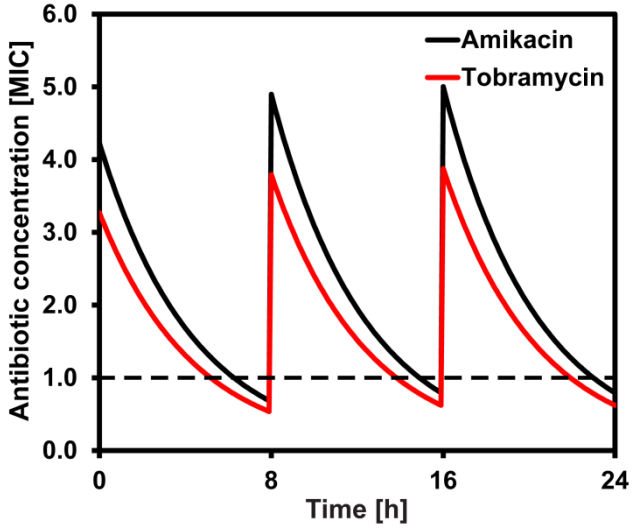

Figure 5.10. Pharmacokinetic modeling to predict the antibiotic concentrations of amikacin and tobramycin in the blood stream over the course of 24 hours.

The antibiotic concentration at the 8^{th} hour is expected to be higher than the initial concentration due to the residual antibiotic prior to the second dose, since the antibiotic does not completely get eliminated after 8 hours. At the end of 8 hour-intervals, both the amikacin and tobramycin concentrations fall below the MIC. Then, we use **Equation 5.9**, **Equation 5.5** and **Equation 5.7**, and the value from **Table 4** to predict the net growth rate over 24 hours (**Fig. 5.11**).

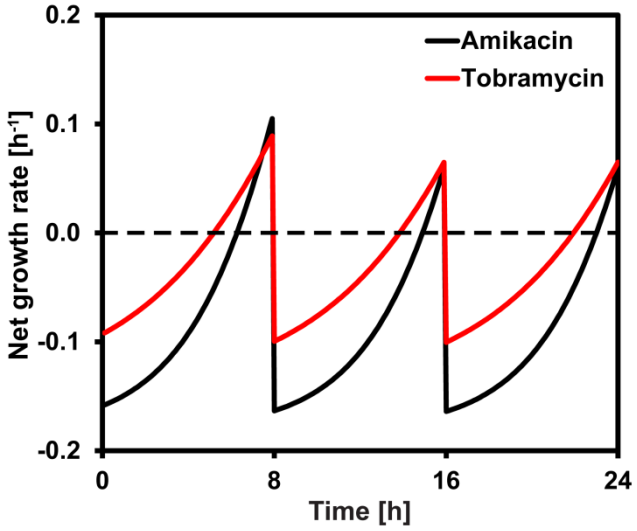

Figure 5.11. Pharmacokinetic modeling to predict *P. aeruginosa* net growth rate in blood stream over the course of 24 hours.

From **Fig. 5.11**, it was observe that the second and third dose of antibiotic yields lower net growth rate at the end of 8 hours period which is due to antibiotic accumulation. Since the tobramycin dose results in higher net growth rate in the first 8 hours than amikacin, it indicates lower drug efficacy than amikacin (even though MIC of tobramycin is lower than amikacin). However, at the end of 8 hours, the net growth rate caused by both tobramycin and amikacin are similar (~ 0.1 h^{-1}). In the case of amikacin, the larger Hill coefficient (1.57) of amikacin correlates with a sharp increase of the net growth rate in contrast to tobramycin, which suggests amikacin's higher drug potency [25]. The smaller negative net growth rate caused by tobramycin also implies that tobramycin is less effective in inhibiting *P. aeruginosa* cell growth. The resulting net growth rate is then used to model the changes in cell numbers over 24 hours by integrating **Equation 5.1** to derive the following equation:

$$B = B_0 e^{(G \cdot t - \int K_t \, dt)} \tag{5.10}$$

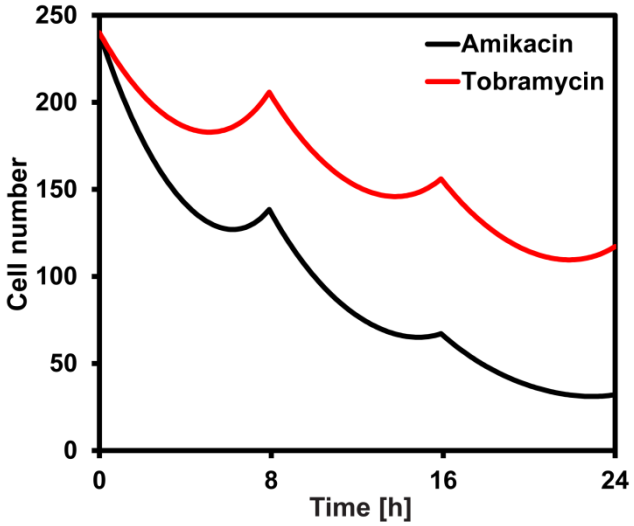

Figure 5.12. Predicted cell numbers of *P. aeruginosa in vivo* over the course of 24 hours.

Fig. 5.12 shows the predicted cell number for *P. aeruginosa in vivo* over the course of 24 hours. The plot demonstrates interesting differences when amikacin and tobramycin are used in the treatment of *P. aeruginosa* infections. Amikacin causes rapid decrease in cell numbers when amikacin concentration is above MIC, while a rapid increase in cell number occurs at concentration below MIC. Since tobramycin concentration falls below MIC faster than amikacin, the treatment with tobramycin allows longer time for cell growth which results in higher cell number at the end of 8 hour. Hence, PK modeling suggests that amikacin suppresses *P. aeruginosa* growth more effectively than tobramycin owing to lower final cell numbers at t = 24 h (even though MIC of tobramycin is lower than amikacin).

5.4 Conclusions

In this chapter, I discussed how high throughput microfluidic platforms can address the limitation of predicting *in vivo* AST results. Specifically, I discuss the utility of microfluidic platforms to perform pharmacokinetic/ pharmacodynamic (PK/PD) modeling from precise time-

kill data obtained from automated AST methods (superior than conventional AST methods) to determine optimal antibiotic dosing regimen for treating monomicrobial and polymicrobial bacterial infections. Furthermore, PK/PD modeling yields more precise prediction of a precise MIC for more accurate prediction of *in vivo* antibiotic action as opposed a range of MIC (the current metric for AST). Hence, microfluidic platforms with the capability for PK/PD modeling have a significant potential to provide a precise antibiotic dosing regimen, thereby minimizing antibiotic resistance.

The discussed microfluidic platforms in this chapter for AST have primarily been used as a research tool to study the interaction of antibiotics and monomicrobial/polymicrobial bacteria. Further studies are required to extend the proof-of-concept PK/PD analysis to study at the clinical level. The current techniques for AST have been used for decades to treat microbial infections, and introduction of a new technology would require collaboration between scientists and clinicians to specifically perform comparative studies on AST and PK/PD modeling using conventional techniques and microfluidic platforms. These types of collaborations will help in overcoming resistance faced by the clinicians in the healthcare for the adoption of new technologies for prescription of antibiotic dosing regimen while utilizing lower sample volumes and delivering more accurate outcomes.

5.5 References

1. McKenzie, C., Antibiotic dosing in critical illness. Journal of Antimicrobial Chemotherapy, 2011. 66(suppl 2): p. ii25-ii31.
2. Nielsen, E.I., et al., Semimechanistic Pharmacokinetic/Pharmacodynamic Model for Assessment of Activity of Antibacterial Agents from Time-Kill Curve Experiments. Antimicrobial Agents and Chemotherapy, 2007. 51(1): p. 128-136.
3. Burgess, D.S., Pharmacodynamic principles of antimicrobial therapy in the prevention of resistance. CHEST Journal, 1999. 115(suppl_1): p. 19S-23S.
4. Schentag, J.J., Antibiotic dosing - does one size fit all? JAMA, 1998. 279(2): p. 159-160.
5. Frimodt-Moller, N., How predictive is PK/PD for antibacterial agents? International Journal of Antimicrobial Agents, 2002. 19(4): p. 333-339.
6. Nafziger, A.N., et al., The application of pharmacodynamics in the optimization of antibiotic therapy. Formulary, 2003. 38: p. 294-319.
7. Nicolau, D.P., Optimizing outcomes with antimicrobial therapy through pharmacodynamic profiling. Journal of Infection and Chemotherapy, 2003. 9(4): p. 292-296.
8. Regoes, R.R., et al., Pharmacodynamic Functions: a Multiparameter Approach to the Design of Antibiotic Treatment Regimens. Antimicrobial Agents and Chemotherapy, 2004. 48(10): p. 3670-3676.
9. Katsube, T., et al., Pharmacokinetic/pharmacodynamic modeling and simulation to determine effective dosage regimens for doripenem. Journal of Pharmaceutical Sciences, 2010. 99(5): p. 2483-2491.
10. Nielsen, E.I., O. Cars, and L.E. Friberg, Predicting In Vitro Antibacterial Efficacy across Experimental Designs with a Semimechanistic Pharmacokinetic-Pharmacodynamic Model. Antimicrobial Agents and Chemotherapy, 2011. 55(4): p. 1571-1579.
11. Yano, Y., et al., Application of logistic growth model to pharmacodynamic analysis of in vitro bactericidal kinetics. Journal of Pharmaceutical Sciences, 1998. 87(10): p. 1177-1183.
12. Moraes, C., et al., Organs-on-a-Chip: A focus on compartmentalized microdevices. Annals of Biomedical Engineering, 2012. 40(6): p. 1211-1227.
13. Kobel, S. and M.P. Lutolf, Biomaterials meet microfluidics: building the next generation of artificial niches. Current Opinion in Biotechnology, 2011. 22(5): p. 690-697.
14. Huh, D., et al., Microengineered physiological biomimicry: Organs-on-Chips. Lab on a Chip, 2012. 12(12): p. 2156-2164.
15. Schütte, J., et al., "Artificial micro organs"—a microfluidic device for dielectrophoretic assembly of liver sinusoids. Biomedical Microdevices, 2011. 13(3): p. 493-501.
16. Reeve, R. and J.R. Turner, Pharmacodynamic Models: Parameterizing the Hill Equation, Michaelis-Menten, the Logistic Curve, and Relationships Among These Models. Journal of Biopharmaceutical Statistics, 2013. 23(3): p. 648-661.
17. Mohan, R., et al., A multiplexed microfluidic platform for rapid antibiotic susceptibility testing. Biosensors and Bioelectronics, 2013. 49(0): p. 118-125.
18. Derendorf, H. and B. Meibohm, Modeling of Pharmacokinetic/Pharmacodynamic (PK/PD) Relationships: Concepts and Perspectives. Pharmaceutical Research, 1999. 16(2): p. 176-185.
19. Duszynska, W., et al., Therapeutic drug monitoring of amikacin in septic patients. Critical Care, 2013. 17(4): p. R165.

20. Akorn - Strides, L. Tobramycin (tobramycin sulfate) Injection 2013 [cited 2013 December 16]; Available from: http://dailymed.nlm.nih.gov/dailymed/lookup.cfm?setid=49151a62-191a-4ba8-8b8c-bd8535f2fdb3.
21. Index, R.-T.I.D. Amikin. 2013 [cited 2013 December 16]; Available from: http://www.rxlist.com/amikin-drug.htm.
22. MedlinePlus. Therapeutic drug levels. 2013 [cited 2013 December 16]; Available from: http://www.nlm.nih.gov/medlineplus/ency/article/003430.htm.
23. Med, D. AMIKACIN SULFATE injection [Teva Parenteral Medicines, Inc.]. 2013 [cited 2013 December 18]; Available from: http://dailymed.nlm.nih.gov/dailymed/lookup.cfm?setid=6ec3129b-c53b-4bdb-913d-a2d0060fa140.
24. Lipsitch, M. and B.R. Levin, The population dynamics of antimicrobial chemotherapy. Antimicrobial Agents and Chemotherapy, 1997. 41(2): p. 363-73.
25. Galimberti, E.S. and B.C. Knollmann, Efficacy and potency of class I antiarrhythmic drugs for suppression of Ca2+ waves in permeabilized myocytes lacking calsequestrin. Journal of Molecular and Cellular Cardiology, 2011. 51(5): p. 760-768.

Chapter 6

Antibiotic susceptibility testing of non-genetically modified bacteria

6.1 Introduction

Since genetically modified bacteria were utilized in all the experiments of AST, direct comparison of the results at the clinical level is challenging. This key limitation described limits the applicability of the platform with real clinical samples. In this chapter, I will discuss ways to address this limitation with the objective of utilization of the clinical samples with the microfluidic platform.

Since some optical dyes are known to induce fluorescence in bacteria [1], I approached to circumvent this issue by utilizing optical dyes. The goal for this study was to search and optimize a dye that fluoresces in live bacterial cells while they proliferate over an extended period (12 hours or more). Long term experiments using this method are challenging since the dye amount per cell is halved in each cell division cycle. This phenomenon makes the fluorescence intensity to drop exponentially and the approach particularly affects the cells with short doubling times. Hence, an ideal optical dye will have several desirable traits including applicability in long term cell proliferation experiments, bright enough for counting bacterial cells over time, stable, and would have low toxicity to the cells or would not negatively affect the bacterial cells physiology. The subsequent paragraphs will discuss several dyes that were tried with the AST techniques using the microfluidic platform.

I first used the dye Alamar Blue that contains an active ingredient of resazurin, which is non-toxic, permeable, blue in color, and does not fluoresce. Alamar blue is widely used in broth

dilution assays for cell viability in AST due to its colorimetric indicator and the dye does not affect cell physiology and growth [2-4]. When resazurin is reduced to resorufin, it induces a very bright red non-toxic fluorescence inside cells *via* cell metabolism (**Fig. 6.1**). Here, the amount of resorufin produced is proportional to the number of living cells.

Fig. 6.1. AlamarBlue indicator mechanism[5]

Next, Cell Tracker^{TM} Green BODIPY was tried that contains fluorescent probing that can pass freely through the cell membranes and get converted to impermeable reaction products [6, 7]. Theoretically, the dye is transferred to several generations and not to adjacent population keeping the bacterial cells viable for up to 24 hours.

STYO BC was also tried for AST because this dye is a mixture of several BC dyes specifically for bacterial staining [8-10]. The dye differs from Alamar Blue and BODIPY because it does not react with intracellular enzymes of the cells and does not remain the cytoplasm of the cells. Specifically, the non-fluorescent dye binds to the nucleic acid and turns fluorescent upon entering the bacterial cells. Hence, this dye is capable of staining both live and dead cells.

Next, I tried Carboxyfluorescein Diacetate Succinimidyl Ester (CFDA-SE) since this particular due is one of the gold standard dyes used for live cell staining because of its stability and low toxicity[11-13]. This dye utilizes incorporates properties of AlamarBlue and BODIPY.

Specifically, initially the CFDA-SE is non-fluorescent and highly cell permeable. However, upon entering the cell the dye is converted CFSE, which is fluorescent and has lower cell permeability. The converted product (CFSE) binds to amine group within the cells and the combination is retained inside the cells for extended time periods. The dye is considered a live staining dye since it can be digested only from intracellular esterase.

CellVue was the last dye tried in the AST experiments. This dye rapidly binds to the cell membrane and hence, has relatively low toxicity compared to previously described nucleic acid stains. The bound dye molecules are stable unlike the CFDA-SE, and hence, eliminate the risk of dye leaking out of the cells. However, the key limitation of dye concentration getting halved with each cell division exists.

This chapter addresses several limitations of the genetically modified bacteria by utilizing optical dyes for its compatibility with TLFM. Specifically five dyes are tested and optimized. Off the dyes tested, CellVue and CFDA-SE provide the most promising results for determination of MIC of antibiotics rapidly (2-4 hours) with non-genetically modified bacteria or "real bacteria".

6.2 Experimental

6.2.1Alamar blue

Preparation of assay was straightforward using this dye. After addition of the dye in the cell culture and after ~ 3 hour incubation time, the assay was ready for fluorescence reading. Specifically, cells at concentrations 1-5x10^7 CFU/mL were first added to the wells. This was

followed by addition of 40 µL of 10x AlamarBlue to each well and absorption of light is measured at 570 nm over a time period of approximately 20 hours (**Fig6. 2**).

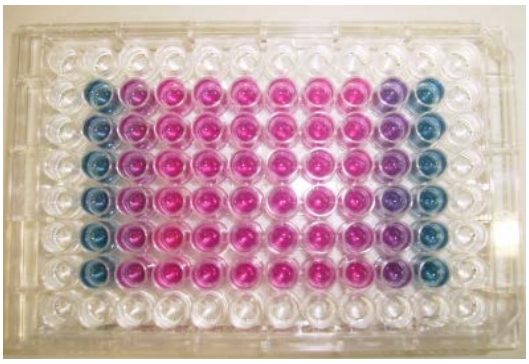

Figure 6.2. AlamarBlue assay using a 96-well plate

6.2.2 Cell tracker™ BODIPY

The working concentration for the dye used was in the range 5-25 µM for fast dividing cells [6]. The procedure to stain the cells is outlined in **Fig. 6.3**. Briefly, the dye vial was first warmed up to room temperature and is dissolved in to DMSO to a final concentration of 10 mM. Next, this stock diluted further to a working concentration of 0.5-25 µM in LB and the dye solution is warmed to a temperature of 37 °C. Overnight cell culture of *E. coli* MG1655 was then collected, centrifuged and the supernatant was removed. Dye solution was then added to the cells and the solution was incubated for 45 minutes as suggested in the dye protocol [6, 14]. The solution was again centrifuged and after removing the supernatant, an equal amount of LB was added, and this solution was incubated for 30 minutes. These bacterial cells were then collected and flowed in the microfluidic device as discussed in previous chapters.

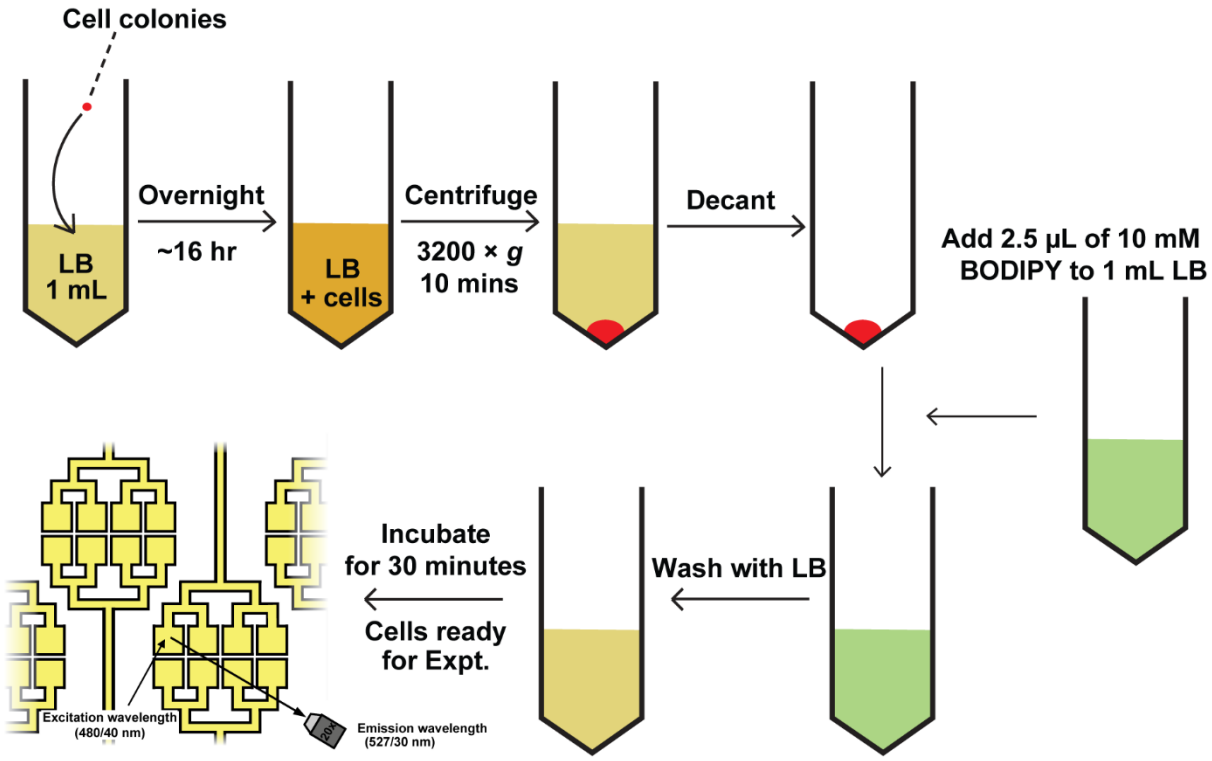

Figure 6.3. BODIPY staining process

6.2.3 STYO BC green nucleic acid stain

The staining procedure is outlined in **Fig. 6.4**. Briefly, the dye is added to the overnight cell culture as above such that the final concentration of the dye is 40-50 µM. The solution is vortexed and covered with aluminum foil to prevent exposure to light since the dye is extremely photosensitive. These cells are then flowed in to the microfluidic device as discussed previously ensuring minimal exposure to light since the dye was known to photo bleach upon exposure to light.

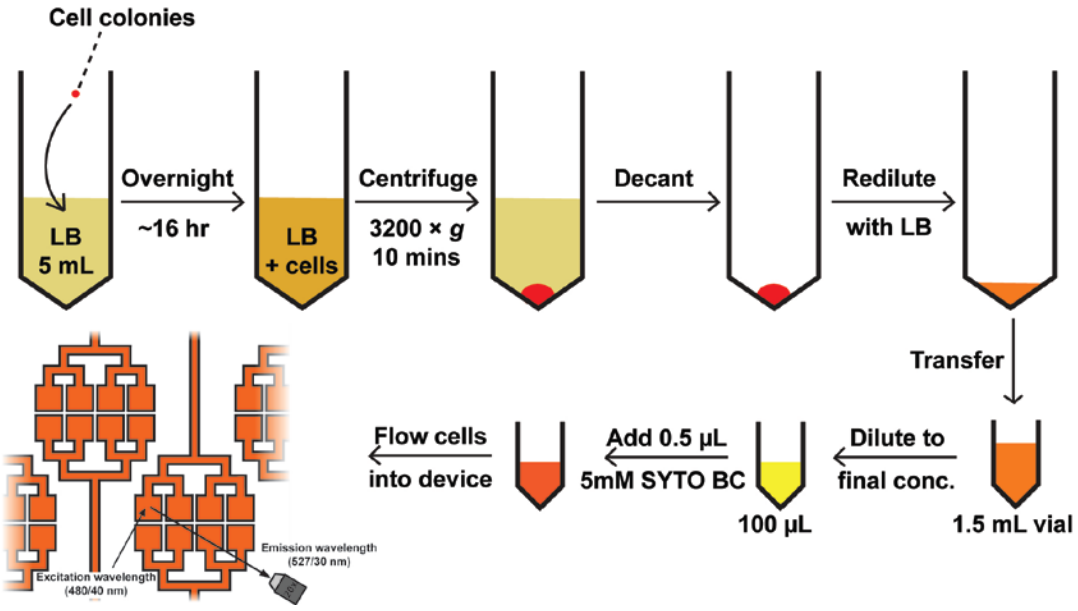

Figure 6.4. SYTO BC staining process

6.2.4 Carboxyfluorescein diacetate succinimidyl ester CFDA-SE

E. coli cells were prepared as described previously. The cell preparation steps are shown in **Fig. 6.5**. Briefly, bacterial concentration ranging between 1-5x10^7 CFU/mL was washed with PBS/0.1 % BSA three times. Next, 1 µL of 100 mM CFDA-SE is pipetted into the bacterial solution prepared in the previous step followed by rigorous vortex. This bacteria-dye solution is incubated for 15 minutes followed by washing with LB and incubation of 30 minutes to ensure the dye molecules gets incorporated in to the bacterial cells. This solution was washed again to remove unstable dye molecules that diffuse out and cause fluorescent background. This solution can be stored overnight at 4ºC or flowed in to the microfluidic device immediately as discussed above.

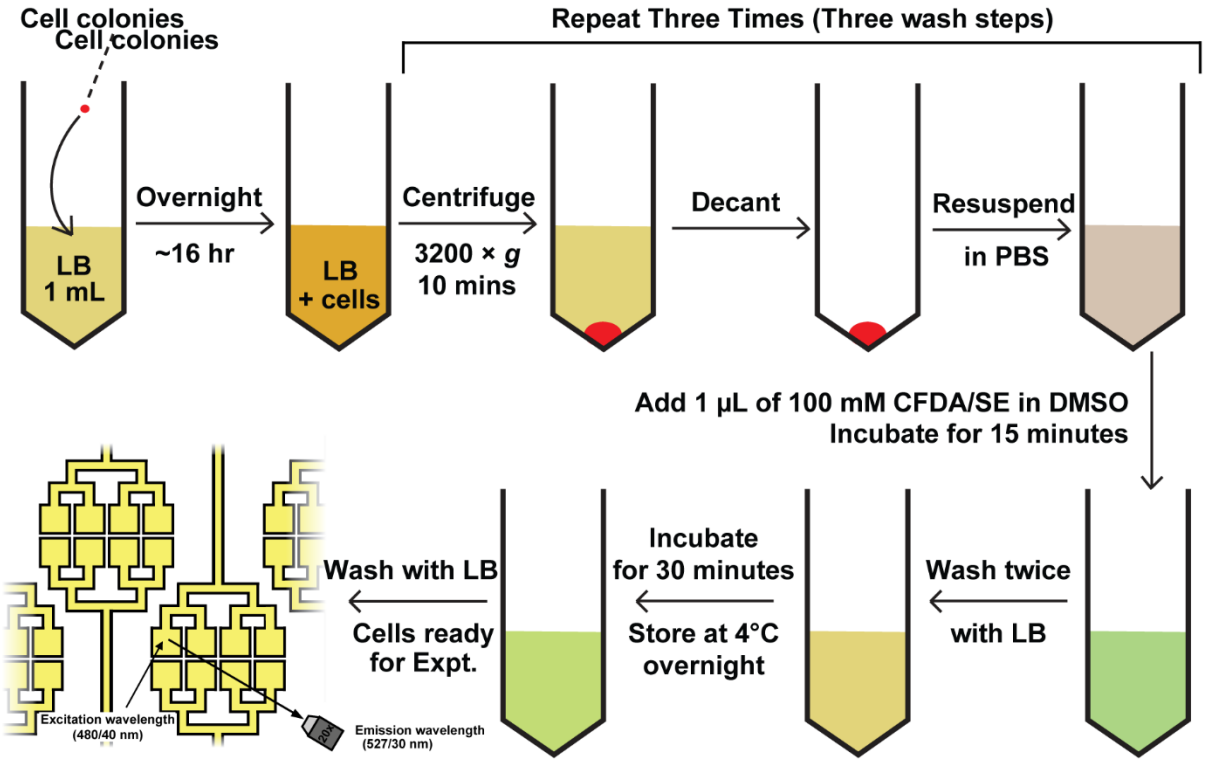

Figure 6.5. CFDA-SE staining process

6.2.5 CellVue (Jade)

To stain *E. coli* cells using CellVue, first the cells were prepared such that the cell density was at $2x10^7$ CFU/mL. Second, the cells were washed with PBS by centrifugation, and then PBS is removed. 1 mL of the diluent C (from the CellVue kit) was added to the cell pellet which was followed by addition of 4 µL of CellVue dye stock into 1 mL of diluent C and mixed without vortexing. This solution was then incubated for 5 minutes and washed three times with LB until the cells were ready for AST experiment.

6.3 Results and Discussion

6.3.1 Alamar blue

Alamar Blue was used first in bulk scale or using 96-well plates (for validation) (**Fig. 6.6**) and then on-chip. I observed that, though AlamarBlue is an appropriate choice for absorbance

measurement, this dye did not work for the application on-chip. The fluorescent resorufin was cell permeable, which leaks out and gave uniform fluorescence in chambers. Due to this leakage, counting the cell numbers was not possible.

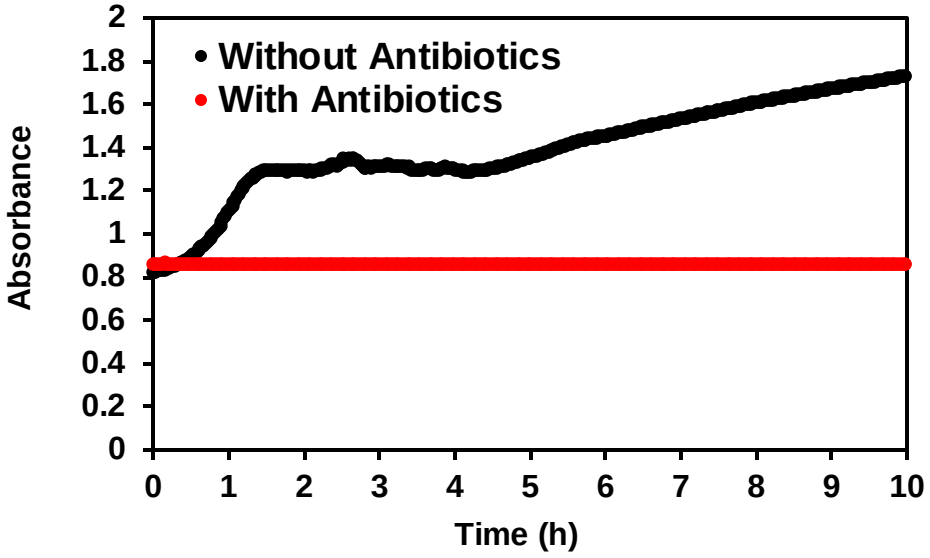

Figure 6.6. Proof-of-principle platform validation using AlamarBlue in 96-well plates

6.3.2 Cell tracker™ BODIPY

Next, Cell Tracker™ Green BODIPY was tried since this dye is impermeable after formation of reaction products. Here, a special mechanism is utilized to first transport dye into the cells. CellTracker BODIPY (8-Chloromethyl-4,4-Difluoro-1,3,5,7-Tetramethyl-4-Bora-3a,4a-Diaza-S-Indacene) dye is cell permeable and upon entering the cells, it gets converted to cell-impermeant product using glutathione transferase. Here too, each successive division of cells halves the fluorescence intensity compared to the previous generation. However, since the dye can be digested only from intracellular enzymes, it makes BODIPY a live cell staining dye. Since the reaction products are cell impermeable, BODIPY dye can be retained within cell

membrane, which results in localized staining. On one hand, BODIPY was successful in staining and counting the cells, and the stained cells are clearly visible under fluorescent microscope (**Fig. 6.7**). On the other hand, only 30% of the cells were stained on-chip, even after several optimizations to the protocol.

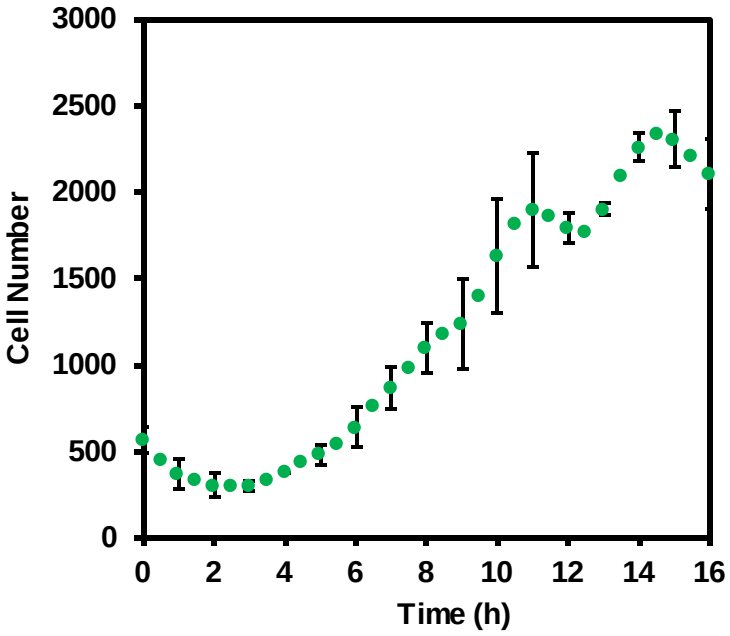

Figure 6.7. Proof-of-principle platform validation using Cell Tracker™ Green Bodipy (only a fraction of the cells get stained)

6.3.3 STYO BC green nucleic acid stain

Compared to BODIPY, although SYTO BC was able to stain up to 95-100% of cells and provided bright fluorescence initially, SYTO dyes photo-bleached rapidly. In addition, I observed the SYTO dyes appeared to alter cell functions (due to changes in doubling times of bacteria) by binding to DNA and RNA of the cells[15]. Specifically, I observed that the cell growth rate is slowed down significantly due to apparent increases in doubling times (**Fig. 6.7**). Further, literature corroborates that DNA damage is not uncommon with these dyes because

excited products can react with DNA and cause mutations within the bacterial cells. Due to the above limitations, I did not try to further optimize this dye.

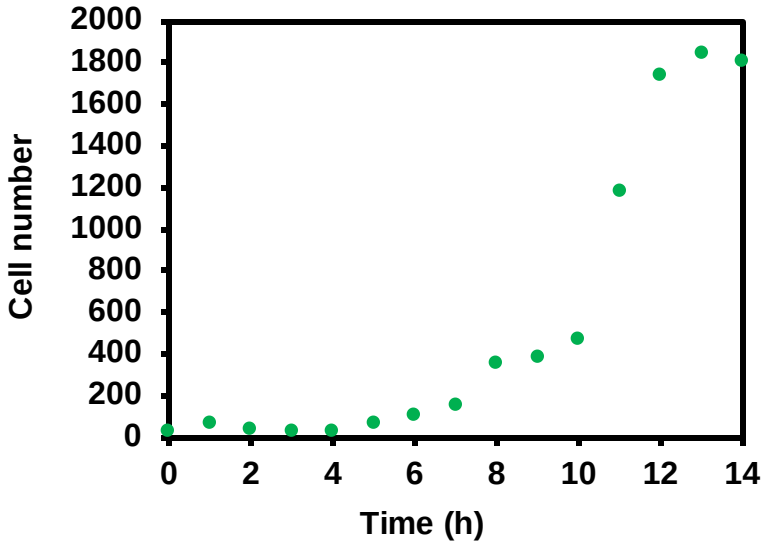

Figure 6.8 Proof-of-principle platform validation using STYO BC on-chip (doubling times are drastically affected.

6.3.4 Carboxyfluorescein diacetate succinimidyl ester CFDA-SE

Even though the dye amount is halved with each division of cells from the previous time, this dye has been the most successful in my microfluidic AST. I was able to determine precise MIC values in 2-4 hours using the dye for *E. coli* cells. **Fig. 6.9** shows MIC of ampicillin and tobramycin against *E. coli* cells using the dye. It can be inferred that the MIC of ampicillin and tobramycin is ~ 2 μg/mL, which is comparable to the values found in literature and the conventional broth dilution methods [16].

Since one of the key limitations of using this dye was the decrease in fluorescence after 3-4 hours, I approached the limitations by mixing CFDA with medium prior to introduction in cells. However, the dye cannot be mixed with medium containing amine because it gets

hydrolyzed, hence; LB was not a viable option. In addition, CFSE gradually leaks out from the cells to the surrounding medium in the first 24 hours after cell lysis which makes the counting cell process tedious. The issue of background fluorescence can be resolved by storing the stained cells in LB broth overnight to let majority of the unstable CFSE leak out overnight. The cells are then washed and flowed the next day which provides with a much brighter fluorescence and low background. Unfortunately, background increases with time but at a lower rate than previously. Furthermore, I observed a fraction of cells turning non-motile after dye staining and consequently not responding to the antibiotic treatment, alluding that the dye was perhaps altering the cell physiology. Another limitation of the dye is that the dye cannot be used to stain *P. aeruginosa* cells[12].

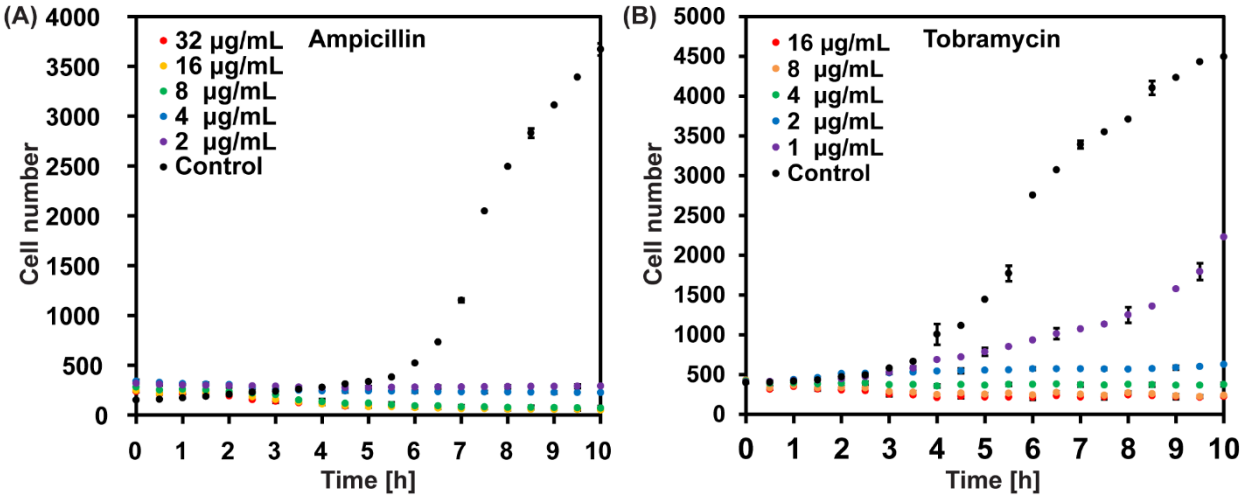

Figure 6.9. Proof-of-principle platform validation using CFDA-SE on-chip using ampicillin and tobramycin against E. coli MG1655 cells.

6.3.5 Cell Vue (Jade)

As discussed previously, staining of the cells was successful with CellVue. The dye was the most effective at low concentrations (2 µM) (**Fig. 6.10**), after which the dye concentrations were perhaps toxic to the cells. Higher concentrations of the dye led to lower cell viability but

brighter cells. With this dye as well, though MIC determination was possible, lowering of fluorescence after a few hours remained the key limitation that hindered long term AST studies for monomicrobial cultures.

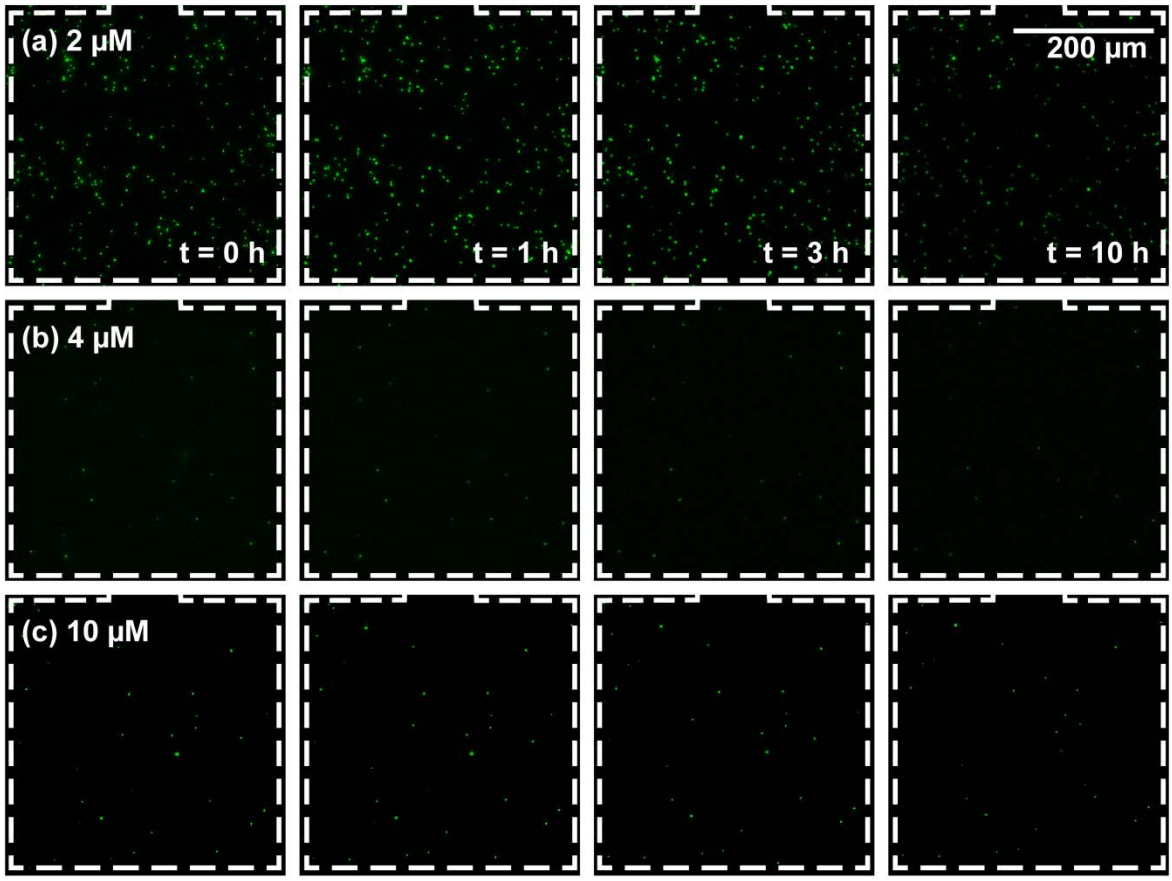

Figure 6.10 Proof-of-principle micrographs showing dye staining at three concentrations for the same cell density (MG1655 strain). The dye staining is most effective at the lowest concentration.

6.4 Conclusions

In summary, CFDA-SE and CellVue were the most effective dyes for the staining of non-genetically modified bacteria for AST. I was able to determine the primary AST parameter (MIC); however, the one key physical limitation still remains is the loss of fluorescence over time. This challenge further limits the ability of the technology to be used for long term studies.

Nevertheless, optical dyes mentioned here can be used in the determination of MICs of non-genetically modified bacteria in a rapid and multiplexed format, an approach that is still far superior to conventional methods of AST (broth dilution and disc diffusion).

In the future, several options exists for observing long term interaction of "real" bacteria and antibiotics including phase contrast microscopy where bacteria can be differentiated based on shapes and motility in polymicrobial infections. In addition, more optical dyes can be tested and/designed where the key objective would be to ensure the fluorescence does not decrease over time such that long term antibiotic screening studies are possible.

6.5 References

1. Hope-Roberts, M., M. Wainwright, and R.W. Horobin, Real-time imaging of bacteria in living mice using a fluorescent dye. Biotechnic and Histochemistry, 2011. 86(2): p. 104-107.
2. Collins, L. and S.G. Franzblau, Microplate alamar blue assay versus BACTEC 460 system for high-throughput screening of compounds against Mycobacterium tuberculosis and Mycobacterium avium. Antimicrobial Agents and Chemotherapy, 1997. 41(5): p. 1004-9.
3. Burt, S.A. and R.D. Reinders, Antibacterial activity of selected plant essential oils against Escherichia coli O157:H7. Letters in Applied Microbiology, 2003. 36(3): p. 162-167.
4. Salvat, et al., Screening of some plants from Northern Argentina for their antimicrobial activity. Letters in Applied Microbiology, 2001. 32(5): p. 293-297.
5. Antczak, C., et al., High-throughput identification of inhibitors of human mitochondrial peptide deformylase. Journal of Biomolecular Screening, 2007. 12(4): p. 521-535.
6. Boleti, H., D.M. Ojcius, and A. Dautry-Varsat, Fluorescent labelling of intracellular bacteria in living host cells. Journal of Microbiological Methods, 2000. 40(3): p. 265-274.
7. De la Fuente, J., et al., Infection of tick cells and bovine erythrocytes with one genotype of the intracellular ehrlichia Anaplasma marginale excludes infection with other genotypes. Clinical and Diagnostic Laboratory Immunology, 2002. 9(3): p. 658-668.
8. Berney, M., et al., Assessment and Interpretation of Bacterial Viability by Using the LIVE/DEAD BacLight Kit in Combination with Flow Cytometry. Applied and Environmental Microbiology, 2007. 73(10): p. 3283-3290.
9. Stocks, S.M., Mechanism and use of the commercially available viability stain, BacLight. Cytometry Part A, 2004. 61A(2): p. 189-195.
10. Rigsbee, W., L.M. Simpson, and J.D. Oliver, DETECTION OF THE VIABLE BUT NONCULTURABLE STATE IN ESCHERICHIA COLI O157:H7. Journal of Food Safety, 1997. 16(4): p. 255-262.
11. Fitzgerald, D.J., et al., Mode of antimicrobial action of vanillin against Escherichia coli, Lactobacillus plantarum and Listeria innocua. Journal of Applied Microbiology, 2004. 97(1): p. 104-113.
12. Fuller, M.E., et al., Development of a Vital Fluorescent Staining Method for Monitoring Bacterial Transport in Subsurface Environments. Applied and Environmental Microbiology, 2000. 66(10): p. 4486-4496.
13. Fuller, M.E., et al., Field-scale evaluation of CFDA/SE staining coupled with multiple detection methods for assessing the transport of bacteria in situ. FEMS Microbiology Ecology, 2001. 37(1): p. 55-66.
14. Scott, R.S., et al., Phagocytosis and clearance of apoptotic cells is mediated by MER. Nature, 2001. 411(6834): p. 207-211.
15. Han, J.H., B.C. Heinze, and J.Y. Yoon, Single cell level detection of Escherichia coli in microfluidic device. Biosensors and Bioelectronics, 2008. 23(8): p. 1303-1306.
16. Mohan, R., et al., A multiplexed microfluidic platform for rapid antibiotic susceptibility testing. Biosensors and Bioelectronics, 2013. 49(0): p. 118-125.

Chapter 7

Summary of accomplishments and future outlook

7.1 Summary of accomplishments

As much as 50% of the antibiotic prescriptions in the clinics are currently inaccurate [1], which is one of the primary reasons for the rise in antibiotic resistance [2-5]. Hence, development of new technologies for prescription of precise antibiotic dosing regimen is critical to address this issue. Conventional technologies including broth dilution and disc diffusion are time consuming, require large sample volumes, have low detection sensitivity and low throughput, and are standardized for monomicrobial infections only [6-13]. In this respect, microfluidics is an attractive technology that can address the issues of these conventional methods for AST. Microfluidic chips/reactors/platforms comprise a simple to complex network of channels, chambers, valves, pumps *etc.* and enable precise spatio-temporal control over the flow of reagents. As a result, microfluidics has been explored for a wide range of applications, from chemical synthesis to fundamental biological studies [11-29]. With respect to performing AST, microfluidics offers several advantages compared to conventional techniques, including assay with low sample volumes (~ 1-10 µL), enhanced detection sensitivity (~ 1 cell), faster analysis (2-4 h), improved portability, and the ability to perform species-specific AST in polymicrobial infections.

The primary objectives of my doctoral thesis focused on the goal of providing precise antibiotic susceptibility results using microfluidics:

- **Optimization of normally-closed (NC) valves for their incorporation into high throughput screening chips:** NC valves have been used previously in different microfluidic

applications [30] but none of these studies specifically focused on the design rules to optimize the performance of NC valves, in particular with respect to minimizing their actuation pressures and improving their reliability. I formulated a set of design rules for these microvalves so they can be utilized in high throughput biological screening applications, such as antibiotic screening and protein crystallization [8]. The design rules have enabled fabrication of valves with dimensions that can be easily achieved with standard soft lithography procedures.

- **Proof-of-concept antibiotic susceptibility testing:** I have successfully designed and implemented a microfluidic platform for antibiotic susceptibility screening [8]. Using *E. coli* as a model organism, I demonstrated the utility of the platform to precisely and rapidly quantify microbial antibiograms. I also showed the importance of rapid determination of pathogen antibiogram by demonstrating the rapid deterioration of antibiotic efficacy with amplification of microbial population. Although I quantified antibacterial effects of antibiotics based on their effects on cell growth in 10 h., a preliminary idea of antibiotic susceptibilities was discernible in ≈ 4 h, which makes the platform ideally suited for rapid diagnosis and management of infections. Furthermore, my results underscore the potential dangers of administering empirical therapies based on combinations of broad-spectrum antibiotics. By accentuating several instances in which antibiotic combinations fare poorly, I expound the need to rigorously evaluate antibiotic cocktails prior to clinical administration.
- **Antibiotic susceptibility testing using clinically relevant pathogens such as *P. aeruginosa* and *K. pneumoniae* in monomicrobial and polymicrobial cultures:** Several infections such as urinary tract infections (UTI) are polymicrobial; yet, most AST studies have focused on monomicrobial AST [31-33]. I performed AST on polymicrobial cultures involving *E. coli*,

P. aeruginosa, and *K. pneumoniae*. Since these types of experiments are challenging to perform using conventional techniques for AST, the current practice often involves extrapolating monomicrobial AST results to determine treatment of polymicrobial infections. Such practices increase the risk of prescribing incorrect antibiotic dosing regimen, consequently antibiotic resistance, bacteria behaves differently in presence of other types of bacteria[31-33]. The approach reported in this thesis offers the potential to prescribe an appropriate antibiotic dosing regimen in a timely fashion based on bacteria-specific polymicrobial AST results. In addition, the technique presents an opportunity to study dynamic bacterial interactions for extended periods of time.

- **Pharmacodynamics/pharmacokinetics (PK-PD) of antibiotics:** PD modeling helps in determination of a precise MIC that can further be used to perform PK modeling for determining a precise *in vivo* antibiotic dosing regimen using experimental data from the microfluidic device. I performed a proof-of-concept study to demonstrate PK-PD modeling from experimental data obtained from time-kill curves for monomicrobial and polymicrobial AST.
- **AST using non-genetically modified bacteria:** Since the tools developed in the work utilize genetically modified bacteria, I attempted to address this issue by optimizing fluorescent dyes to be used with non-genetically modified bacteria. Though determination of MIC is possible using optical dyes mentioned here, more work is needed to advance this part of the study for performing long-term cell studies with "real" clinical samples.

7.2 Future directions

The discussed microfluidic platforms in this thesis for AST have primarily been used as a research tool to study the interaction of antibiotics and monomicrobial/polymicrobial bacteria.

Although these platforms have led to interesting microbiological insights, two key advances are required to translate the microfluidic technology to clinics. **First**, since most of the microfluidic-based AST studies have utilized genetically modified bacteria for assays, optimized microfluidic platforms need to be developed that utilize non-genetically modified bacteria, which is representative of the actual clinical samples. Though this aspect was tested in **chapter 6** of my thesis, more studies are needed to further advance the technology since the current optimization allows determination of MIC only and no long-term studies are possible due to loss of fluorescence overtime. **Second**, since the current technology is dependent on ancillaries such as microscope for TLFM and the current set up requires trained personnel for performing AST, the technology needs to be further optimized for point-of-care applications. Cell-phone based colorimetric detection could be an approach to realize the goal of a point-of-care technology. Finally, the current techniques for AST have been used for decades to treat microbial infections, and introduction of a new technology would require collaboration between scientists and clinicians to specifically perform comparative studies on AST and PK/PD modeling using conventional techniques and microfluidic platforms. These types of collaborations will help in overcoming resistance faced by the clinicians in the healthcare for the adoption of the new technologies that will enable prescription of accurate antibiotic dosing regimen, which would ultimately help in addressing the global health issue of antibiotic resistance.

7.3 References

1. Carr NF, Wales SG, Young D. 1994. Reported management of patients with sore throat in Australian general practice. British Journal of General Practice 44: 515-8.
2. Alanis AJ. 2005. Resistance to antibiotics: are we in the post-antibiotic era? Archives of medical research 36: 697-705.
3. Bisht R, Katiyar A, Singh R, Mittal P. 2009. Antibiotic resistance - A global issue of concern. Asian Journal of Pharmaceutical and Clinical Research 2: 34-9.
4. Kauffman CA, Hedderwick SA, Bradley SF, High. 1999. Antibiotic resistance: Issues in long-term care. Infections in Medicine 16: 122-8.
5. Kunin CM. 1993. Resistance to antimicrobial drugs - A worldwide calamity. Annals of Internal Medicine 118: 557-61.
6. Boedicker JQ, Li L, Kline TR, Ismagilov RF. 2008. Detecting bacteria and determining their susceptibility to antibiotics by stochastic confinement in nanoliter droplets using plug-based microfluidics. Lab on a Chip - Miniaturisation for Chemistry and Biology 8: 1265-72.
7. Cira NJ, Ho JY, Dueck ME, Weibel DB. 2012. A self-loading microfluidic device for determining the minimum inhibitory concentration of antibiotics. Lab on a Chip 12: 1052-9.
8. Mohan R, Mukherjee A, Sevgen SE, Sanpitakseree C, et al. 2013. A multiplexed microfluidic platform for rapid antibiotic susceptibility testing. Biosensors and Bioelectronics 49: 118-25.
9. Murray CK, Hospenthal DR, Kotwal RS, Butler FK. 2011. Efficacy of Point-of-Injury Combat Antimicrobials. The Journal of Trauma: Injury, Infection, and Critical Care 71: S307-S13.
10. Sun P, Liu Y, Sha J, Zhang Z, et al. 2011. High-throughput microfluidic system for long-term bacterial colony monitoring and antibiotic testing in zero-flow environments. Biosensors and Bioelectronics 26: 1993-9.
11. Velve-Casquillas G, Le Berre M, Piel M, Tran PT. 2010. Microfluidic tools for cell biological research. Nano Today 5: 28-47.
12. Zheng XT, Yu L, Li P, Dong H, et al. 2013. On-chip Investigation of Cell-drug Interactions. Advanced drug delivery reviews 65: 1556–74.
13. Ziółkowska K, Kwapiszewski R, Brzózka Z. 2011. Microfluidic devices as tools for mimicking the in vivo environment. New Journal of Chemistry 35: 979-90.
14. Abou-Hassan A, Sandre O, Cabuil V. 2010. Microfluidics in inorganic chemistry. Angewandte Chemie International Edition 49: 6268-86.
15. Andersson H, Berg AVd. 2003. Microfluidic devices for cellomics: a review. Sensors and Actuators B: Chemical 92: 315-25.
16. deMello AJ. 2006. Control and detection of chemical reactions in microfluidic systems. Nature 442: 394-402.
17. Dittrich PS, Manz A. 2006. Lab-on-a-chip: microfluidics in drug discovery. Nature Reviews Drug Discovery 5: 210-8.
18. El-Ali J, Sorger PK, Jensen KF. 2006. Cells on chips. Nature 442: 403-11.
19. Khandurina J, Guttman A. 2002. Bioanalysis in microfluidic devices. Journal of Chromatography A 943: 159-83.
20. Kobel S, Lutolf MP. 2011. Biomaterials meet microfluidics: building the next generation of artificial niches. Current Opinion in Biotechnology 22: 690-7.

21. Kraly JR, Holcomb RE, Guan Q, Henry CS. 2009. Review: Microfluidic applications in metabolomics and metabolic profiling. Analytica chimica acta 653: 23-35.
22. Lecault V, White AK, Singhal A, Hansen CL. 2012. Microfluidic single cell analysis: from promise to practice. Current Opinion in Chemical Biology 16: 381-90.
23. Li L, Ismagilov RF. 2010. Protein crystallization using microfluidic technologies based on valves, droplets, and slipchip. Annual review of biophysics 39: 139-58.
24. Mason BP, Price KE, Steinbacher JL, Bogdan AR, et al. 2007. Greener approaches to organic synthesis using microreactor technology. Chemical Reviews 107: 2300-18.
25. Park JI, Saffari A, Kumar S, Günther A, et al. 2010. Microfluidic synthesis of polymer and inorganic particulate materials. Annual Review of Materials Research 40: 415-43.
26. Streets AM, Huang Y. 2013. Chip in a lab: Microfluidics for next generation life science research. Biomicrofluidics 7: 011302.
27. Tu Q, Pang L, Zhang Y, Yuan M, et al. 2013. Microfluidic Device: A Miniaturized Platform for Chemical Reactions. Chinese Journal of Chemistry 31: 304-16.
28. Wang J, Ren L, Li L, Liu W, et al. 2009. Microfluidics: a new cosset for neurobiology. Lab on a Chip 9: 644-52.
29. Zhang C, Xing D. 2010. Single-molecule DNA amplification and analysis using microfluidics. Chemical Reviews 110: 4910-47.
30. Mohan R, Schudel BR, Desai AV, Yearsley JD, et al. 2011. Design considerations for elastomeric normally closed microfluidic valves. Sensors and Actuators, B: Chemical 160: 1216-23.
31. Chu W, Zere TR, Weber MM, Wood TK, et al. 2012. Indole production promotes escherichia coli mixed-culture growth with Pseudomonas aeruginosa by inhibiting quorum signaling. Applied and Environmental Microbiology 78: 411-9.
32. Riedele C, Reichl U. 2011. Interspecies effects in a ceftazidime-treated mixed culture of Pseudomonas aeruginosa, Burkholderia cepacia and Staphylococcus aureus: analysis at the single-species level. Journal of Antimicrobial Chemotherapy 66: 138-45.
33. Riedele C, Reichl U. 2012. Time-kill studies with a ceftazidime-treated mixed culture consisting of Pseudomonas aeruginosa, Burkholderia cepacia and Staphylococcus aureus. Engineering in Life Sciences 12: 188-97.

Appendix A

A.1 Distribution of cells in the microfluidic device

Distribution of cells was studied in the microfluidic device that helped in optimization of the device in polymicrobial studies. The primary objective here was to model distribution of particles in the microfluidic device discussed in chapter 3 under conditions such as high and low density of beads and longer actuation of valves. The key goal was the optimization of the platform based on the results obtained experimentally and using COMSOL modeling. Fluorescent beads of the same size as typical bacterial cells were used as model particles in the experiment. Experiment was performed on 18 devices using micro fluorescence beads solution at three different concentrations. (C1: $500x10^6$, C2: $50x10^6$, and C3: $5x10^6$ beads/mL).

Theoretical values

C1, C2, C3: 1500, 150, 15 beads/chamber

$500x10^6$, 50x106, $5x10^6$ beads/mL

Experimental values (before actuation)

C1, C2, C3: 1693, 170, 19 beads/chamber

$564x10^6$, 57x106, $6x10^6$ beads/mL

Experimental values (after actuation)

C1, C2, C3: 1264, 166, 22 beads/chamber

$421x10^6$, $55x10^6$, $7x10^6$ beads/mL

Note that standard deviation of errors in the bead counts increase as the beads solutions were diluted and beads distribution was more uniform (lower standard error) when fluid valves were closed.

Standard deviation with fluid valves closed (C1, C2, and C3): 0.87%, 0.94%, 1.99%
Standard deviation with fluid valves actuated (C1, C2, and C3): 5.14%, 8.87%, 34.70%

In order to analyze the beads distribution, number of beads within a column was normalized by minimum (# of beads in each chamber/minimum beads in that column).

Beads distribution within a column was more uniform at higher concentration (lower normalized values) and fluid valves actuation had negligible effect on beads distribution within a column.

With fluid valves closed, average highest (C1, C2, C3): 1.09, 1.22, 1.72

With fluid valves actuated, average highest (C1, C2, C3): 1.08, 1.19, 1.71

Standard errors of normalized values (% compare to normalized values) increase as the beads solutions were diluted. Fluid valves actuation had no effect on of normalized values.

With fluid valves closed (C1, C2, C3): 0.91%, 2.46%, 6.98%

With fluid valves actuated (C1, C2, C3): 0.93%, 1.68%, 5.85%

Table A.1 : Distribution of beads with valves closed

	Device#1	Device #2	Device #3	Average
Dilute 10 folds ($500x10^6$ beads/mL)				
Average	1597.31	1575.33	1907.33	1693.33
S.E.	9.68	12.44	15.71	14.66 (0.87%)
Range	276	333	525	
Dilute 100 folds ($50x10^6$ beads/mL)				
Average	166.02	175.63	167.40	169.68
S.E.	2.29	3.58	2.08	1.60 (0.94%)
Range	64	110	64	
Dilute 1000 folds ($5x10^6$ beads/mL)				
Average	19.25	18.65	17.83	18.58
S.E.	0.64	0.57	0.68	0.37 (1.99%)
Range	24	17	21	

Normalization by minimum: maximum beads in a column/minimum beads in the column

	Device#1	Device #2	Device #3	Average
Dilute 10 folds ($500x10^6$ beads/mL)				
Average	1.08	1.11	1.09	1.09
S.E.	0.01	0.01	0.01	0.01 (0.91%)
Dilute 100 folds ($50x10^6$ beads/mL)				
Average	1.20	1.25	1.20	1.22
S.E.	0.03	0.04	0.03	0.03 (2.46%)
Dilute 1000 folds ($5x10^6$ beads/mL)				

Average	1.60	1.70	1.86	1.72
S.E.	0.08	0.12	0.18	0.12 (6.98%)

Table A.2 : Distribution of beads with valves open

	Device#1	Device #2	Device #3	Average
Dilute 10 folds ($500x10^6$ beads/mL)				
Average	1248.19	1262.83	1281.56	1264.19
S.E.	59.40	52.32	77.50	64.97 (5.14%)
Range	258	214	329	267
Dilute 100 folds ($50x10^6$ beads/mL)				
Average	169.96	169.40	159.02	166.13
S.E.	13.62	14.88	13.26	14.73 (8.87%)
Range	56	65	56	59
Dilute 1000 folds ($5x10^6$ beads/mL)				
Average	18.83	19.23	28.42	22.16
S.E.	4.57	5.27	8.44	7.69 (34.70%)
Range	20	24	48	31

Normalization by minimum: maximum beads in a column/minimum beads in the column

	Device#1	Device #2	Device #3	Average
Dilute 10 folds ($500x10^6$ beads/mL)				
Average	1.08	1.08	1.10	1.08
S.E.	0.01	0.01	0.01	0.01 (0.93%)
Dilute 100 folds ($50x10^6$ beads/mL)				
Average	1.19	1.21	1.18	1.19
S.E.	0.02	0.02	0.02	0.02 (1.68%)
Dilute 1000 folds ($5x10^6$ beads/mL)				
Average	1.70	1.67	1.75	1.71
S.E.	0.09	0.09	0.13	0.10 (5.85%)

COMSOL modeling was performed to see the distribution of particles in the device (**Fig A.1-A.8**). Modeling results demonstrated accumulation of beads more likely on the ends and non-uniform distribution of beads, perhaps due to inconsistent hydrodynamic resistance.

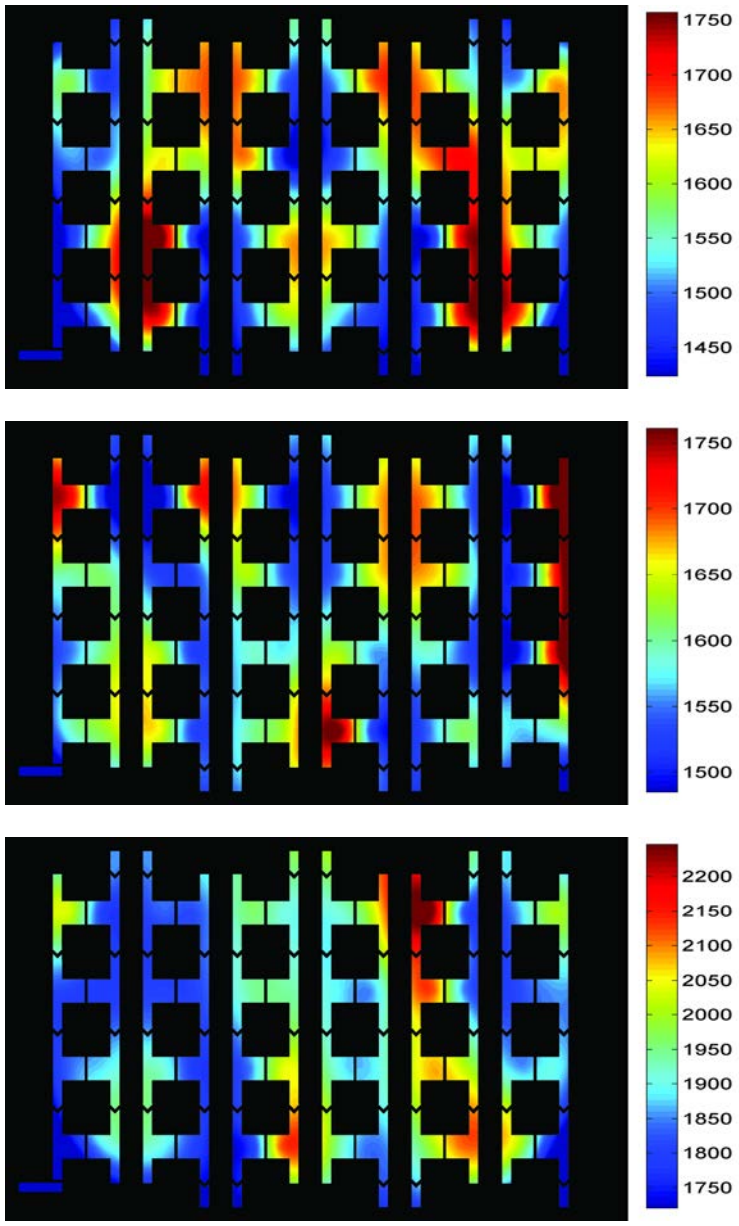

Figure A.1. Heat map with no normalization and cell culture diluted by 10 folds with LB

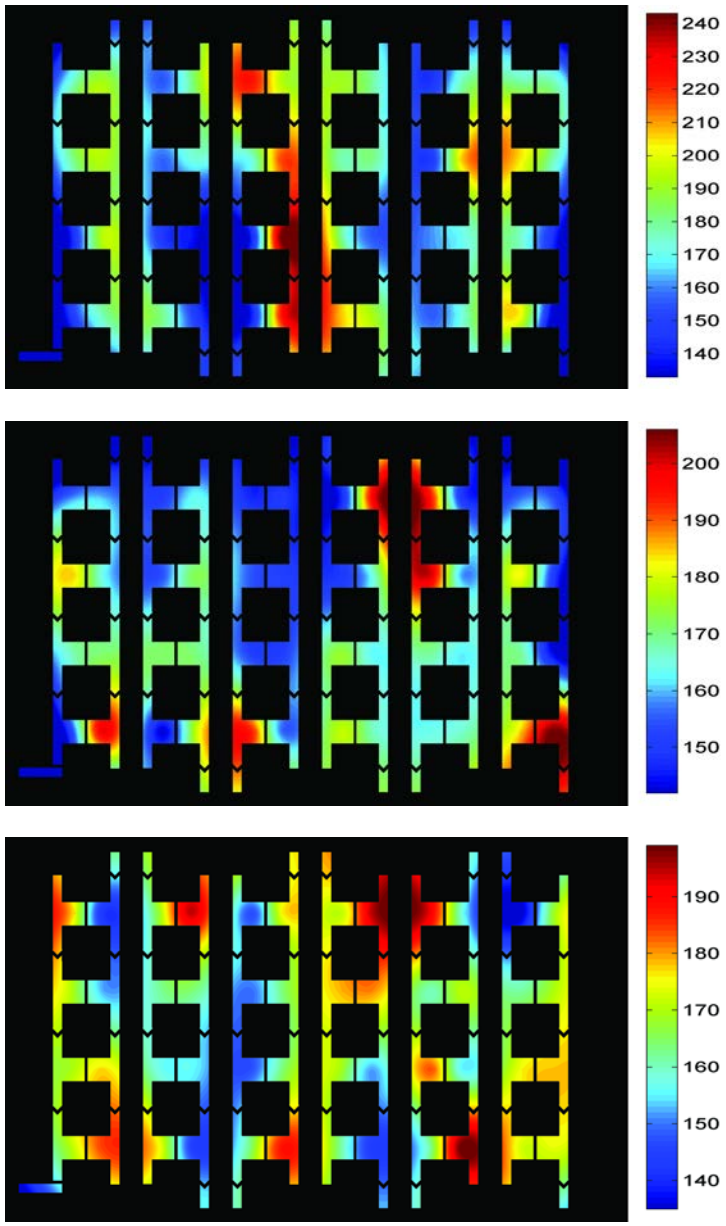

Figure A.2. Heat map with no normalization and cell culture diluted by 100 folds with LB

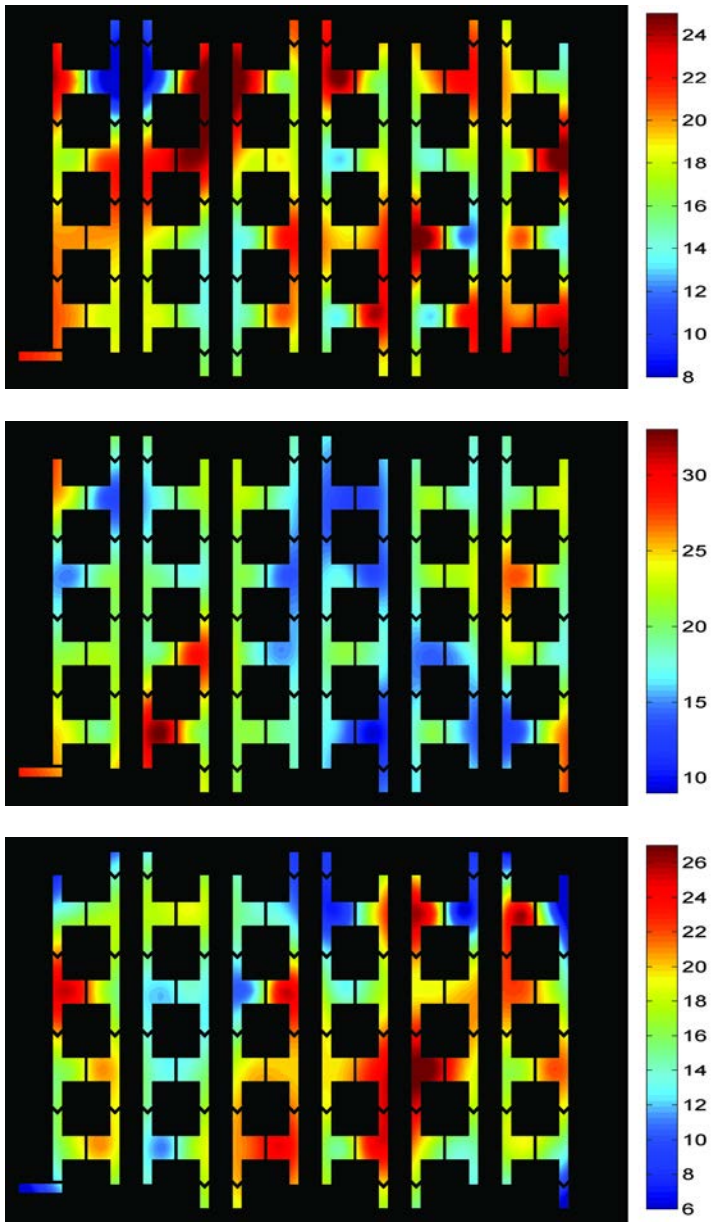

Figure A.3. Heat map with no normalization and cell culture diluted by 1000 folds with LB

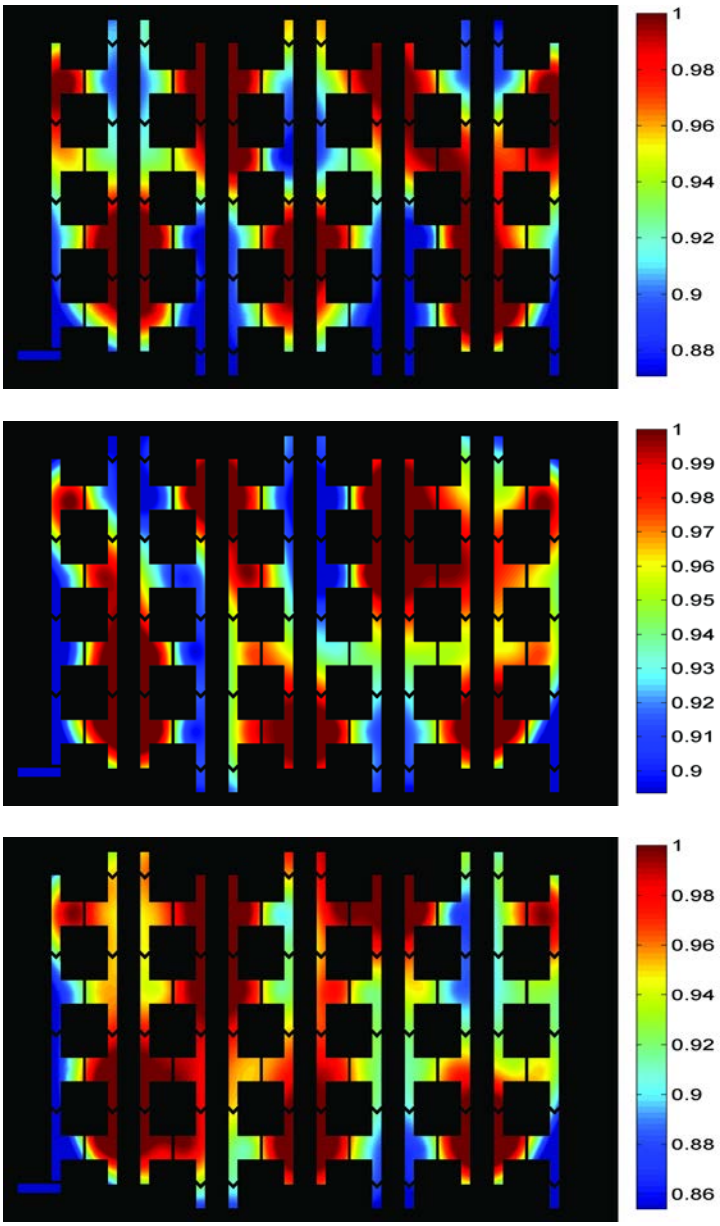

Figure A.4. Heat map with normalization (max) and cell culture diluted by 10 folds with LB

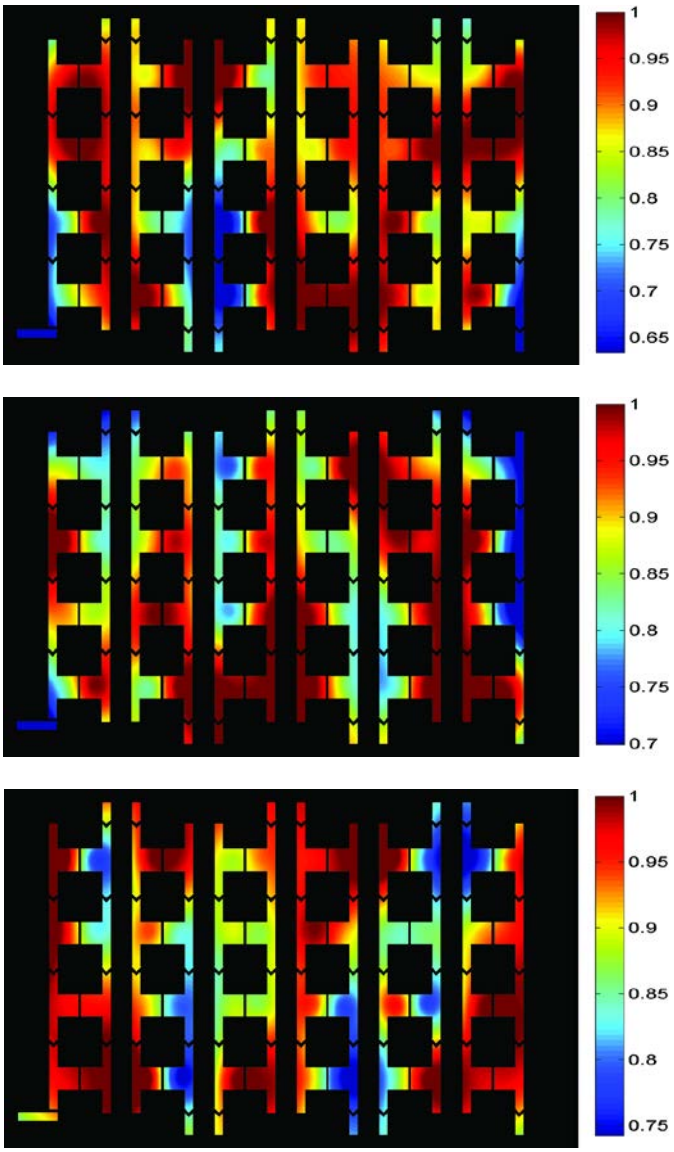

Figure A.5. Heat map with normalization (max) and cell culture diluted by 100 folds with LB

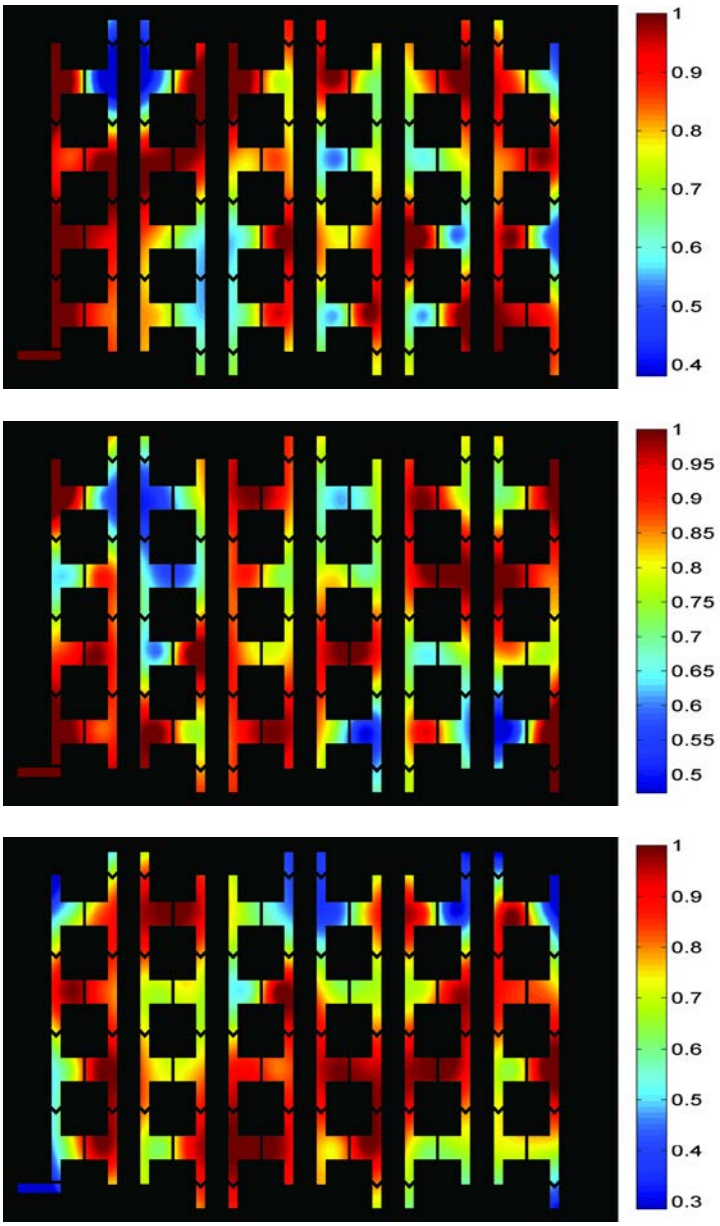

Figure A.6. Heat map with normalization (max) and cell culture diluted by 10 folds with LB

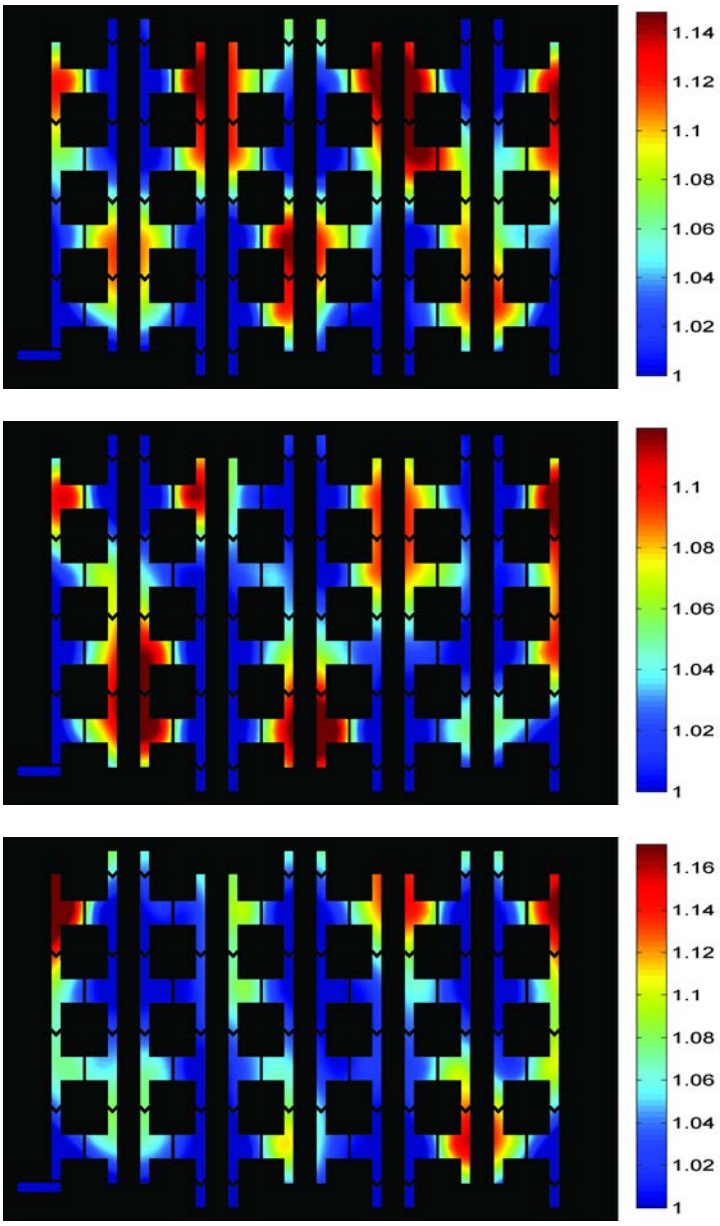

Figure A.7. Heat map with normalization (min) and cell culture diluted by 10 folds with LB

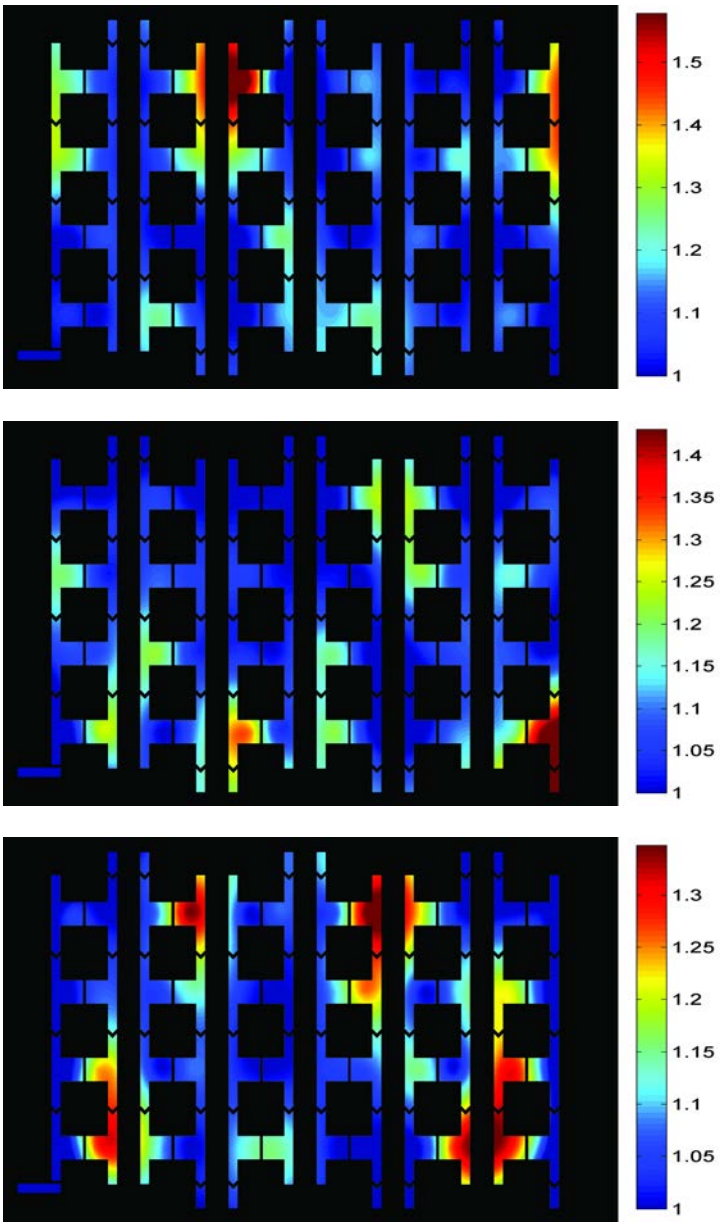

Figure A.8. Heat map with normalization (min) and cell culture diluted by 100 folds with LB

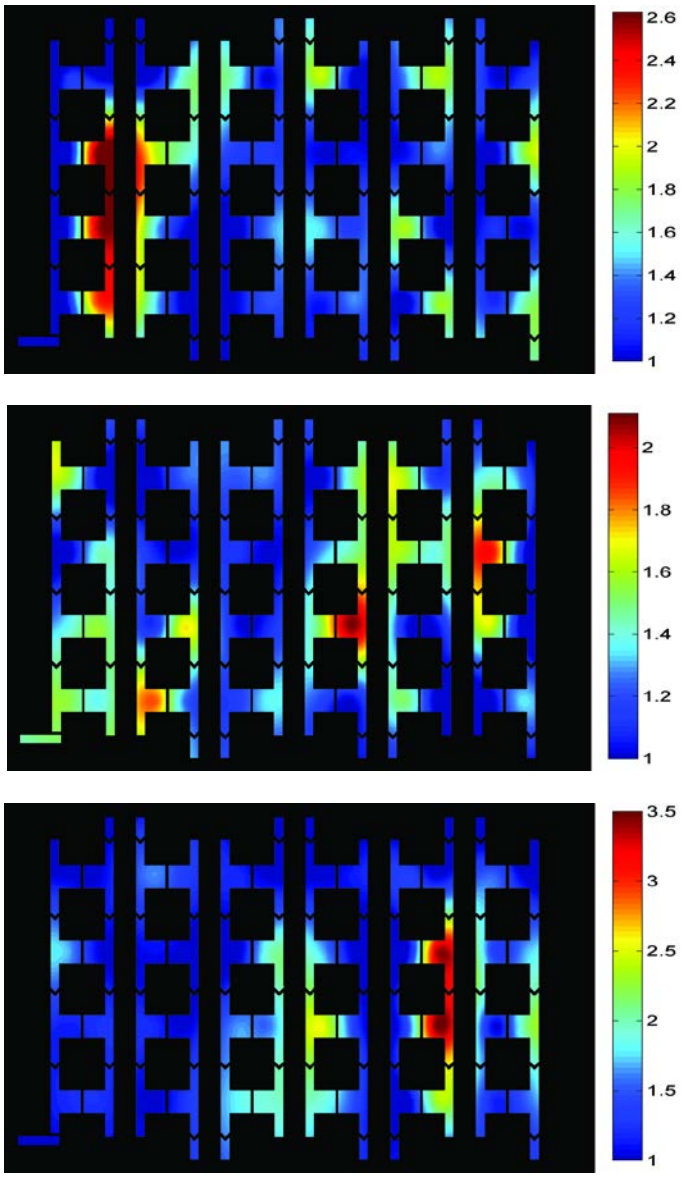

Figure A.9. Heat map with normalization (min) and cell culture diluted by 1000 folds with LB

I changed the dimensions of the mixing valves and determined growth rate to see effect of valve dimensions on the physiology of the cells. All chambers that initially had the same material (LB/cells) gave a similar growth curve. Thus, width and height of mixing valve does not alter the growth rate (**Fig. A.9**). The following graphs show growth of cells in adjacent chambers. The graph on the left shows growth in the chamber where cells are added and the one on right show growth rate where medium (LB) is added. **Fig. A.10** utilizes COMSOL modeling to show dimensions of the mixing valve that give the most efficient mixing.

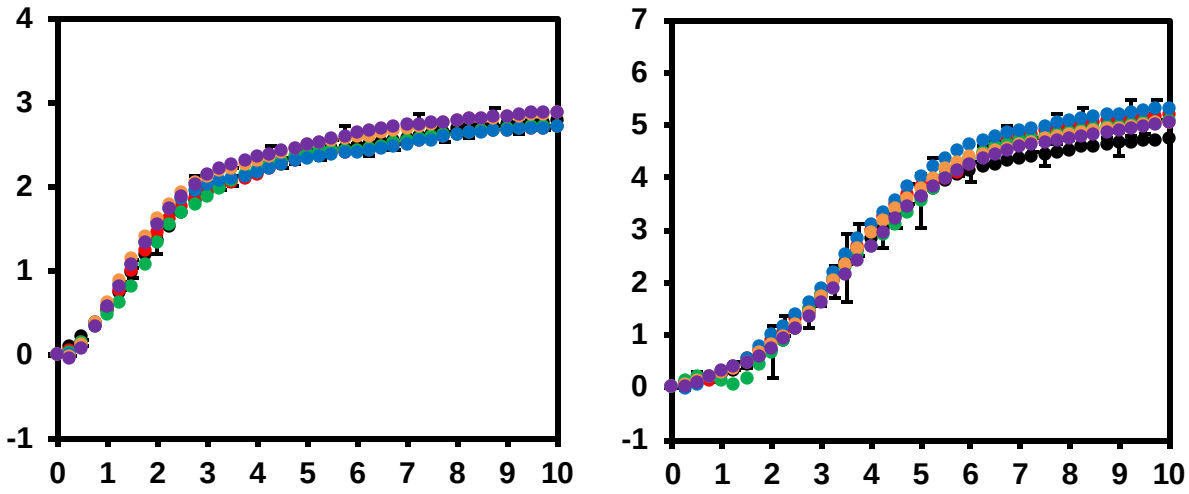

Figure A.10. Growth rate of bacteria in when different mixing valve dimensions are utilized. Negligible change in growth rate is seen for all cases.

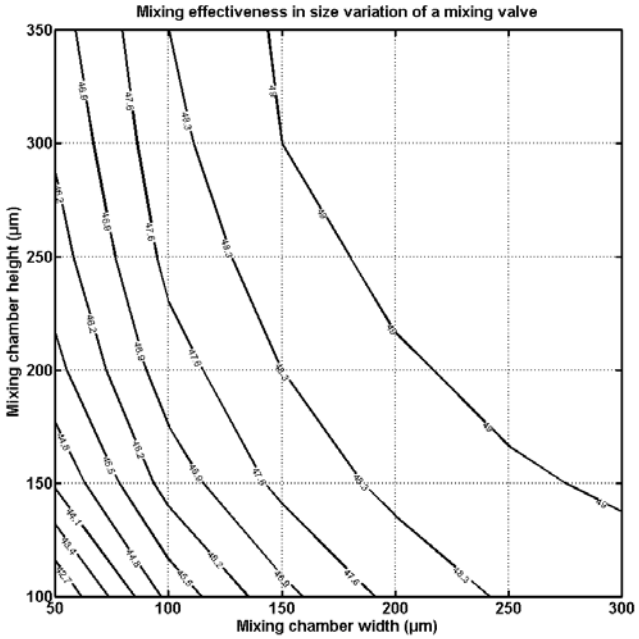

Figure A.11. Mixing is the most efficient (~ 1:1) with valve dimensions 300 x 350.

Appendix B

B.1 MATLAB codes for image analysis

MATLAB codes have been divided into three categories. First describes the codes used in chapter 3, second describes when 20x objective is utilized, and third category describes codes used in polymicrobial AST experiments in chapter 4.

Sorting the images after acquisition [Chapter 3 - with 10x objective]

```
function 10x_single_sort()
clc % clear existing text on the screen
disp('Image sorting - sort RAW IGB images into chambers.')
path =  uigetdir('C:\Users\pkgroup\Desktop');% show folder selection
toolbox
disp('Sorting....')
global blank
blank = 0;
manage(path,path);% Use recursive function to sort all *.tif files
into corresponding folders
rmdir(fullfile(path,'sorted',num2str(blank,'%02d')),'s'); % remove
blank background images after sorting
disp('     Done!')
end

function manage(path,givenpath)
global blank
listing = dir(fullfile(path,'\'));% list all the files/folders inside
the selected folder
for i = 3:numel(listing)% work on each file/folder one by one
     subpath = fullfile(path,listing(i).name);
    [~, name, ext] = fileparts(listing(i).name);
if isdir(subpath)==1
     manage(subpath,givenpath);% if a folder is found inside a given
folder, run function 'manage' with that folder
elseif strcmpi(ext,'.tif')
% create the chamber folders. Since one image contains two chambers
(10x), a copy of an image set is created to make a folder for each
chamber.
foldername = sprintf('%02d',str2num(name(end-1:end))*2-1);
foldernext = sprintf('%02d',str2num(name(end-1:end))*2);
     if exist(fullfile(givenpath,'sorted',foldername),'dir')==0
          mkdir(fullfile(givenpath,'sorted',foldername));
       mkdir(fullfile(givenpath,'sorted',foldernext));
            if blank<str2num(foldernext)
               blank = str2num(foldernext);
            end
    end
```

```
copyfile(fullfile(subpath),fullfile(givenpath,'sorted',foldernext));
     movefile(fullfile(subpath),fullfile(givenpath,'sorted',foldername
));% move the file to corresponding chamber folder
end
end
end
```

Cropping the images after sorting

```
function 10x_single_crop()
clc % clear the existing text on the screen
disp('IGB cropping code - Please select experiment folder to
proceed.')
disp('The last chamber must be a blank')
mainpath = uigetdir();% shows folder selection dialog box
path1 = fullfile(mainpath,'sorted');
list = dir(path1);% make a list of folders inside
% create 'stackimage' folder if not already exists
if ~exist(fullfile(mainpath,'stackimage'), 'dir')
     mkdir(fullfile(mainpath,'stackimage'));
end

disp('cropping, please wait...')

% Gather all background reference images
i=numel(list);
if isdir(fullfile(path1,list(i).name))==1
        subpath = fullfile(path1,list(i).name);
        piclist = dir(subpath);% make a list of blank images at
different time
        blank = zeros(600,800,numel(piclist)-3,'uint8'); % create a
variable for storing blank images
        for j=3:1:numel(piclist
            [~, ~, ext] =
fileparts(fullfile(subpath,piclist(j).name));
            if strcmpi(ext,'.TIF')==1
                blank(:,:,j-2) =
imread(fullfile(subpath,piclist(j).name));% store blank images for in
variable ‘blank’
            end
        end
end

% work on cropping folder by folder
for i=3:1:(numel(list)-1)
    if isdir(fullfile(path1,list(i).name))==1
        subpath = fullfile(path1,list(i).name);
        piclist = dir(subpath);% make a list of images in each chamber
folder
        allpic = zeros(600,800,numel(piclist)-3,'uint8');% create a
blank variable for storing chamber images
```

```
        for j=3:1:numel(piclist)
            [~, name, ext] =
fileparts(fullfile(subpath,piclist(j).name));
            if strcmpi(ext,'.TIF')==1
                allname(j-2) = {name};
                allpic(:,:,j-2) =
imread(fullfile(subpath,piclist(j).name));%store images in the
variable created
            end
        end
    end
% This code relies on user to indicate the chamber position. The
following commands will allows the 'chamber shape' to be seen easily.
I = sum(allpic,3);
I = histeq(I/max(max(I)));
s = warning('off', 'Images:initSize:adjustingMag');
imshow(I);% display stacked image on screen for cropping
set(gcf,'NumberTitle','off');
set(gcf,'Name',strcat(list(i).name,'/',list(end-1).name));
warning(s);

h = imrect(gca, [250 200 289 289]);% display cropping rectangle on the
stack image
setResizable(h,false);

% record the stacked image
ipath = fullfile(mainpath,'stackimage',strcat(list(i).name,'.jpg'));
imwrite(I,ipath,'jpg');

%subtract each image with corresponding background reference, crop,
and then save as *.jpg files
pause
position = getPosition(h);% get the cropping rectangle position
for k=1:1:numel(blank(1,1,:))
allpic(:,:,k) = allpic(:,:,k)-blank(:,:,k);%subtract chamber images
with blank reference images
despath = fullfile(subpath,strcat(allname{k},'.jpg'));
cropped = imcrop(allpic(:,:,k),position);% crop images in that chamber
at the given rectangle position
imwrite(cropped,despath,'jpg','Quality',100);%write jpg image in the
same chamber folder
end
end
close

disp('Deleting *tiff files....')

rmdir(fullfile(path1,list(numel(list)).name),'s');% remove blank
images
recycle off;
```

```
manage(mainpath,mainpath);% delete every *tif files using recursive
function
recycle on;
disp('     Done!')

end

function manage(path,givenpath)
listing = dir(fullfile(path,'\'));
for i = 3:numel(listing)
     subpath = fullfile(path,listing(i).name);
    [~, name, ext] = fileparts(listing(i).name);
if isdir(subpath)==1
     delete(fullfile(subpath,'*.tif'));
     manage(subpath,givenpath);
end
end
end
```

Counting the cells

```
function 10x_single_count()
clc% clear existing images on the screen
disp('Configuring necessary parameters...')
warning off all;
clear global variable
clear java

% Request for the threshold inputs for ‘Find Maxima’ algorithm
threshold = str2double(input('Please enter the threshold: ','s'));

% This code relies on ImageJ function (Requires ImageJ)
javaaddpath('C:/Program Files (x86)/ImageJ/ij.jar');
javaaddpath('C:/Program Files/ImageJ/ij.jar');
import('ij.IJ.*'); % Import ImageJ functions
import('ij.plugin.filter.*'); % Import more ImageJ functions
% 'Find Maxima' function is avaiable only in version 1.46 or later
if versionLessThan('1.46')==1
    return
end

disp('Please locate the sorted, cropped experiment folder...')
folder = uigetdir();% locate experiment folder
path = fullfile(folder,'sorted');

listing = dir(path);% make a list of chamber folders inside channal
folders
disp('Counting cells in chamber number:  ')

for a=3:(numel(listing))% count cells folder by folder
    filelist = dir(fullfile(path,listing(a).name,'*.jpg'));% make a
list of chamber images inside each chamber folder
```

```
    fprintf(1,'\b\b%s',listing(a).name);
    chambername(1,a-2) = str2num(listing(a).name);
    chambername(2,a-2) = 1;
    first = imread(fullfile(path,listing(a).name,filelist(1).name));
    overall = sum(sum(first));% obtain intensity sum of the first
image in that folder.
% for each file, load image into Java variable, then use getMaxima
function to achieve the cell count.
    for b=1:numel(filelist)
        imp =
openImage(fullfile(path,listing(a).name,filelist(b).name));
        ip = imp.getProcessor();
        mf = MaximumFinder;
        maxima = mf.getMaxima(ip,threshold, 0);% call function Maximum
Finder using the defined threshold
        maximacount(b,a-2) = maxima.npoints;%get the cell count from
ImageJ
% alternative counting method: count by comparing intensity sum with
the first image intensity sum. The cell count is then related to the
first image cell count.
        I = imread(fullfile(path,listing(a).name,filelist(b).name));
        intensity = sum(sum(I));
        intensitycount(b,a-2) =
floor(intensity/overall*maximacount(1,a-2)); % record cell count by
intensity (relative to the first image) in an array
        rawintensity(b,a-2) = floor(intensity);% record raw intensity
of each image in another array
    end
end
fprintf('\n')
disp('Done counting cells. ')

% record the cell counts in Excel file.
disp('Writing result in .xls file...')
filename = 'Cell Count.xls';
timepoints = numel(dir(fullfile(path,listing(3).name,'*.jpg')))-1;
time = transpose(0:30:timepoints*30);

A1 = sprintf('threshold = %d',threshold);

xlswrite(fullfile(folder,filename), {A1;'Y/N = 1/0';'time(min)'},
3,'A1');
xlswrite(fullfile(folder,filename), chambername, 3,'B1');
xlswrite(fullfile(folder,filename), time, 3,'A4');
xlswrite(fullfile(folder,filename), rawintensity, 3,'B4');

xlswrite(fullfile(folder,filename), {A1;'Y/N = 1/0';'time(min)'},
2,'A1');
xlswrite(fullfile(folder,filename), chambername, 2,'B1');
xlswrite(fullfile(folder,filename), time, 2,'A4');
xlswrite(fullfile(folder,filename), intensitycount, 2,'B4');
```

```
xlswrite(fullfile(folder,filename), {A1;'Y/N = 1/0';'time(min)'},
1,'A1');
xlswrite(fullfile(folder,filename), chambername, 1,'B1');
xlswrite(fullfile(folder,filename), time, 1,'A4');
xlswrite(fullfile(folder,filename), maximacount, 1,'B4');

e = actxserver ('Excel.Application'); % open Activex server
ewb = e.Workbooks.Open(fullfile(folder,filename)); % open file (enter
full path!)
ewb.Worksheets.Item(1).Name = 'Local Maxima';% rename 1st sheet
ewb.Worksheets.Item(2).Name = '# from Intensity';
ewb.Worksheets.Item(3).Name = 'Raw Intensity';
ewb.Save % save to the same file
ewb.Close(false)
e.Quit

fprintf('Output file: %s\n', filename)
clear all
clear global variable
clear java
disp('     Done!')
warning on all;
end
```

MATLAB codes with 20x objective

Sorting code

```
function 20x_single_sort()
clc % clear existing text on the screen
disp('Image sorting - sort RAW IGB images into chambers.')
path =  uigetdir('C:\Users\pkgroup\Desktop'); % show folder
selection toolbox
disp('Sorting....')
manage(path,path); % Use recursive function to sort all *.tif
files into corresponding folders
disp('     Done!')
end

function manage(path,givenpath)
listing = dir(fullfile(path,'\')); % list all the files/folders
inside the selected folder
for i = 3:numel(listing)
     subpath = fullfile(path,listing(i).name);
    [~, name, ext] = fileparts(listing(i).name);
if isdir(subpath)==1
     manage(subpath,givenpath); % if detect folder inside, run
‘manage’ function on this folder again
```

```
elseif strcmpi(ext,'.tif') % if detect *.tif file, create
chamber folder and move the file into corresponding chamber
folder
    foldername = sprintf('%02d',str2num(name(end-1:end)));
     if exist(fullfile(givenpath,'sorted',foldername),'dir')==0
          mkdir(fullfile(givenpath,'sorted',foldername));
    end
     movefile(fullfile(subpath),fullfile(givenpath,'sorted',fold
ername));
end
end
end
```

Cropping the images

```
function 20x_single_crop()
clc % clear existing text on the screen
disp('IGB cropping code - Please select experiment folder to
proceed.')
disp('The last chamber must be a blank')
mainpath = uigetdir(); % show folder selection toolbox
path1 = fullfile(mainpath,'sorted');% go to ‘sorted’ folder
list = dir(path1);% list all chamber folders
if ~exist(fullfile(mainpath,'stackimage'), 'dir')
     mkdir(fullfile(mainpath,'stackimage'));% create
‘stackimage’ folder
end

disp('cropping, please wait...')

% start collecting noise images (last chamber)
i=numel(list);
if isdir(fullfile(path1,list(i).name))==1
        subpath = fullfile(path1,list(i).name);% locate the last
folder
        piclist = dir(subpath);% list all files (images) in the
last folder
        blank = zeros(600,800,numel(piclist)-3,'uint8');% create
a blank variable for blank background image storage.
        for j=3:1:numel(piclist)%% from j=1
            [~, ~, ext] =
fileparts(fullfile(subpath,piclist(j).name));
            if strcmpi(ext,'.TIF')==1
blank(:,:,j-2) = imread(fullfile(subpath,piclist(j).name)); %
store blank images in ‘blank’ variable
            end
        end
```

```
else
    disp('error: non folder is the last item in sorted folder')
    return
end

% start collecting real images
for i=3:1:(numel(list)-1) % work on each chamber folder one by
one
    if isdir(fullfile(path1,list(i).name))==1
        subpath = fullfile(path1,list(i).name);
        piclist = dir(subpath);
        allpic = zeros(600,800,numel(piclist)-3,'uint8'
for j=3:1:numel(piclist)
            [~, name, ext] =
fileparts(fullfile(subpath,piclist(j).name));
            if strcmpi(ext,'.TIF')==1
                allname(j-2) = {name};
                allpic(:,:,j-2) =
imread(fullfile(subpath,piclist(j).name)); % read images in that
folder into ‘allpic’ variable
            end
        end
    end
% This code relies on user to indicate the chamber position. The
following commands will allows the 'chamber shape' to be seen
easily.
I = sum(allpic,3);
I = imadjust(histeq(I/max(max(I))));
s = warning('off', 'Images:initSize:adjustingMag');
imshow(I); % display an enhanced image of that chamber for
cropping
set(gcf,'NumberTitle','off');
set(gcf,'Name',strcat(list(i).name,'/',list(end-1).name));
warning(s);
h = imrect(gca, [50 20 559 559]); % display a cropping rectangle
setResizable(h,false);

% record a stacked image
ipath =
fullfile(mainpath,'stackimage',strcat(list(i).name,'.jpg'));
imwrite(I,ipath,'jpg');

%subtract each image with corresponding background reference,
crop the green channel, and then save as *.jpg files
pause
position = getPosition(h); % get position from the cropping
rectangle
```

```
for k=1:1:numel(blank(1,1,:))
allpic(:,:,k) = allpic(:,:,k)-blank(:,:,k); % subtract every
images in that chamber with a blank image at the same time point
despath = fullfile(subpath,strcat(allname{k},'.jpg'));
cropped = imcrop(allpic(:,:,k),position); % crop images
imwrite(cropped,despath,'jpg','Quality',100); % write cropped
images in the same folder as the original images
end

end
close

% delete original *tiff files
disp('Deleting *tiff files....')
rmdir(fullfile(path1,list(numel(list)).name),'s');
recycle off;
manage(mainpath,mainpath); % recursive function for deleting
*.tiff files
recycle on;
disp('     Done!')

end

function manage(path,givenpath)
listing = dir(fullfile(path,'\'));
for i = 3:numel(listing)
     subpath = fullfile(path,listing(i).name);
    [~, name, ext] = fileparts(listing(i).name);
if isdir(subpath)==1
     delete(fullfile(subpath,'*.tif'));
     manage(subpath,givenpath);
end
end
end
```

Counting the cells

```
function 20x_single_count()
clc  % clear existing text on the screen
disp('Configuring necessary parameters...')
warning off all;
clear global variable
clear java

% Request for threshold input for ‘Find Maxima’ algorithm
threshold = str2double(input('Please enter the threshold:
','s'));
```

```
% This code relies on ImageJ function as it's core, thus ImageJ
is needed
javaaddpath('C:/Program Files (x86)/ImageJ/ij.jar');
javaaddpath('C:/Program Files/ImageJ/ij.jar');
import('ij.IJ.*'); % Import ImageJ functions
import('ij.plugin.filter.*'); % Import more ImageJ functions
if versionLessThan('1.46')==1 % 'Find Maxima' function is
avaiable only in version 1.46 or later
    return
end

% locate experiment folder and update the counting progress
disp('Please locate the sorted, cropped experiment folder...')
folder = uigetdir();
path = fullfile(folder,'sorted');

listing = dir(path);
disp('Counting cells in chamber number:  ')

for a=3:(numel(listing)) % count cells folder by folder
    filelist = dir(fullfile(path,listing(a).name,'*.jpg'));
    fprintf(1,'\b\b%s',listing(a).name);
    chambername(1,a-2) = str2num(listing(a).name);
    chambername(2,a-2) = 1;
    first =
imread(fullfile(path,listing(a).name,filelist(1).name));
    overall = sum(sum(first)); % obtain intensity sum of the
first image in that folder.

% for each file, load image into Java variable, then use
getMaxima function to achieve the cell count.
    for b=1:numel(filelist)
        imp =
openImage(fullfile(path,listing(a).name,filelist(b).name));
        ip = imp.getProcessor();
        mf = MaximumFinder;
        maxima = mf.getMaxima(ip,threshold, 0);% call function
Maximum Finder using the defined threshold
        maximacount(b,a-2) = maxima.npoints;%get the cell count
from ImageJ
% alternative counting method: count by comparing intensity sum
with the first image intensity sum. The cell count is then
related to the first image cell count.
        I =
imread(fullfile(path,listing(a).name,filelist(b).name));
        intensity = sum(sum(I));
```

```
        intensitycount(b,a-2) =
floor(intensity/overall*maximacount(1,a-2));
        rawintensity(b,a-2) = floor(intensity);
    end
end

% record the counting result in Excel file.
fprintf('\n')
disp('Done counting cells. ')
disp('Writing result in .xls file...')
filename = 'Cell Count.xls';
timepoints = numel(dir(fullfile(path,listing(3).name,'*.jpg')))-
1;
time = transpose(0:30:timepoints*30);

A1 = sprintf('threshold = %d',threshold);

xlswrite(fullfile(folder,filename), {A1;'Y/N =
1/0';'time(min)'}, 3,'A1');
xlswrite(fullfile(folder,filename), chambername, 3,'B1');
xlswrite(fullfile(folder,filename), time, 3,'A4');
xlswrite(fullfile(folder,filename), rawintensity, 3,'B4');

xlswrite(fullfile(folder,filename), {A1;'Y/N =
1/0';'time(min)'}, 2,'A1');
xlswrite(fullfile(folder,filename), chambername, 2,'B1');
xlswrite(fullfile(folder,filename), time, 2,'A4');
xlswrite(fullfile(folder,filename), intensitycount, 2,'B4');

xlswrite(fullfile(folder,filename), {A1;'Y/N =
1/0';'time(min)'}, 1,'A1');
xlswrite(fullfile(folder,filename), chambername, 1,'B1');
xlswrite(fullfile(folder,filename), time, 1,'A4');
xlswrite(fullfile(folder,filename), maximacount, 1,'B4');

e = actxserver ('Excel.Application'); % open Activex server
ewb = e.Workbooks.Open(fullfile(folder,filename)); % open file
ewb.Worksheets.Item(1).Name = 'Local Maxima';% rename 1st sheet
ewb.Worksheets.Item(2).Name = '# from Intensity';
ewb.Worksheets.Item(3).Name = 'Raw Intensity';
ewb.Save % save to the same file
ewb.Close(false)
e.Quit

fprintf('Output file: %s\n', filename)

clear all
```

```
clear global variable
clear java
disp('     Done!')
warning on all;
end
```

The following codes are for polymicrobial AST (Chapter 4)

Sorting the images

```
function 20x_poly_sort()
clc % clear existing text on the screen
disp('Image sorting - sort RAW IGB images into chambers.')
path =  uigetdir('C:\Users\pkgroup\Desktop'); % show a folder
selection dialog box
disp('Sorting....')
manage(path,path); % recursive function, repeat function
'manage' with everything inside the selected folder
disp('     Done!')
end

function manage(path,givenpath)
listing = dir(fullfile(path,'\')); % list all the files/folders
inside the selected folder

% create FITC and Texas Red folder if they are not already
existed
mkdir(fullfile(path,'FITC'));
mkdir(fullfile(path,'Texas Red'));
for i = 3:numel(listing) % work on each file/folder one by one
subpath = fullfile(path,listing(i).name);
    [~, name, ext] = fileparts(listing(i).name);
if isdir(subpath)==1
     manage(subpath,givenpath); % if a folder is found inside a
given folder, run function 'manage' with that folder

elseif ((strfind(name,'Texas Red')~=0)&(strcmpi(ext,'.tif')==1))
% if a tif file name includes 'Texas Red'
    foldername = sprintf('%02d',str2num(name(end-1:end)));
     if exist(fullfile(givenpath,'Texas
Red',foldername),'dir')==0 % if the chamber folder is not
already created
          mkdir(fullfile(givenpath,'Texas Red',foldername)); %
create the chamber folder
    end
       movefile(fullfile(subpath),fullfile(givenpath,'Texas
Red',foldername)); % move the file to corresponding chamber
folder
```

```
elseif ((strfind(name,'FITC')~=0)&(strcmpi(ext,'.tif')==1)) % if
file name includes FITC
    foldername = sprintf('%02d',str2num(name(end-1:end)));
     if exist(fullfile(givenpath,'FITC',foldername),'dir')==0 %
if the chamber folder is not already created
          mkdir(fullfile(givenpath,'FITC',foldername)); % create
the chamber folder
    end

movefile(fullfile(subpath),fullfile(givenpath,'FITC',foldername)
); % move the file to corresponding chamber folder
end
end
end
```

Cropping the images

```
function 20x_poly_crop()
clc % clear the existing text on the screen
disp('IGB cropping code - Please select experiment folder to
proceed.')
mainpath = uigetdir(); % shows folder selection dialog box
path1 = fullfile(mainpath,'FITC'); % define path1 as FITC folder
path2 = fullfile(mainpath,'Texas Red'); % define path 2 as Texas
Red folder

list1 = dir(path1); % make a list of folders inside FITC
list2 = dir(path2);% make a list of folders inside Texas Red
if ~exist(fullfile(mainpath,'stackimage'), 'dir') % create
'stackimage' folder if not already exists
     mkdir(fullfile(mainpath,'stackimage'));
end

disp('cropping, please wait...')

% Gather all background reference images
i=numel(list1);% index the number of 'blank' folder
% Get blank images for FITC
if isdir(fullfile(path1,list1(i).name))==1
        subpath = fullfile(path1,list1(i).name);
        piclist = dir(subpath);% make a list of blank images at
different time
        blank1 = zeros(600,800,numel(piclist)-3,'uint8');%
create an array for storing blank images
        for j=3:1:numel(piclist)
            [~, ~, ext] =
fileparts(fullfile(subpath,piclist(j).name));
```

```
            if strcmpi(ext,'.TIF')==1
                blank1(:,:,j-2) =
imread(fullfile(subpath,piclist(j).name)); % store blank images
for FITC in variable ‘blank1’
            end
        end
end

% Get blank images for Texas Red
if isdir(fullfile(path2,list2(i).name))==1
        subpath = fullfile(path2,list2(i).name);
        piclist = dir(subpath);
        blank2 = zeros(600,800,numel(piclist)-3,'uint8');
        for j=3:1:numel(piclist)
            [~, ~, ext] =
fileparts(fullfile(subpath,piclist(j).name));
            if strcmpi(ext,'.TIF')==1
                blank2(:,:,j-2) =
imread(fullfile(subpath,piclist(j).name));% store blank images
for Texas Red in variable ‘blank2’
            end
        end
end

% work on cropping folder by folder
for i=3:1:(numel(list1)-1)
    if isdir(fullfile(path1,list1(i).name))==1
        subpath1 = fullfile(path1,list1(i).name);
        piclist = dir(subpath1);% make a list of images in each
chamber folder
        allpic1 = zeros(600,800,numel(piclist)-3,'uint8'); %
create a blank variable for storing chamber images
        for j=3:1:numel(piclist)
            [~, name, ext] =
fileparts(fullfile(subpath1,piclist(j).name));
            if strcmpi(ext,'.TIF')==1
                allname1(j-2) = {name};
                allpic1(:,:,j-2) =
imread(fullfile(subpath1,piclist(j).name)); %store images in the
variable created
            end
        end
    end
% repeat the image storing process with red channel folders
    if isdir(fullfile(path2,list2(i).name))==1
        subpath2 = fullfile(path2,list2(i).name);
        piclist = dir(subpath2);
```

```
        allpic2 = zeros(600,800,numel(piclist)-3,'uint8');
        for j=3:1:numel(piclist)
            [~, name, ext] =
fileparts(fullfile(subpath2,piclist(j).name));
            if strcmpi(ext,'.TIF')==1
                allname2(j-2) = {name};
                allpic2(:,:,j-2) =
imread(fullfile(subpath2,piclist(j).name));
            end
        end
    end
% This code relies on user to indicate the chamber position. The
following commands will allows the 'chamber shape' to be seen
easily.
I = sum(allpic1,3)+sum(allpic2,3);
I = imadjust(histeq(I/max(max(I))));
s = warning('off', 'Images:initSize:adjustingMag');
imshow(I); % display stacked image on screen for cropping
set(gcf,'NumberTitle','off');
set(gcf,'Name',strcat(list1(i).name,'/',list1(end-1).name));
warning(s);

h = imrect(gca, [50 20 559 559]); % display cropping rectangle
on the stack image
setResizable(h,false);

% record the stacked image
ipath =
fullfile(mainpath,'stackimage',strcat(list1(i).name,'.jpg'));
imwrite(I,ipath,'jpg');

%subtract each image with corresponding background reference,
crop the green channel, and then save as *.jpg files
pause
position = getPosition(h); % get the cropping rectangle position
for k=1:1:numel(blank1(1,1,:))
allpic1(:,:,k) = allpic1(:,:,k)-blank1(:,:,k); %subtract chamber
images with blank reference images
despath = fullfile(subpath1,strcat(allname1{k},'.jpg'));
cropped = imcrop(allpic1(:,:,k),position); % crop images in that
chamber at the given rectangle position
imwrite(cropped,despath,'jpg','Quality',100); %write jpg image
in the same chamber folder
end

% Repeat cropping with other channel (red)
for k=1:1:numel(blank2(1,1,:))
```

```
allpic2(:,:,k) = allpic2(:,:,k)-blank2(:,:,k);
despath = fullfile(subpath2,strcat(allname2{k},'.jpg'));
cropped = imcrop(allpic2(:,:,k),position);
imwrite(cropped,despath,'jpg','Quality',100);
end
end
close

disp('Deleting *.tiff files....')
rmdir(fullfile(path1,list1(numel(list1)).name),'s');% remove
blank images in FITC
rmdir(fullfile(path2,list2(numel(list2)).name),'s');% remove
blank images in Texas Red
recycle off;
manage(mainpath,mainpath); % delete every *tif files
recycle on;
disp('     Done!')
end

function manage(path,givenpath)
listing = dir(fullfile(path,'\'));
for i = 3:numel(listing)
     subpath = fullfile(path,listing(i).name);
    [~, name, ext] = fileparts(listing(i).name);
if isdir(subpath)==1
     delete(fullfile(subpath,'*.tif'));
     manage(subpath,givenpath);
end
end
end
```

Counting the cells

```
function 20x_poly_count()
clc % clear existing images on the screen
disp('Configuring necessary parameters...')
warning off all;
clear global variable
clear java

% This code relies on ImageJ function as it's core, thus ImageJ
is needed
javaaddpath('C:/Program Files (x86)/ImageJ/ij.jar');% Locate
ImageJ (default location for ImageJ in both 32 and 64 bit
systems)
javaaddpath('C:/Program Files/ImageJ/ij.jar');
import('ij.IJ.*');% Import ImageJ functions
import('ij.plugin.filter.*');% Import more ImageJ functions
```

```
if versionLessThan('1.46')==1 % 'Find Maxima' function is
avaiable only in version 1.46 or later
    return
end

% Request for the threshold inputs for ‘Find Maxima’ algorithm
th1 = str2double(input('Threshold for FITC: ','s'));
th2 = str2double(input('Threshold for Texas Red: ','s'));

disp('Please locate the sorted, cropped experiment folder...')
folder = uigetdir();% locate experiment folder

for i=1:1:2
% display the thresholds assigned by user
if i==1
    celltype = 'FITC';
    disp('-----FITC-----')
    threshold = th1;
    fprintf('The sensitivity is %d \n',threshold);
elseif i==2
    celltype = 'Texas Red';
    disp('-----Texas Red-----')
    threshold = th2;
    fprintf('The sensitivity is %d \n',threshold);
else
    disp('Error!')
end

path = fullfile(folder,celltype);

listing = dir(path);% make a list of chamber folders inside
channal folders
disp('Counting cells in chamber number:  ')

for a=3:numel(listing) % count cells folder by folder
    filelist = dir(fullfile(path,listing(a).name,'*.jpg'));%
make a list of chamber images inside each chamber folder
    fprintf(1,'\b\b%s',listing(a).name); %display progress
during counting
    chambername(1,a-2) = str2num(listing(a).name);
    chambername(2,a-2) = 1;
    first =
imread(fullfile(path,listing(a).name,filelist(1).name));
    overall = sum(sum(first)); % obtain intensity sum of the
first image in that folder.
```

```
% for each file, load image into Java variable, then use
getMaxima function to achieve the cell count.
    for b=1:numel(filelist)
        imp =
openImage(fullfile(path,listing(a).name,filelist(b).name));
        ip = imp.getProcessor();
        mf = MaximumFinder;
        maxima = mf.getMaxima(ip,threshold, 0);% call function
Maximum Finder using the defined threshold
        maximacount(b,a-2) = maxima.npoints;%get the cell count
from ImageJ
% alternative counting method: count by comparing intensity sum
with the first image intensity sum. The cell count is then
related to the first image cell count.
I = imread(fullfile(path,listing(a).name,filelist(b).name));
        intensity = sum(sum(I));
        intensitycount(b,a-2) =
floor(intensity/overall*maximacount(1,a-2));% record cell count
by intensity (relative to the first image) in an array
        rawintensity(b,a-2) = floor(intensity);% record raw
intensity of each image in another array
    end
end
fprintf('\n')

disp('Done counting cells. ')
disp('Writing result in .xls file...')

% record the counting result in Excel file.
filename = strcat('Cell Count_',celltype,'.xls');
timepoints = numel(dir(fullfile(path,listing(3).name,'*.jpg')))-
1;
time = transpose(0:30:timepoints*30);

A1FTIC = sprintf('threshold = %d',threshold);

xlswrite(fullfile(folder,filename), {A1FTIC;'Y/N =
1/0';'time(min)'}, 3,'A1');
xlswrite(fullfile(folder,filename), chambername, 3,'B1');
xlswrite(fullfile(folder,filename), time, 3,'A4');
xlswrite(fullfile(folder,filename), rawintensity, 3,'B4');

xlswrite(fullfile(folder,filename), {A1FTIC;'Y/N =
1/0';'time(min)'}, 2,'A1');
xlswrite(fullfile(folder,filename), chambername, 2,'B1');
xlswrite(fullfile(folder,filename), time, 2,'A4');
xlswrite(fullfile(folder,filename), intensitycount, 2,'B4');
```

```
xlswrite(fullfile(folder,filename), {A1FTIC;'Y/N =
1/0';'time(min)'}, 1,'A1');
xlswrite(fullfile(folder,filename), chambername, 1,'B1');
xlswrite(fullfile(folder,filename), time, 1,'A4');
xlswrite(fullfile(folder,filename), maximacount, 1,'B4');

e = actxserver ('Excel.Application'); % open Activex server
ewb = e.Workbooks.Open(fullfile(folder,filename)); % open file
(enter full path)
ewb.Worksheets.Item(1).Name = 'Local Maxima';% rename 1st sheet
ewb.Worksheets.Item(2).Name = '# from Intensity';
ewb.Worksheets.Item(3).Name = 'Raw Intensity';
ewb.Save % save to the same file
ewb.Close(false)
e.Quit

fprintf('Output file: %s\n', filename)

end
clear all
clear global variable
clear java
disp('     Done!')
warning on all;
end
```